André Filipe de Oliveira Almeida

Mestre em Engenharia Civil

PUNCHING IN FLAT SLABS SUBJECTED TO CYCLIC HORIZONTAL LOADING

Dissertação para obtenção do Grau de Doutor em

Engenharia Civil

Orientador: Prof. Doutor António Manuel Pinho Ramos
Professor Auxiliar, FCT/UNL

Co-orientador: Prof. Doutor Válter José da Guia Lúcio
Professor Associado, FCT/UNL

Júri:

Presidente: Prof. Doutor Fernando M. A. Henriques

Arguentes: Prof. Doutor Carlos Manuel Chastre Rodrigues
Prof. Doutor Mário Jorge de Seixas Pimentel

Vogais: Prof. Doutor António Manuel Pinho Ramos
Prof. Doutor Rui Pedro César Marreiros
Profª Doutora Ana Rita Faria Conceição de Sousa Gião
Prof. Doutor Manuel José Andrade Loureiro Pipa

Setembro, 2019

FACULDADE DE CIÊNCIAS E TECNOLOGIA
UNIVERSIDADE NOVA DE LISBOA

PUNCHING IN FLAT SLABS SUBJECTED TO CYCLIC HORIZONTAL LOADING

Acknowledgments

This dissertation would not have been possible without the strength of God and the support of those who were by my side, helping me going through the difficult times and being responsible by the good ones. My most profound thanks to all those extraordinary people.

I am grateful for the best team of supervisors that I could ever had, Professor António Pinho Ramos and Professor Válter Lúcio. Thank you for the best scientific guidance, for the support, for the limitless patience and for the immense trust that allowed me to go ahead with the oddest ideas.

To my dear friend Micael Inácio, my research companion, a brilliant investigator, tireless worker, who lift me up and pushed me forward in the most difficult periods of this work, my thoughtful thanks.

I would like to thank my friends Rui Marreiros and Carla Marchão for the scientific guidance, true friendship and therapy sessions.

To my friends and office colleagues Ana Rita, Nuno Mamede, Noel Franco and Alessia Masini for all the laughs, technical support and help in random tasks whenever I need them.

I truly thank the help of Eng. Ricardo Faria, Eng. Nuno Ornelas, Eng. Bruno Alcobia and Eng, Gonçalo Antunes for their collaboration with both labour and data that enriched this work.

I would like to thank the laboratory technicians Jorge Silvério, José Gaspar and Vitor Silva for all the labour and technical support.

This work received the support from the Fundação para a Ciência e a Tecnologia - Ministério da Ciência, Tecnologia e Ensino Superior through scholarship number SFRH/BD/119772/2016.

A special thanks to Concremat - Soluções de Betão, S.A. Precast Facility for making possible the fabrication of the specimens. To all their work team, namely Eng. Romeu Reguengo, Eng. José and Eng. David, thank you.

I would like to thank TECNO2004 Lda for the fabrication of the steel elements of the test setup. A special thanks to José Carlos Carmo.

To my closest friends André Ramos, Filipa Lopes, Goretti, Jorge and Susana, Luís Mota, Mário Alves, Pedro and Lucía, Pedro Tiago, Ricardo and Cátia, Tiago Vilarinho, Vale family and many more, that were always by my side, a very special thank you.

I thank my dear friends Pe. Ricardo Jacinto and the late D. Sebastião Perestrello, for the spiritual guidance and for helping me growing up to be the person I am today.

I would like to thank my close family for all the support. To my late grandparents José de Oliveira and Brígida Rosa. I miss you every day.

A very special thank you to Joana Reis, for all the love we shared, for picking me up when I most needed, for showing me the way, for all the wonderful moments we shared and for being the most wonderful person.

To Noémia and Diamantino, the best parents that I could hope for. All this is a result of your wok. Thank you for the superhuman effort that you have to go through to allowing me to continue to pursuit this goal. I hope I am the son you hoped for. Love you both.

The most special acknowledge to Inês Almeida. You are the best sister that I could ever wish. You lift me when, you lectured me and you let me stumble and learn by myself, when I needed. I will always be in debt to you for everything you did for me. Love you to eternity.

Abstract

The aim of this work is to study the behaviour of reinforced concrete flat slab structures under combined vertical and horizontal cyclic loading. A total of eleven similar reinforced concrete slabs were cast and tested, measuring 4.25x1.85x0.15m³.

The cyclic tests were performed using an innovative test setup that aimed to simulate the boundary conditions of a flat slab, representing the slab between middle spans in one direction and between zero bending moment points in the other direction. It was designed to allow bending moment redistribution, mobility of the line of inflection, assure equal vertical displacements and rotations at the opposite free borders, and, therefore, symmetrical shear forces and equal bending moments, as expected in a real structure.

The slab specimens were connected to two steel half columns, by 0.25x0.25m² rigid steel plates prestressed against the slab using steel bolts, to ensure monolithic behaviour. The slabs were divided in groups, according to the characteristics of the test protocol and the tested variables. A reference specimen was subjected to centred punching, and the results were used to predict the punching capacity of the remaining slabs. One specimen was tested under constant vertical loading and monotonically increased eccentricity until failure. In the cyclic tests, the vertical load was first applied and kept constant during the test, while the cyclic horizontal loading, was increased, in steps of three cycles, until failure. Three specimens were tested under constant vertical load, at different shear ratios, and cyclic increasing horizontal loading. Two slabs were tested using post installed shear bolts arranged in two different solutions, one using a radial distribution around the column and another using a cross distribution. Four slab specimens with shear reinforcement were tested with different shear reinforcement ratios and number of stirrup layers.

Results show that cyclic horizontal actions are very harmful to the slab-column connection, resulting in low horizontal drift, if no adequate shear reinforcement is provided, and low energy dissipation. The post installed steel bolts were proven to be an efficient solution for strengthening existing structures, improving the structural behaviour and the punching resistance. Also, the use of steel stirrups as shear reinforcement is very effective, increasing shear, drift and energy dissipation capacities. Finally, design recommendations and a proposition for the calculation of a minimum shear reinforcement are suggested.

Keywords

Flat slab, reinforced concrete, cyclic, shear ratio, punching stirrups, bolts, shear reinforcement

Resumo

Este trabalho teve como objetivo estudar o comportamento de lajes fungiformes de betão armado sujeitas a cargas verticais gravíticas combinadas com cargas horizontais cíclicas. Foram ensaiadas onze lajes de características semelhantes com dimensões de 4.25x1.85x0.15m³.

Nos ensaios realizados foi usado um sistema de ensaio inovador, concebido para aplicar as condições de fronteira de uma laje fungiforme real, num modelo de uma laje truncado entre meios-vãos numa das direções e entre pontos de inflexão para cargas gravíticas na direção perpendicular. Este sistema de ensaio foi concebido para permitir redistribuição de momento positivo, mobilidade da linha de inflexão e permitir deslocamentos verticais iguais e rotações iguais nos bordos opostos, assegurando assim, esforço transverso simétrico e momentos iguais, como esperado no meio vão de uma laje real.

Os modelos foram ligados a dois meios pilares metálico por meio de chapas metálicas rígidas de dimensões 0.25x0.25m², pré-esforçadas contra a laje por varões roscados de aço, para garantir um comportamento monolítico. Os modelos foram agrupados de acordo com as variáveis estudadas e as caraterísticas do protocolo ed ensaio utilizado. Foi ensaiada uma laje de referência ao punçoamento centrado, cujos resultados foram usados para extrapolar a capacidade de carga das restantes lajes. Um dos modelos foi ensaiado sob carga vertical constante e excentricidade unidirecional crescente até à rotura. Nos ensaios cíclicos, a carga vertical foi mantida constante, enquanto se aplicaram ciclos de drift crescente até se atingir a rotura. Foram ensaiadas três lajes com diferentes valores de shear ratio e incrementos de drift alternados. Em duas lajes foram testados parafusos pós-instalados como armadura de punçoamento em disposições radial e cruciforme. Nas últimas quatro lajes, utilizaram-se estribos com duas taxas de armaduras com disposições de três e cinco perímetros.

Os resultados mostraram que as ações cíclicas horizontais são gravosas para as ligações laje-pilar o que apresentam capacidades de drift reduzidas. O uso de armadura de punçoamento pré e pós instalada mostrou-se eficaz no aumento da capacidade de drift e ductilidade da ligação pilar-laje. Por fim, são feitas recomendações de projeto e é proposta uma armadura mínima a utilizar em zonas sísmicas.

Palavras Chave

Laje fungiforme, betão armado, cíclico, shear ratio, punçoamento, estribos, parafusos, armadura de punçoamento

Contents

List of Figures

List of Tables

Nomenclature

Roman letters

a	constant
A_{cw}	influence area of the first layer of shear reinforcement
A_{sw}	sum of the cross-section areas from all the steel reinforcement that efficiently contribute to punching resistance (well anchored and crossing a 45º crack)
$A_{w,\,s}$	the area of the cross section of the shear reinforcement in a single perimeter around the column to be used for seismic actions
b	constant
$b_{0,\,ACI}$	control perimeter of the punching failure zone in ACI 318
$b_{0,\,EC2}$	control perimeter of the punching failure zone
$b_{0,\,MC2010}$	control perimeter according to MC2010
b_1	dimension of the perimeter b_0 in the direction of the application of the horizontal loading
$b_{1,\,red}$	reduced control perimeter due to non uniform stress distribution
b_2	dimension of the perimeter b_0 in the direction of the application of the horizontal loading
b_s	width of the slab strip according to MC2010
b_u	diameter of circle with an area equal to the area of the control perimeter
b_y	maximum dimension of the control perimeter in the direction of the application of the horizontal loading
b_z	maximum dimension of the control perimeter in the direction perpendicular to the application of the horizontal loading
c	constant
c_1	column dimension in the direction of the horizontal loading
c_2	column dimension in the direction perpendicular to the horizontal loading
c_L	distance from the centre of the column to the line of the control perimeter in the direction of the horizontal loading

$C_{Rd,c}$	parameter that takes into account the uncertainty of the concrete characteristics
d	average effective depth of the slab
d_g	maximum dimension of the aggregates
d_{g0}	reference aggregate size equal to 16 mm
dr	inter-story drift
d_v	effective depth of the slab considering support penetration
E	Modulos of Elasticity (Young)
e_L	distance parallel to the eccentricity from each point of the control perimeter to the bending moment action axis
E_s	modulus of elasticity of the flexural reinforcement
E_s	modulus of elasticity of the shear reinforcement
e_u	eccentricity of the shear force relative to the centroid of the control perimeter
f_{bd}	design bond strength
f_c	average concrete compressive strength in cylinders
$f_{c,cube}$	average concrete compressive strength in cubes
f_{cd}	design compressive strength of the concrete
f_{ck}	characteristic compressive strength of the concrete
$f_{ct,sp}$	average concrete traction strength by splitting test
f_y	average yield strength of the flexural reinforcement
f_{yt}	characteristic value of the yield stress of the shear reinforcement
$f_{ywd,ef}$	effective stress in the shear reinforcement
J_c	parameter analogous to the moment of inertia
k	factor that takes size effect into account
k_c	factor that takes into account the ratio of the dimensions of the column
k_e	eccentricity coeficiente

k_{sys}	concrete confinement parameter due to shear reinforcement
M_{Ed}	design unbalanced moment in the column region
$M_{f, ACI}$	parcel of the unbalanced moment transferred by flexure from the column to the slab
m_{Rd}	average design flexural strength per unit of length
$M_{s, ACI}$	parcel of the unbalanced moment transferred by shear from the column to the slab
M_{sc}	total unbalanced moment to be transferred from the column to the slab
m_{sd}	average distributed bending moment
r_s	distance from the centre of the column to the counter-flexure point
$r_{s, x}$	distance from the centre of the column to the counter-flexure point in the x direction
$r_{s, y}$	distance from the centre of the column to the counter-flexure point in the y direction
SR	vertical shear ratio
s_0	distance from the face of the column to the first shear reinforcement layer
s_r	distance between shear reinforcement perimeters
V	shear force
V_c	value for the concrete contribution for the punching resistance
$V_{c, ACI}$	ACI 318 value for the concrete contribution for the punching resistance
$V_{c, EC2}$	EC2 value for the concrete contribution for the punching resistance
$V_{c,MC2010}$	MC2010 value for the concrete contribution for the punching resistance
$V_{crush, ACI}$	ACI 318 concrete crushing resistance near the column
$V_{crush, EC2}$	EC2 concrete crushing resistance near the column
$V_{crush, MC2010}$	MC2010 concrete crushing resistance near the column
V_{Ed}	design shear force
$V_{Ed, s}$	design shear force for the seismic combination

V_{exp}	experimental vertical load
V_{flex}	shear force associated to the failure of the slab by flexure
$V_{out, ACI}$	ACI 318 provision of the punching resistance outside the shear reinforcement
$V_{out, EC2}$	EC2 provision of the punching resistance outside the shear reinforcement
V_R	CSCT provision of the punching resistance
V_{Rd}	EC2 provision of the punching resistance
$V_{s, ACI}$	ACI 318 provision of the shear reinforcement contribution in the punching resistance
$V_{s, MC2010}$	MC2010 provision of the shear reinforcement contribution in the punching resistance
$V_{sr, ACI}$	ACI 318 provision of the punching resistance for slabs with shear reinforcement
$V_{sr, EC2}$	EC2 provision of the punching resistance for slabs with shear reinforcement
W_1	function of the distance between each point of the control perimeter and the axis of action of the unbalanced moment

Greek letters

ε_y	average yield strain
$\varepsilon_{yk, w}$	design yield strain of the shear reinforcement
$\varepsilon_{w, max}$	maximum allowed strain for the shear reinforcement
$\emptyset$	reduction factor
$\emptyset_w$	diameter of the shear reinforcement
ρ_l	weighted flexural reinforcement ratio of the slab
ρ_y	flexural reinforcement ratio of the slab in the longitudinal direction
ρ_z	flexural reinforcement ratio of the slab in the transverse direction
σ_{swd}	average design flexural strength per unit of length
ψ	rotation of the slab

α	angle between the shear reinforcement and the plane of the slab (top towards the column)
α_s	parameter that takes into account the position of the column within the slab (40 for interior columns, 30 for edge columns and 20 for corner columns
β	magnifying factor due to moment eccentricity
β_c	ratio of the longest over the shortest column side
γ_c	reduction factor for the concrete according to the ruling regulation
γ_f	fraction of the total moment to be transferred by flexure
δ_{col}	horizontal displacement due to the flexibility of the column
λ	parameter that takes into account the type of concrete (1 for regular concretes)
υ_u	shear stress at the control perimeter
γ_c	reduction factor to be applied in the calculation of the concrete crushing resistance near the column
υ_{cr}	reduction factor for cracked concrete under shear

Chapter 1

Introduction

1.1 Background

Earthquakes can be devastating events with numerous losses both human and economical. To minimize those losses, special cares must be taken by civil engineers when designing structures in seismic zones. Flat slab structures have been widely used lately. Its architectural and economic advantages made them a top choice for both office and residential buildings. Its main advantage, the beam absence, leads to one of its main weakness: the punching failure. Although this is a reasonably well-known phenomenon for monotonic vertical loading, flat slab punching failure under cyclic horizontal loads is not yet sufficiently understood. Being a quite complex case study, with a large number of variables to consider, the amount of experimental information regarding the behaviour of flat slabs under reversed cyclic horizontal loading is clearly insufficient.

To study this subject, various methods were used by researchers. The first approach was to try to create a simplified experimental model of the slab-column connection. This simplification was introduced by Hanson [1] and inspired all the simplified test setups used in future works. Some researchers opted to follow a multi frame experimental approach (eg. Robertson [2], [3], Durrani [4], [5], Dechka [6], Hwang [7], Rha [8]). The multi frame test setup has the main advantage of being more faithful to the real structure, however, it is more expensive and difficult to implement in a laboratorial context. Other researchers such as Hawkins [9], Pan [10], Tegos [11], Warnitchai [12], Robertson [13], Gayed [14], Ritchie [15], Han [16], Park [17], Benavent-Climent [18], [19], [20], Anggadjaja [21], Eder [22] and Himawan [23] continued working in the subject of flat slabs under vertical and seismic actions, using variations of the simplified test setup, progressively changing details trying to overcome the limitations of the simplified approach. All tests led to the conclusion that flat slabs are susceptible to fail by punching under seismic actions, leading in some cases to progressive collapse as documented in recent events.

Researchers started to test ways to improve the behaviour of flat slab structures by adding various types of shear reinforcement such as steel stirrups (Hawkins [24], Robertson [25]), shear studs (Megally [26] and Isufi [27]), and other methods (Park [28], Esfahani [29], Kang [30], Cheng [31], Song [32], Al-Nasra [33]) with satisfactory results. For existing structures, there is the need to strength them. Two main methods were tested for this purpose: Fiber Reinforced Polimer (FRP) bands (Stark [34], Widianto [35]) and shear bolts (El-Salakawy [36]. Polak [37], Lawler [38], Topuzi [39]). The various shear reinforcement methods enhanced the behaviour of the flat slabs by increasing drift capacity, moment transfer capacity and energy dissipation.

1.2 Motivation and objectives

Throughout the years, researchers have studied the subject of the behaviour of flat slabs under gravity and horizontal cyclic loads using, mostly, simplified test setups that fail to replicate the real boundary conditions at the borders of the truncated models used as test specimens. The complexity of the deformed shape of flat slab structures when subjected to seismic loads is difficult to replicate in a simplified system, which results in a progressive search for improvements by the researchers introducing variations to the test setups when developing and implementing their own. The improvements done along the last decades although important, did not solve all the problems associated with the simplified test setups.

The objective of this dissertation is to contribute to the research on this topic by introducing a new and improved approach to the simplified test setup, as well as contribute with experimental test results regarding the influence of parameters such as shear ratio, shear reinforcement ratio, shear reinforcement arrangement and post installed shear reinforcement. A test setup with passive real time systems to approximate the real force distribution and therefore, the real deformed shape was developed and used to test eleven specimens, that were grouped as follows: one monotonic centred, one monotonic eccentric, three cyclic tests with different shear ratios, four with steel stirrups as shear reinforcement and two cyclic tests with steel bolts as post installed shear reinforcement. By using test specimens with similar characteristics as well as the same test setup and test protocol, it was possible to directly compare the influence of each studied parameter, with minimal unknown variables.

1.3 Dissertation organization

This dissertation is organized in five chapters, including the present one.

Chapter 2 summarizes the experimental tests performed in flat slabs subjected to horizontal cyclic actions, through the last decades. Special importance was given to the test setups developed and used by the authors that have been constantly evolving in order to achieve in the laboratory environment, the most accurate approximation to the behaviour of the real slabs. Tests in slabs without shear reinforcement, slabs with stirrups and slabs with post-installed reinforcement are shown and the obtained results are presented. The methodology proposed by three building codes for the design of flat slabs with and without shear reinforcement are presented.

Chapter 3 describes the thought process behind the development of the test setup used in the experimental campaign. The predesign and the design of the test setup and the test specimens is shown, followed by the production of the specimens and the results of the characterization tests of the used materials. The different test specimens are presented, as well as the details of the test assembly, instrumentation, protocols and proceedings.

Chapter 4 is where the results of the experimental campaign are shown, compared and discussed. The specimens are presented arranged in groups, sorted by type of test (with or without eccentricity) and studied variable. Results of the hysteretic response, stress distribution, slab deformation and energy dissipation are shown for each tested specimen.

In Chapter 5, the tested slabs and the obtained results are applied in a real design situation. The difficulties in the quantification of the vertical shear ratio, the scattering of the test results from literature and the need for shear reinforcement are addressed. Finally, a minimum shear reinforcement is proposed.

Chapter 6 presents the conclusions of the dissertation, a synthesis of the design proposals and suggestions for future researches on this dissertation scope.

Chapter 2

Literature Review

In this chapter, a review of a number of studies about the subject of this dissertation is presented, and arranged by authors. The first sub-chapter approaches studies where smaller simplified specimens were used. The second sub-chapter describes tests on larger multi frame specimens. Lastly, the specifications from Eurocode, ACI, and Model Code 2010 for punching, eccentric punching and, when applicable, punching under cyclic horizontal actions are presented.

2.1 Experimental tests using simplified setups

The transference of unbalanced moment from the column to the slab has been studied since the 1960s, however, the amount of experimental studies in this subject is massively small when compared to the number of tests on flat slabs subjected to centred punching.

Hanson and Hanson, 1968

The first studies where an unbalanced moment was considered consisted in the application of a monotonic eccentricity which prompted an unbalanced moment to be absorbed by the slab through the slab-column connection. The studies of Hanson [1], published in the decade of 1960, presented experimental tests using three types of loading: horizontal displacement without vertical load (with reversed cycles in some cases), vertical load without eccentricity and vertical load with eccentricity.

Sixteen specimens representing an interior slab-column connection were tested, as well as one specimen with an edge column. The dimensions of the slab were 2135 mm by 1220 mm (1143 mm by 1220 mm in the case of the slab with edge column) and the thickness of the slab was 76 mm. The top and bottom reinforcement consisted in a mesh of 9.5 mm diameter reinforcement bars spaced 76 mm from each other. The clear cover was 10 mm and the higher effective depth was parallel to the longitudinal axis. The columns were made of reinforced concrete with a steel plate welded to the reinforcement bars at the bottom end, to further be connected to a hinged support. The top end of the column was pinned to four

braces that were also fixed to the strong floor. A scheme of the test setup can be seen in Figure 2.1.

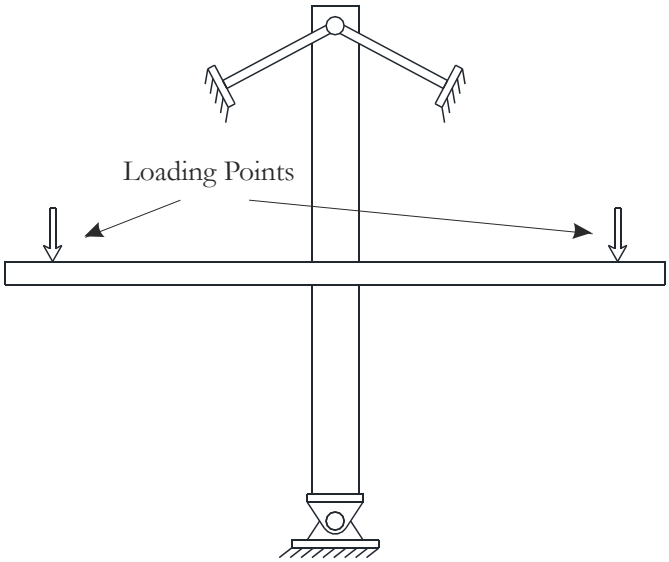

Figure 2.1: Test setup adapted from Hanson [1].

The parameters under consideration were, the type of loading, the geometry of the column, the position of the column and the existence of holes (25 mm by 152 mm) in opposite sides of the slab-column connection. All the details are summarized in Table 2**.1**.

The loading was applied as line forces by means of two steel spreader beams with two steel rods each. In the Type I test, antisymmetric forces were applied in the opposite borders to simulate eccentricity without vertical load. The Type II test consisted in symmetric vertical forces simulating the action of vertical loading only. Only one side was loaded in the Type III protocol in order to simulate both eccentricity and vertical load. The eccentric cyclic action was applied by load control, making it impossible to accurately measure the corresponding inter-story drift. Failure modes are also shown in Table 2.1.

Table 2.1: Characteristics of the specimens, test protocol and failure (adapted from Hanson [1]).

Specimen	Column (mm²)	Load Type	Holes	f_c (MPa)	f_y (MPa)	Failure
A1	152x152 Interior	Eccentric without vertical load.	-	30.3	365.4	Shear
A2				31.3	375.8	
A3L			//Long	37.0	364.0	
A4L				33.4	373.7	
A5C		A2, A4L and A6C were Cyclic	//Short	35.0	371.6	
A6C				34.9	368.2	
B7	152x305 Interior		-	33.0	354.4	
C8	305x152 Interior			32.8	410.9	
A9	152x152 Interior	Vertical load only	-	34.7	368.9	Flexure
A10L			//Long	30.9	354.4	
A11C			//Short	33.4	348.2	
A12		Eccentric with vertical load.	-	33.2	372.3	Shear
A13L			//Long	32.8	370.2	
A14C			//Short	35.6	372.3	
D15	152x152 Edge		-	31.1	365.4	
B16	152x305 Interior			30.4	3340.6	
C17	305x152 Interior			36.0	341.3	

Hawkins, Mitchell et al, 1974-1976

In the late 1970s, Hawkins [24], [40] acknowledged the importance of the capacity of the flat slab structures to convey the designed deformations without shear failure. With the recent Alaska (1964), Caracas (1967) and San Fernando (1971) earthquakes in mind, the author studied the behaviour of slabs with and without shear reinforcement. During the development of the studies, ten specimens designed to simulate full scale interior slab-column connections representative of a prototype building. This work was followed by Symonds [41], that tested 5 five additional slabs, using the same test setup and type of specimens with the same geometry and dimensions.

The specimens measured 3962 mm by 2134 mm with a thickness of 152 mm. The column consisted in two halves, with 1067 mm length each and a square cross section of 305 mm width. Both top and bottom extremities of the column were pinned to tie rods and to the

strong floor, respectively, in order to prevent them from moving while allowing rotation as seen in Figure 2.2. The vertical load was applied by hydraulic jacks with shared hoses assure balanced forces. The eccentric load was applied as a line load, along the most distant opposite borders, by push-pull jacks at a distance of 1829 mm from the centre of the column. From a total of fifteen specimens, eight had no shear reinforcement (S1, S2, S3, S4, S5 [40] [24], S6, S7 and S8 [41]) and seven had two legged steel stirrups as shear reinforcement (SS1, SS2, SS3, SS4, SS5 [40] [24], SS6 and SS7 [41]) displaced along the orthogonal axis with a spacing of 38 mm, varying the distance from the column to the last layer (shear reinforcement radius).

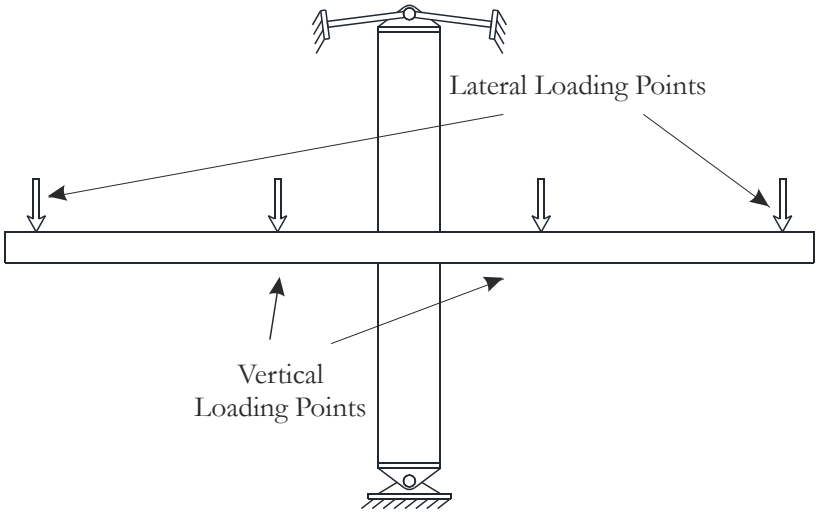

Figure 2.2: Test setup used by Hawkins (adapted from Hawkins [40]).

The flexural reinforcement was also a tested variable, both in ratio and arrangement of the reinforcement bars. The clear cover was 19 mm and the higher effective depth was parallel to the longer sides of the specimens. Details of the specimens are depicted in **Table 2.2**.

Table 2.2: Characteristics of the specimens and failure modes (adapted from [40], [24] and [41]).

Name	f_c (MPa)	Flexural reinforcement ratio (%)		Gravity load (kN)	Shear reinforcement		Failure
		Top	Bottom		Ø (mm)	Radius* (mm)	
S1	30.3	1.29	0.59	128.1	-	-	Punching
S2	30.7	0.90	0.49	142.3	-	-	Punching
S3	31.4	0.57	0.40	138.8	-	-	Punching
S4	54.7	1.29	0.59	149.9	-	-	Punching
S5	-	1.10	0.56	Unknown	-	-	Unknown
S6	23.2	1.10	0.56	271.3	-	-	Punching
S7	26.5	0.90	0.49	271.3	-	-	Punching
S8	30.8	0.57	0.40	235.8	-	-	Flexure
SS1	27.6	1.29	0.59	133.0	9.5	400	Crushing
SS2	25.7	0.90	0.49	126.3	6.4	286	**
SS3	25.9	1.10	0.56	126.8	9.5	362	Punching (out)
SS4	27.6	1.10	0.56	127.7	9.5	362	Punching (out)
SS5	32.2	0.90	0.49	125.9	6.4	324	Punching (out)
SS6	24.2	0.90	0.49	271.3	9.5	324	Punching (out)
SS7	26.9	1.10	0.56	271.3	6.4	514	Punching (out)

*radius of the reinforced area

**premature failure due to malfunction.

The lateral loading cycles were given in order to achieve a target load or a target ductility, therefore, because of the way the test setup was conceived and due to the non-linearity of the deformed shape, an accurate measurement of the drift was not possible. The authors used different test protocols varying the number of cycles and the target loads. When failure was not achieved, a monotonic centred load was applied until failure.

The authors observed that the reinforcement bars that pass through the column, as well as the ones right next to it, were the most stressed due to the moment transfer from the column to the slab, however, yielding was reached for the top reinforcement later in the test and it never occurred for the bottom reinforcement. The authors concluded that stirrups are effective if well detailed and applied [24] resulting in an increase in ductility, energy absorption, shear capacity and moment transfer.

Ghali and Dilger, 1976

A different test setup was used by Ghali [42] to compare the behaviour of slab-column connections subjected to cyclic horizontal loads to the specimens under quasi-static eccentricity, along with different flexural reinforcement ratios. The test setup had the specimen held along the two edges perpendicular to the eccentricity direction. To facilitate

the test assembly, the specimens were placed with a 90 degree angle from the normal position (the slab rests vertically and the column, horizontally). Both the vertical and horizontal loading were applied in the column. The eccentric load consisted in applying antisymmetric forces in both column edges while the gravity load resulted from compression in the bottom column edge, as shown in Figure 2.3.

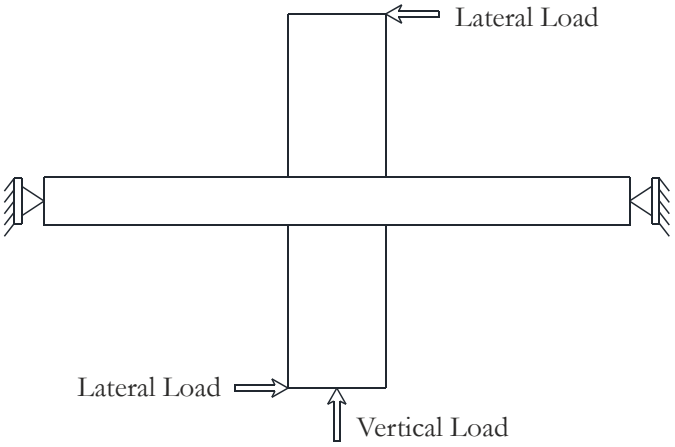

Figure 2.3: Test setup adapted from Ghali [42].

A total of six specimens were tested. The specimens, representing square slabs with 1830 mm width and 152 mm thick, were truncated at the theoretical inflection line for the vertical load. From end to end, the column measured 1170 mm divided in two halves in each side of the slab and its square cross section was 305 mm width. Three different flexural reinforcement ratios were used (0.5%, 1.0% and 1.5%) with a clear cover of 19 mm. For each reinforcement ratio, two tests were performed: a quasi-static horizontal loading combined with vertical load and a cyclic eccentric loading combined with vertical load.

All specimens failed by punching in the slab-column connection however, the specimen with the smaller reinforcement ratio presented generalized reinforcement yielding. Among the main findings of this work, the test speed was shown to influence the response of the materials that show an increase in strength for faster actions. The increase in the flexural reinforcement ratio, resulted in an increased strength, but reduced ductility and energy abortion capacity.

Morrison et al, 1983

To study the influence of the dynamic horizontal actions on the slab-column connection with and without vertical load, Morrison [43] used a different approach regarding the test setup. The specimen was supported by a hinged support at the bottom of the column and double pinned struts at the borders perpendicular to the imposed displacement. The struts

worked as a simple support that prevented vertical displacements only at the supported borders while an imposed displacement was applied at the top edge of the column. Some specimens were loaded vertically in four equidistant points at a distance of 467 mm from the closest corner of the column, as shown in Figure 2.4.

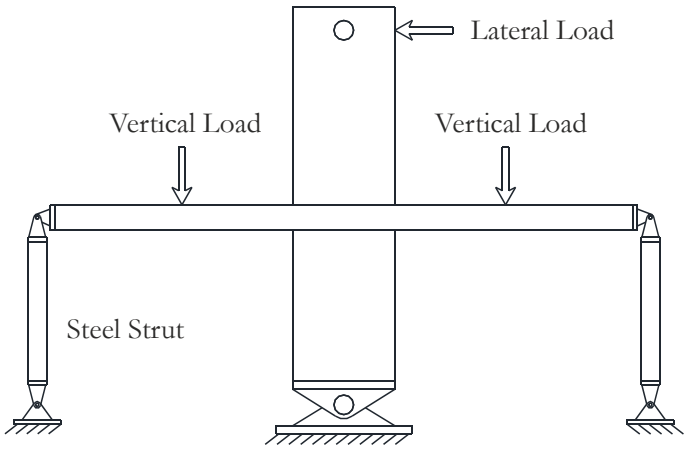

Figure 2.4: Test setup adapted from Morrison [43].

All slabs had similar geometry and were designed to be a reduced scale model of 1/3 of a typical flat slab structure, cut at mid-span. This resulted in square specimens with 1829 mm width and a thickness of 76 mm. The column had a total length of 1118 mm and a 305 mm width square cross section.

The flexural reinforcement ratios of 0.65 %, 0.98 % and 1.31 % were used for S1, S2 and S3 specimens (no vertical load), respectively. The S4 and S5 specimens had a flexural reinforcement ratio of 0.98% and were subjected to vertical loads of 14.3 kN and 28.6 kN respectively. The effective depth along the direction of the imposed displacement was 64 mm. The concrete compressive strength for the S1 specimen was 45.8 MPa while for the remaining ones, it averaged 34.8 MPa.

The cyclic imposed displacement protocol consisted in ten reversed complete cycles in each drift step, increasing the imposed displacement in each step, until a total of thirty cycles were achieved. Then, two more cycles with a higher displacement were applied followed by a non-cyclic increasing displacement until failure. The author also used an analytical model based in beams to approximate the behaviour of the experimental models.

The failures occurred by yielding of the flexural reinforcement and, for reinforcement ratios over 1.0 %, it happened for loads lower than provisioned, which means that the results were against safety. The specimens with higher reinforcement ratios showed less ductility. The

experimental results showed that the vertical load had little influence on the strength of the specimens. The beam based analytical model was a good approximation for this case.

Pan and Mohele, 1993

A different test setup was used by Pan [10] in order to study the effect of bi-directional cyclic horizontal loading in interior slab-column connections of flat slab structures. The specimens were supported by bi-directional bearings at both ends of the column and at the edges, representing the mid-span of the slab (where the inflection point for the horizontal loading was assumed), as detailed in Figure 2.5.

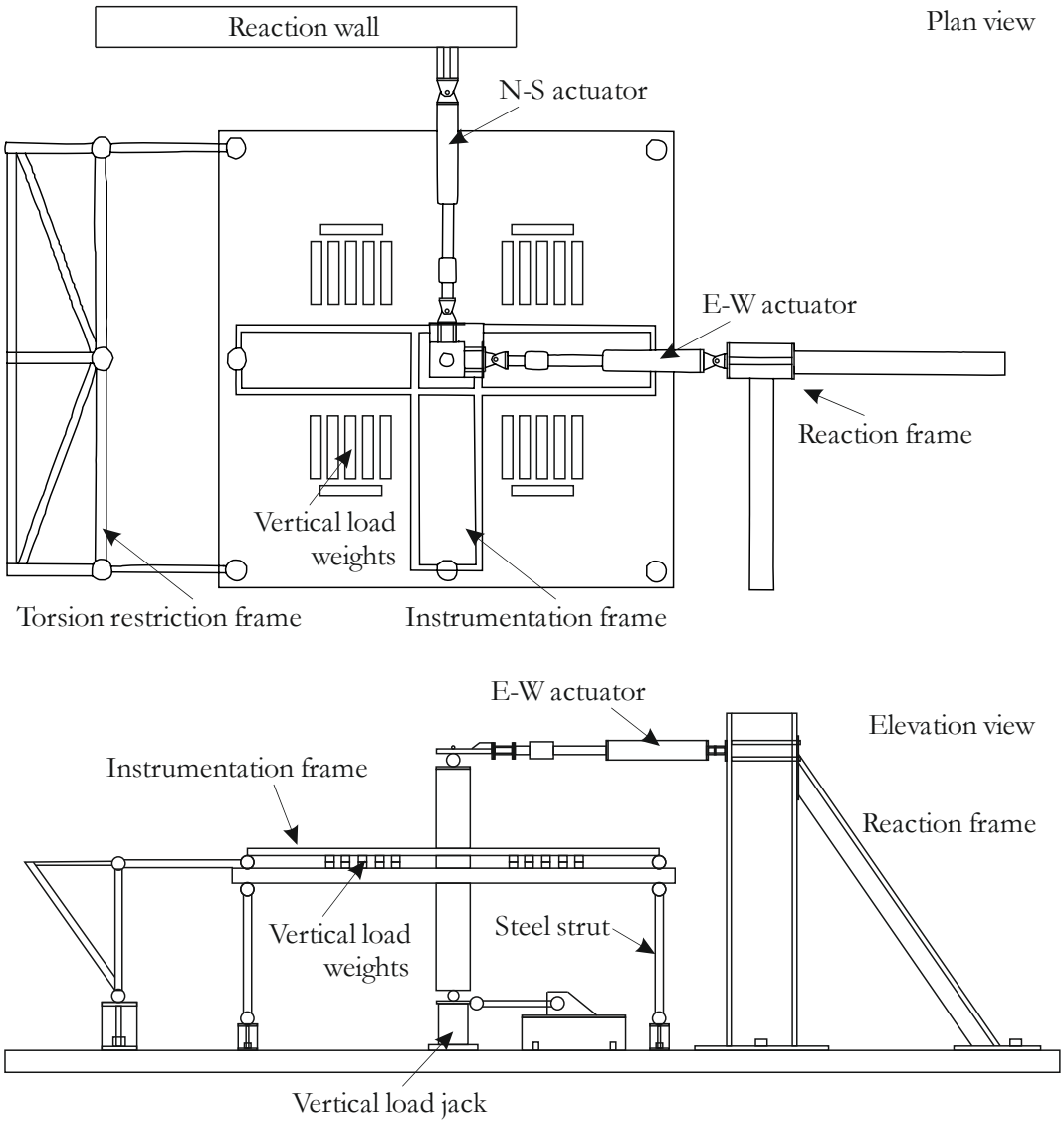

Figure 2.5: Test setup adapted from Pan [10].

To apply the horizontal displacements at the top of the column in two orthogonal directions two actuators were used, as well as a vertical jack, under the column, to apply the vertical

load. To better approximate the theoretical shear distribution curve, weights were added at the top of the slab. A restraining frame was used to prevent torsion during the test. A total of five tests were performed on four specimens, as summarized in Table 2.3.

The slabs were 3/5 reduced models of a typical flat slab building, and consequentially square 3.97 m width slabs, with 122 mm of thickness, with an 1.83 m length column with a square cross section with 274 mm width. All specimens had similar flexural reinforcement ratio of 0.76 % in the column region.

Table 2.3: Characteristics of the specimens and test protocol (adapted from Pan [10]).

Specimen	f_c (MPa)	Test	Vertical Load (MPa)
1	33.3	Uniaxial	0.7
2	33.3	Biaxial	0.7
3	31.4	Uniaxial	0.4
4	31.4	Biaxial	0.4
5*	51.0**	Biaxial	0.4

*Specimen 4 after failure and being repaired by cleaning and adding grout.

**Mean compressive strength of the repair grout.

The obtained results indicate that the vertical load has a central role in the resistance of the specimens. The slabs with the smaller vertical load presented increased stiffness and strength to the horizontal load. The biaxial action reduced the ductility, drift capacity and the overall strength. The use of bottom reinforcement bars that pass though the column is essential for post failure behaviour, to prevent progressive collapse. The repaired specimen presented satisfactory ductility but was not able to mobilize as much horizontal load that the other specimens did.

Soares, 1993

In 1993, Soares [44] assessed the suitability of the ruling codes regarding monotonic eccentric horizontal loads in reinforced concrete flat slabs. Two monotonic eccentric tests were performed in 3.00 m width square specimens with a thickness of 100 mm. The concrete columns had a cross section of 200 mm by 200 mm and a total length of 1700 mm from top to bottom, that represented the distance between inflection points.

The test setup, showed in Figure 2.6, had the specimens supported by steel tendons at the free borders perpendicular to the eccentricity direction and a passive system to impose positive bending moments in all free borders. Because the free borders represented the mid-span of the slab, under vertical load, the behaviour of the specimen would be similar to a cantilever, resulting in higher bending moments in the column region. Thus, a system consisting in four pinned struts (two in each direction) connected to hanging steel profiles solidly connected to the slab was used. The length of the struts was adjusted for each slab prior to the application of the vertical load. The vertical load was applied in sixteen equidistant points by means of spreader beams connected to two hydraulic jacks by steel tendons.

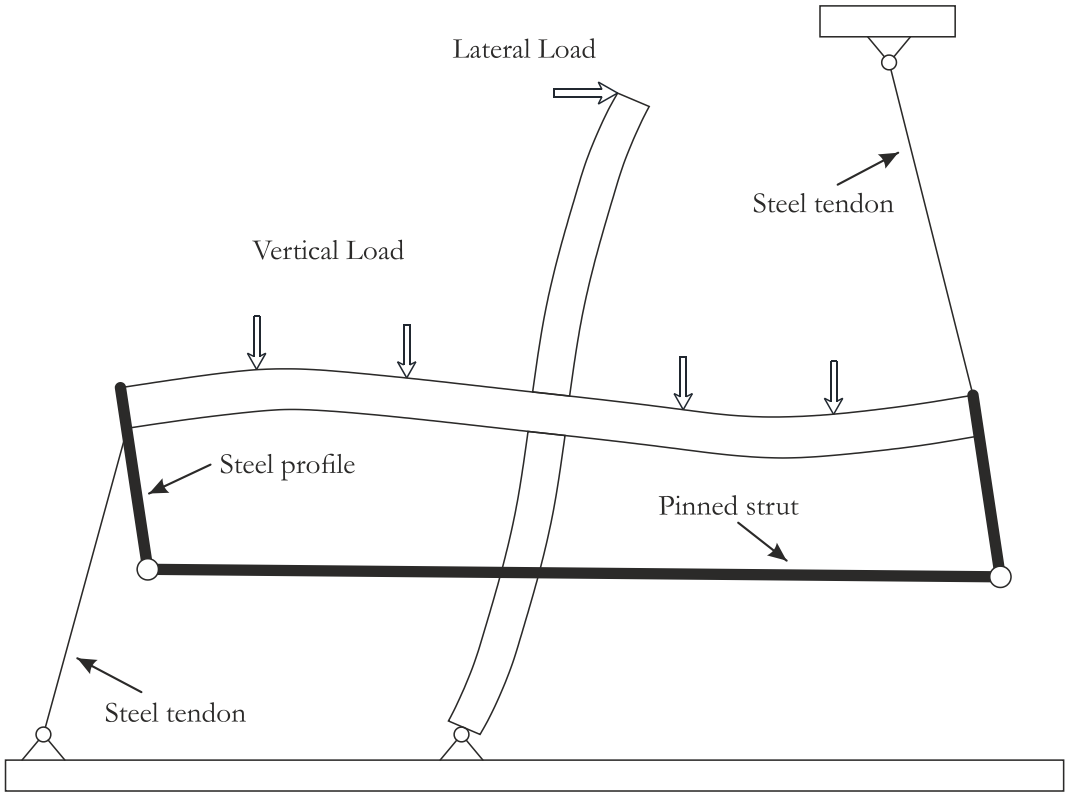

Figure 2.6: Test setup used by Soares (adapted from Soares [44]).

A flexural reinforcement ratio of 1.0 % was used for both slabs with the higher effective depth in the direction of the horizontal loading. The test protocol was different for both specimens. The specimens were first subjected to a vertical load of 140.9 kN. Then, a horizontal displacement at the top of the column was applied to the JS2 specimen until failure. The JS3 specimen was unloaded until a vertical load of 97.3 kN was reached and then, a horizontal displacement at the top of the column was applied until failure.

The author concluded that the moment imposition system worked well, however, the border restraining system had to be improved in order to control the transverse loads applied to the specimens. The codes predictions showed dispersion regarding slabs under eccentric loading.

Tegos and Tsonos, 1996

Using a similar approach to Ghali [42], Tegos [11] developed a test setup that consisted in a slab specimen rotated ninety degrees and supported at the borders being the horizontal and vertical loads applied at the end of the column. The supports prevented displacements on the borders perpendicular to the horizontal action while allowing rotations. The slabs were squares with 1.60 m width and 120 mm thick with a column 650 mm long and 200 mm width square cross section. The column was hanged from the bottom of the slab, as depicted in Figure 2.7.

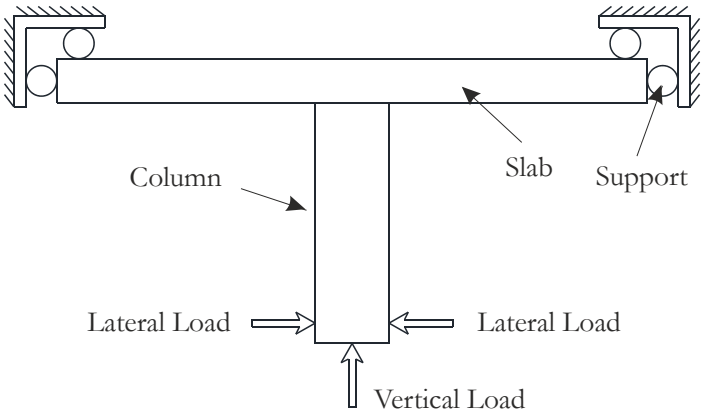

Figure 2.7: Test setup adapted from Tegos [11].

Three specimens, with an average cylinder concrete compressive strength of 25 MPa, were cast and tested: L1 had no shear reinforcement; S1 had six 8 mm diameter reinforcement bars going through the column and bent down with a 45º angle; in specimen F1 a fiber reinforced concrete was used, with 30 kg/m³ of 50 mm long steel fibers. The flexural reinforcement was similar for all specimens and consisted in 8 mm diameter reinforcement bars spaced of 100 mm with a higher concentration in the column region (ten bars spaced of 50 mm) and an effective depth of 100 mm.

The test protocol consisted in loading the specimen vertically with 75 kN and kept constant, followed by reversed cyclic horizontal loads at the end of the column.

Both L1 and F1 failed by punching, however the presence of steel fibres changed the failure from brittle to gradual. The S1 specimen developed significant cracking over the column and presented a mix of flexural and punching failure. In this test, inclined reinforcement bars performed better than steel fibres but both solutions enhanced the performance of the specimens.

Robertson et al, 2002-2006

Robertson tested the efficiency of three different types of shear reinforcement [45] and the influence of vertical shear ratio and continuous flexural reinforcement [13] in the load capacity of flat slab interior column connections subjected to seismic and gravity loading. The test setup approach was similar to the one used by Morrison [43]. The specimens were supported by double pinned steel struts at the edges perpendicular to the horizontal load direction, representing the mid-span of the slab, and by the bottom column. The column consisted in two elements, being the horizontal load applied at the top one, as shown in Figure 2.8.

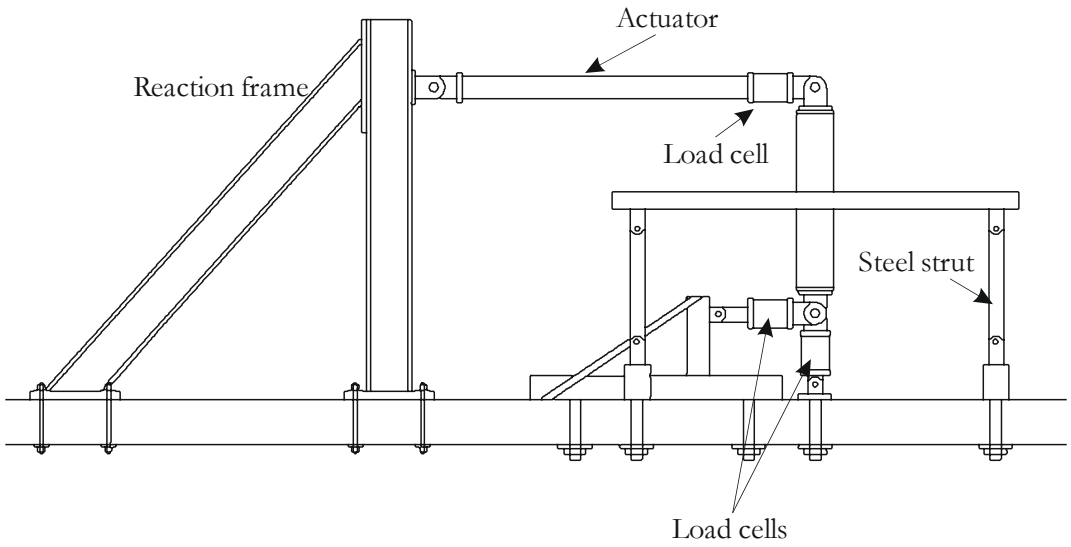

Figure 2.8: Test setup used by Robertson (adapted from Robertson [45]).

All specimens were similar in dimensions, measuring 2743 mm by 3048 mm, in plan, supported on the shorter edges. The thickness was 114 mm and the reported effective depth was 100 mm. The distance between both ends of the column, representing the inflection points of the column, was 1372 mm and it had a square cross section of 254 mm width. The first batch of specimens had eleven layers of eight 6 mm diameter bars as shear reinforcement, spaced of 65 mm in the radial direction, and continuous flexural reinforcement while the second set had discontinuous flexural reinforcement with different ratios as well as different vertical shear ratios. All the details of the specimens are summarized in Table 2.4

Table 2.4: Characteristics of the specimens (adapted from Robertson [45] [13]).

Specimen	ρ (%)	f_c (MPa)	Shear reinforcement	Average vertical load (kN)	Drift (%)	Failure
1C	0.80	35.4	-	38.9	3.5	Punching
2CS	0.80	31.4	Closed stirrups	33.7	8.0	-
3SL	0.80	43.4	Single leg stirrups	24.9	8.0	-
4HS	0.80	38.2	Shear studs	35.4	8.0	-
ND1C	0.53	29.6	-	60.8	8.0	Flexure/Punching
ND4LL	0.53	32.3	-	93.4	4.0	Flexure/Punching
ND5XL	0.53	24.1	-	104.8	2.0	Punching
ND6HR	0.93	26.3	-	67.2	4.5	Punching
ND7LR	0.39	18.8	-	68.5	4.5	Flexure/Punching
ND8BU	0.93	39.2	-	65.3	4.5	Flexure/Punching

The vertical load was applied using concrete blocks suspended from underneath the slab while the horizontal load was imposed at the top of the column by an actuator, in increasing

drift steps up to 4.0 %, of three cycles per drift step. Afterwards, increasing positive only steps of three cycles per step were imposed until a maximum of 8.0 %.

The obtained results showed that the three types of shear reinforcement were equally efficient in preventing failure until the end of the test protocol for the considered vertical load and increased the horizontal peak load by 22 %. Specimens with discontinuous bottom flexural reinforcement presented a similar behaviour to the ones with continuous bars, however, the lack of inferior reinforcement bars passing through the column lead to full loss of load transmission from the slab to the column, what may lead to progressive collapse in a real structure. The author concluded that increased gravity load reduced the drift capacity and, slabs with higher flexural reinforcement ratio, may suffer from premature punching failure due to increased moment transfer.

Megaly, Ritchie, Gayed et al, 1998-2006

Following the studies performed by Ghali and Dilger [42], similar specimens and the same test setup were used by Megally [46] [26], Ritchie [15] and Gayed [14]. Edge and interior connections were tested using several variables, to be detailed further. The test setup was an upgrade of the one used by Ghali [42]. The specimens were rotated 90º (with the slab plan in the vertical position) and were supported by the edges (at quarter-span lines) with neoprene supports. The gravity load was imposed by a horizontal actuator while two vertical actuators applied the horizontal loading at both ends of the column. An elevation view of the test setup is presented in Figure 2.9.

Two sets of specimens were cast: interior slab-column connections and edge slab-column connections some of which were prestressed. The interior column-slab connection specimens measured 1.90 m by 1.90 m with the edge ones measuring 1.90 m by 1.35 m. All specimens were 150 mm thick. The column consisted in two 700 mm long half columns with a 250 mm width square cross section.

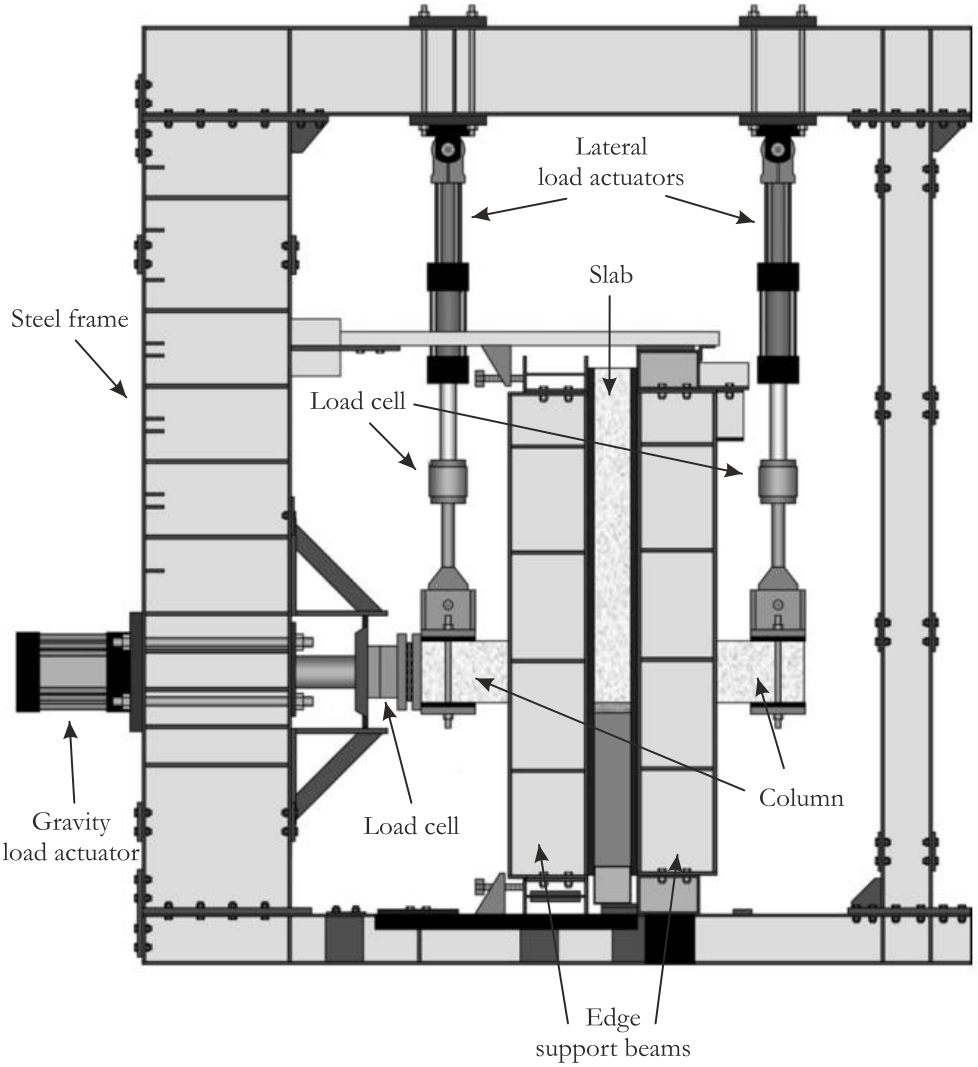

Figure 2.9: Test setup adapted from Ritchie [15].

Details on the flexural reinforcement are presented in Table 2.5. The reported effective depth was 114 mm for the non prestressed bars. The prestress strands were bonded. Each strand had a dead-end anchorage inside the slab and a stressing anchor were the prestress was applied. The flexural resistance was kept similar by reducing the number of ordinary reinforcement bars when the number of prestress strands increased. The shear reinforcement consisted in eight single legged studs by layer, with 9.5 mm diameter each. Details on the number of layers and stud spacing are presented in Table 2.5. A vertical load was applied and kept constant during the test for a combined action of gravity and horizontal loads. The cyclic loading followed a protocol comprised of increasing drift steps of four cycles per step, until a total of eight steps were completed. Then, increasing cycle steps were performed until failure was achieved.

Table 2.5: Characteristics of the specimens and test parameters (adapted from Megally [26], Ritchie [15] and Gayed [14]).

Specimen	ρ (%)		f_c (MPa)	Type	Prestress (kN)		Studs	Vertical load (kN)
	x	y			x	y	layers; spacing	
MG-2A	1.66	1.69	32	Edge	-	-	-	120
MG-3	1.66	1.69	34		-	-	7; 0.75d	120
MG-4	1.66	1.69	32		-	-	7; 0.75d	180
MG-5	1.66	1.69	28		-	-	7; 0.75d	60
Mg-6	1.66	1.69	30		-	-	5; 0.44d	120
EC0C	1.39	1.43	28		-	-	8; 0.48d	110
EC3C	1.02	0.78	26		3x35	1x105	8; 0.48d	110
EC5C	0.92	0.65	26		5x35	2x88	8; 0.48d	110
EC7C	0.74	0.52	29		7x35	2x82	8; 0.48d	110
EC9C	0.37	0.26	28		9x35	2x105	8; 0.48d	110
IPS-9	0.37	0.37	23	Interior	9x35	3x105	8; 0.48d	240
IPS-9R	0.37	0.37	26		9x35	3x105	8; 0.48d	240
IPS-7	0.55	0.46	31		7x35	3x82	8; 0.48d	240
IPS-5	0.65	0.46	29		5x35	3x88	8; 0.48d	240
IPS-5R	0.65	0.46	28		5x35	3x88	8; 0.48d	240
IPS-3	0.83	0.65	27		3x35	3x105	8; 0.48d	240
IPS-0	1.11	0.83	26		-	-	8; 0.48d	240

x represents the horizontal loading direction

d is the effective depth (d=114 mm)

All the edge slab-column connection specimens failed by punching near the column, while the interior ones, failed by punching outside the shear reinforced area. The MG-2A specimen achieved a maximum drift of 1.25%. The use of shear studs increased the drift capacity by 450%. The use of prestress does not affect adversely the drift capacity of the specimens. Prestressed slabs presented less stiffness loss and less energy dissipation capacity.

Warnitchai and Prawatwong, 2004-2012

Warnitchai [12] and Prawatwong [47] Used a test setup similar to the one used by Robertson [45], schematized in Figure 2.10, by using vertical double pinned struts to fasten the borders of the slab. Similar specimens were used to test the effect of post-tension in the behaviour of flat slab structures under seismic actions [12] and the efficiency of a drop panel in the column region [47].

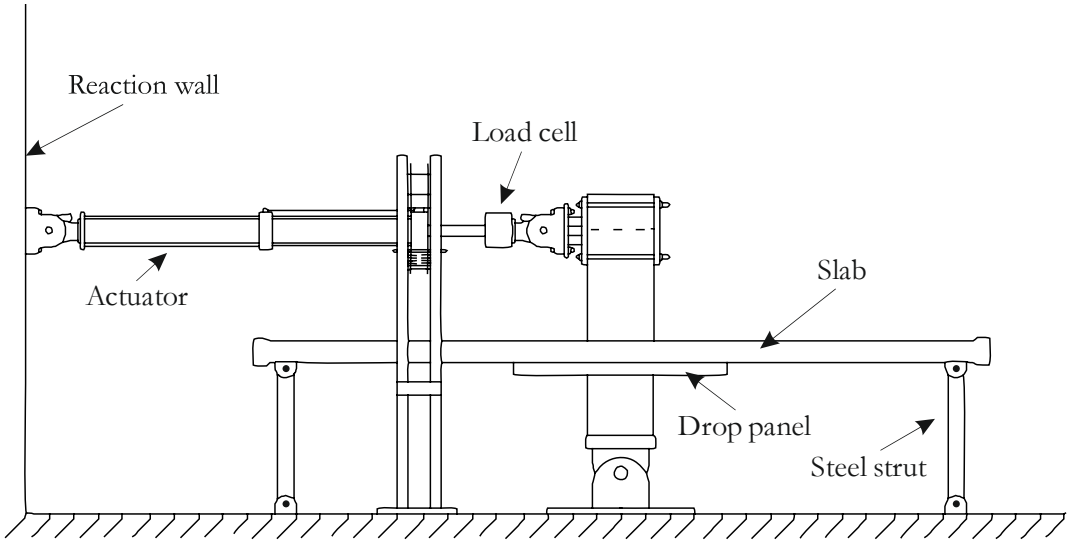

Figure 2.10: Test setup used by Prawatwong (adapted from Prawatwong [47]).

Two specimens (S1 and S2) with a square plan view with 5700 mm width and a thickness of 120 mm were tested. The cross section of the column was rectangular with 500 mm by 250 mm sides, being the higher dimension aligned with the imposed displacement direction. The column had a total length of 1.80 m between the top and bottom hinges that simulate its inflection points.

The top regular flexural reinforcement was placed in the column region only, and consisted in bars of 10 mm diameter and 2.00 m long, of which eight were parallel to the longer column width and ten were arranged in the perpendicular direction, spaced of 80 mm. The bottom reinforcement was a mesh of 10 mm diameter bars with 550 mm spacing. The specimens were post-tensioned with eight 12.7 mm diameter strands in each direction, spaced of 350 mm in the horizontal loading direction and 700 mm in the transverse direction and with a 147.2 kN effective prestress force.

A square drop panel of 1.60 m width and 80 mm thick, reinforced with a mesh of 10 mm diameter bars anchored in the slab and spaced of 200 mm was used. The drop panel influenced the effective depth of the S2 specimen, resulting in an average effective depth of 70 mm for S1 and 150 mm for S2. The concrete cylinder compressive strength at the date of the test was 41.1 MPa and 45.9 MPa for S1 and S2, respectively. The test protocol comprised two cycle drift steps, increasing each step by 0.25 % up to 3.00 % and, after, a 1.00 % increase for each step up to failure. Throughout the test, a non-specified vertical load was imposed by means of weights laid on the surface of the specimen in order to achieve an average shear ratio for a representative building.

The presence of prestress did not avoid a brittle punching failure for the S1 specimen for a 2.0 % drift while, the use of a drop panel, increased the drift capacity up to 6.0 % and the ductility of specimen S2.

Benavent-Climent et al, 2008-2009

Both edge and interior slab-column connections were tested, using a test setup similar to the one used by Robertson [45]. Waffle flat slab structures were the subject of a series of studies by Benavent-Climent [18] [19] in order to assess how structures designed according to old European standards perform in an earthquake situation. A prototype building was designed and specimens of interior and edge columns were scaled down from it. The specimens corresponding to interior column connections measured 1.74 m by 3.85 m, with the smaller side coinciding with the width of the solid square area in the column region. The webs width was 60 mm and 360 mm clear distance between ribs. The depth of the rib and the slab measured 180 mm and 36 mm, respectively.

Specimens representing edge connections share the same dimensions except for the span length in the loading direction that was 2.08 m long. The top flexural reinforcement consisted in one 12 mm bar in each outer web and grouped in pairs in the three middle webs. Along the webs, two legged stirrups with a diameter of 6 mm and spaced of 130 mm were used. The solid zone had additional reinforcement in both directions, passing through the column, by means of two beam like element of four 8 mm diameter bars at the corners of 6 mm diameter two legged closed stirrups, spaced of 45 mm. A mesh of 6 mm diameter bars spaced of 60 mm was placed on top of the flexural reinforcement all across the slab. The reported effective depth was 160 mm. The column was a squared section with 270 mm width (240 mm in the edge connection specimen) and 1450 mm long double hinged concrete element. The concrete cylinder compressive strength for both specimens was 19.4 MPa.

To simulate the vertical load of the prototype building, weights were placed on top of the slab specimen, 40 kN and 20 kN, together with a prestress load applied to the column of a magnitude of 335 kN and 287 kN, for the interior and edge specimen, respectively. The vertical loading was followed by the imposition of increasing cyclic horizontal displacements at the top of the column. The displacements summed up as series of three cycles per step. In the first step, the drift increased in each cycle, however, in the following steps were equal within the same drift step.

On both slabs, all instrumented flexural reinforcement bars yielded before shear failure. The observed lateral load and stiffness degradation was on pair with the results reported in the bibliography for solid flat slabs under similar loading.

Han et al, 2006

The resistance of edge connections with prestress was approached by Han [16], by performing experimental tests, subjecting specimens to vertical and biaxial horizontal loading, by using a test setup based in the one used by Morrison [43] with the specimens cut right next to the column in one of the sides, simulating an edge connection. Two specimens (PE-B50 and PE-D50) measuring 3.60 m (edge were the column was placed) by 2.45 m with a thickness of 130 mm and a column of 300 mm by 300 mm cross section and a 2.10 m distance between hinges, were tested. A third specimen (RE-50) with similar dimensions but 1.85 m long in the direction orthogonal to the edge of the slab was also cast, to be tested without prestress, totalizing three specimens.

The PE-B50 and PE-D50 specimens had a similar flexural reinforcement ratio of 0.61 % with an effective depth of 110 mm. The PE-B50 specimen had the prestress applied parallel to the smallest length side while PE-D50 was prestressed in the other direction. Both prestressed slabs had an average compressive stress of 1.21 MPa. The remaining slab had no prestress, so, a reinforcement ratio of 1.24 % was used in order to compensate for the absence of prestress tendons that provided an extra reinforcement ratio in the other slabs. The average cylinder concrete compressive strength was 32.3 MPa for all the tested specimens. The used test protocol was similar to the one adopted by Pan [10] with applied vertical loads of 84.2 kN, 80.2 kN and 86.8 kN for PE-B50, PE-D50 and RE-50, respectively.

The results showed that the specimens with prestress reached flexural failure prior to punching, reaching higher drifts (from 2.5 % to 4.0 %) and dissipating more energy when compared to the non-prestressed specimen, however, those results may have been influenced by the different span to thickness ratio due to the different dimensions of the specimens.

Anggadjaja, Himawan and Teng, 2008-2014

Anggadjaja and Himawan performed bi-directional cyclic tests on five edge slab-column connections [21], and on three prestressed specimens with interior slab-column connections [23]. A similar arrangement to the one by Pan [10], was used in order to apply horizontal loading along orthogonal axis, however, in this test setup, the vertical load was mainly applied

using a vertical jack placed under the column. The edge connection specimens measured 2.90 m (North-South direction) by 4.00 m and a thickness of 135 mm. The cross section of the column was a 900 mm by 180 mm rectangle, with the longer side parallel to the North-South (N-S) direction, and a length between ends of 2.70 m.

The top flexural reinforcement was more concentrated in the column strip with a ratio of 1.1 % in both directions. The effective depth was 107 mm with the outmost bars in the North-South direction. The prestressed slabs with interior slab-column connections measured 3.50 m (North-South direction) by 2.54 m with a thickness of 115 mm. In those specimens, the cuts were considered to be at the inflection points for the vertical loads. The columns were equal to the ones from the edge connection specimens, but, measuring 0.95 m above and 1.15 m below the slab. All the columns were prestressed (15 % of the axial capacity) to simulate the effect of the weight of the upper floors. The regular flexural reinforcement ratio was the same as in the edge connection specimens as well as the orientation of the outmost reinforcement bars. The flexural reinforcement ratio was 1.01 % in the North-South direction and 0.47 % in the orthogonal direction, with an average effective depth of 118 mm. Values for the concrete compressive strength and the compressive tension in the specimen due to prestress is given in **Table 2.6**. The test protocol used for all the specimens consisted in the application of a vertical load to the specified load target or shear ratio, followed by the imposition of the lateral load in the form of two cycles increasing drift steps (**Table 2.6**).

Table 2.6: Characteristics of the specimens (adapted from Anggadjaja [21] and Himawan [23]).

Slab	f_c (MPa)	Lateral load	Vertical load (kN)	PS* (MPa)		Peak drift N-S (%)	Peak drift E-W (%)
				N-S	E-W		
E1H	33.0	North-South	100	-	-	3.02	-
E2H	32.5	East-West	100	-	-	-	4.29
E12H	34.4	Biaxial	100	-	-	2.51	2.02
E12L	35.4	Biaxial	50	-	-	2.10	1.60
E0U	33.3	-	To failure	-	-	-	-
PI-0	33.0	-	To failure	1.87	0.95	-	-
PI-1	36.1	North-South	164.0	1.70	0.91	2.50	-
PI-2	34.0	Biaxial	170.6	1.62	0.95	1.52	1.49

* Prestress compressive stress

The specimens that were vertically loaded without lateral loading, E0U and PI-0, failed for 245 kN and 511.8 kN, respectively. All specimens failed by punching in the column region. It was observed that more unbalanced moment could be transferred when the horizontal load acted in the stronger direction of the column, however the higher stresses in the

connection promoted a brittle punching failure. The biaxial horizontal load proved to be more damaging to the connection. The use of prestress increased the shear strength of the connection.

Stark et al, 2005

Post installed Carbon Fibre Reinforced Polymer (CFRP) was used to strengthen existing slab-column connections in two different patterns, by Stark [34]. Four specimens were tested, two of them strengthened (A4-S and B4-S) and two to be used as control specimens. Three specimens were designed according to ACI 318-63 (C-63, A4-S and B4S) and one was design using ACI 318-02 specifications (C-02). The test setup used by the research team was inspired by the one by Robertson [45], but instead of using weights to apply the vertical load, a vertical jack placed between the strong floor and the bottom of the column was used. The slabs had a square shape of 2.85 m width and a thickness of 115 mm. A steel column was used to simplify the cast of the specimens as well as the test setup assemblage. The column was made of two steel profiles welded to a 305 mm by 305 mm square plate that simulated the column cross-section in contact with the concrete slab. Both top and bottom plates were fastened against each other by eight bolts that crossed the slab. Grout was used to fill the existing voids between the surfaces. The distance from the top hinge to the bottom hinge of the column was 1635 mm.

A value for the flexural reinforcement ratio was not reported, however, it was computed to be 0.95%, with an effective depth of 82 mm. The average effective cylinder compressive strength of the concrete used in all the specimens was 30.9 MPa. The shear reinforcement was performed by drilling holes in the slab, in the vicinity of the column, followed by sewing the slab with CFRP bands. Two different placements for the CFRP bands were tested: a cross geometry and a radial geometry, both with four perimeters of CFRP bands. A vertical load of 90 kN was applied and kept constant during the horizontal cyclic loading that consisted in increasing steps of three cycles each.

The test results showed that the steel column worked well and no concrete crushing was noticed in the steel-concrete interface. The difference in performance between the specimen designed according to ACI 318-63 and the one designed respecting the ACI 318-02 specifications was noticeable, with the specimens reaching drifts of 2.3 % and 3.2 % at failure, respectively. The use of post installed CFRP as shear reinforcement increased the lateral load capacity, energy dissipation and the drift capacity from 2.3 % up to 7.2 %.

Kang and Wallace, 2008

Thin plate stirrups were tested against shear studs to evaluate if this type of shear reinforcement was suitable to improve flat slab resistance to lateral loads. Kang [30] tested four specimens in a setup configuration similar to the one used by Stark [34]. The specimens were two-third scale representations of interior connections, resulting in 3.00 m by 1.80 m rectangular slabs with a thickness of 150 mm. The column had a square 250 mm width cross-section and was wrapped in glass fibre reinforced polymer (GFRP), along its 1.80 m length, to prevent column degradation. The top flexural reinforcement had a reported ratio of 0.52 %, with an effective depth of 130 mm.

Specimen C0, to be tested without shear reinforcement, presented a concrete compressive cylinder strength of 38.6 MPa while the remaining specimens (PS2.5, PS3.5 and HS2.5) had a 35.1 MPa concrete compressive strength. The thin plate used as stirrups consisted in a 25.4 mm by 1.5 mm cross section steel strip, with holes along the length, to promote anchorage to the concrete. A continuous strip was used to wrap the top and bottom reinforcement, providing the shear reinforcement. The PS2.5, and PS3.5 specimens had the plate reinforcement spanned 255 mm and 135 mm from the face of the column, respectively. The studs used in the HS2.5 specimen had a diameter of 9.5 mm, spaced of 63.5 mm and arranged in eight studs by layer, being the farthest layer at 255 mm from the face of the column. The specimens were loaded vertically with 125 kN followed by the imposition of the horizontal cyclic loads in increasing drifts.

The specimen without shear reinforcement (C0) and the specimen with the smaller amount of thin plates, failed by brittle punching at the slab-column connection and outside the reinforced area, respectively. The two other specimens (PS2.5 and HS2.5) presented a better ductility and strength. The PS2.5 specimen presented less cracking and a punching failure was avoided while in the HS2.5 case, more cracking was visible and a circular crack appeared outside the reinforced area, suggesting a possible punching failure. The use of shear reinforcement up to a distance of 255 mm from the face of the column proved to be effective in increasing the drift capacity from 1.85 % to 5.0 %.

Cheng and Parra-Montesinos, 2010

Two different grades of steel fibres (2300 MPa and 1100 MPa yield stress) were used as a way to enhance the strength and drift capacity of flat slabs under seismic actions. Cheng [31] tested the use of steel fibre reinforced concrete (SFRC) in the vicinity of the column. The

test setup had the specimens supported at the borders with "S" shaped section steel profiles, secured to the strong floor with double pinned struts. The bottom edge of the column was pinned to the strong floor and the top edge connected to the actuator responsible for the imposition of the horizontal load. The vertical load was applied by four strands connected to the slab at mid-distance between the column and the borders, stretched by four hydraulic jacks. The vertical load was nor kept constant during the cycles but was adjusted, from time to time, when no drift was applied. A scheme of the test setup is shown in Figure 2.11.

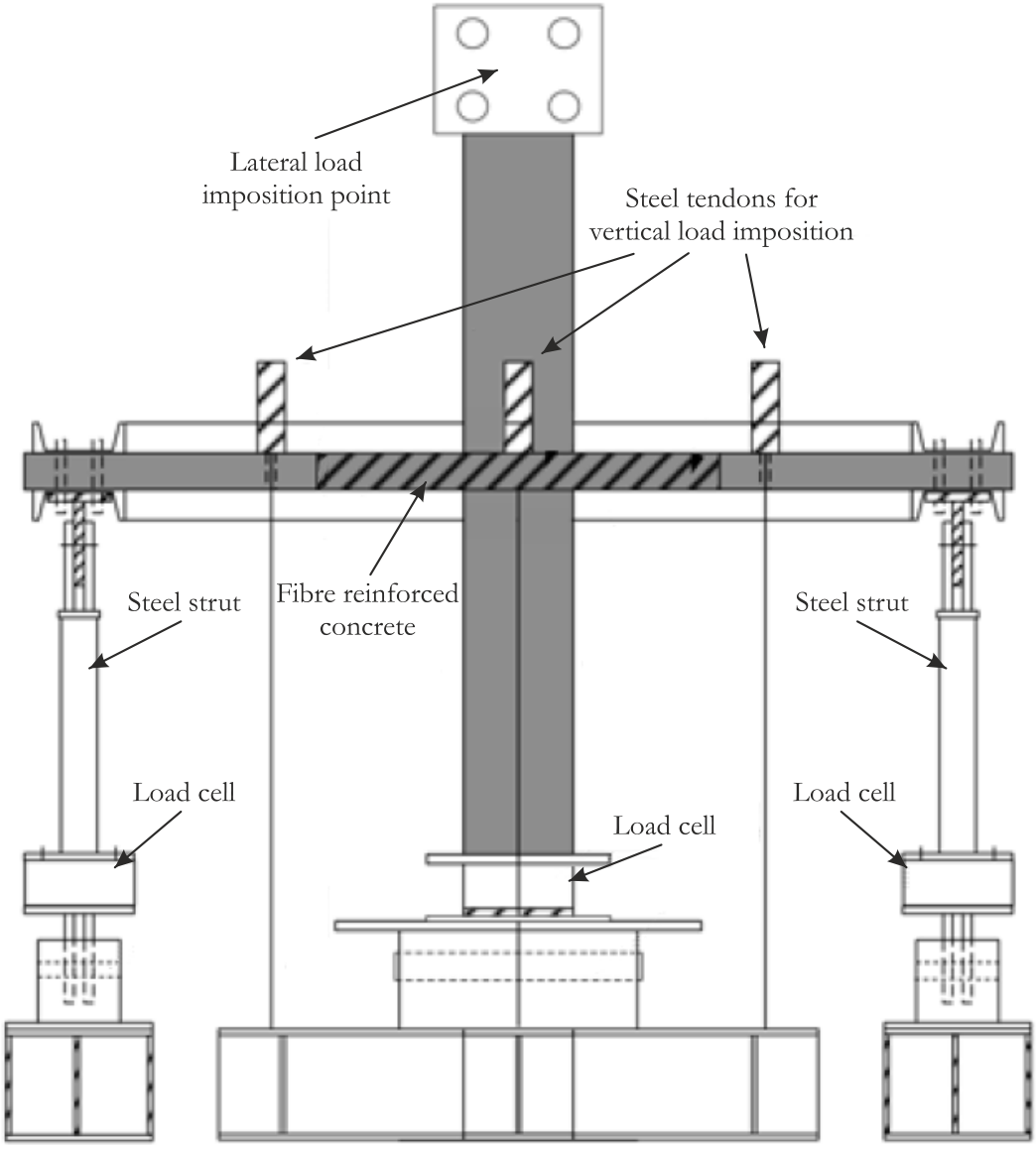

Figure 2.11: Test setup used by Cheng (adapted from Cheng [31]).

Two specimens with plan view dimensions of 2438 mm by 2743 mm and 102 mm of thickness with a square 305 mm width cross section column, measuring in length 2540 mm, were tested. A ratio of 0.57 % reinforcement ratio with an effective depth of 83 mm was used in both specimens.

The average compressive strength of the plain concrete and the fibre reinforced concrete used in the tested specimens were, respectively, 33.4 MPa and 58.5 MPa for the SU1 specimen and, 50.2 MPa and 47.8 MPa for the SU2 specimen. The fibres with the higher yield stress (2300 MPa) were used in the SU1 specimen, being the other one reinforced with the lower grade fibres (1100 MPa), both with a ratio of 1.5% of the concrete volume. The fibre reinforced concrete was placed in the vicinity of the column in a square area with 1117 mm width.

The test proceedings started with the application of the vertical load. A value for this load was not reported, however, the target shear ratio was 50 % of the predicted centred shear capacity of each slab. This procedure was followed by increasing steps of two cycles each until completion (4.0 % drift for SU1 and 5.0 % for SU2). The gravity load was then increased to a target load of 63 % and again, the specimens were subjected to the cyclic loading protocol.

The data obtained from the load cell under the column showed that the shear ratio dropped significantly when the drift increased due to stiffness loss and force absorption by the double pinned struts that supported the edges of the specimens. None of the specimens failed during the test, having reached drifts of 5.0 % under a 63 % shear ratio, however, measured strains showed yielding of the flexural reinforcement for drifts over 2.0 %.

Song et al, 2012

A test setup inspired in the one used by Stark [34] was used to compare three types of shear reinforcement in interior slab-column connections, by Song [32]. Square 3.00 m width specimens with 135 mm of thickness were reinforced with steel stirrups, shear studs and thin steel bands. The reinforced slabs were then compared to a reference specimen without shear reinforcement, making a total of four specimens. The column was asymmetric, being the top extent longer (825 mm) than the bottom one (655 mm), totalising 1615 mm between the top and the bottom hinges. The cross section of the column was a 300 mm width square. The same flexural reinforcement ratio of 1.06 % was used for all the specimens, as well as the same effective depth, gauging 113.5 mm and a concrete cylinder compressive strength of 38.7 MPa.

Specimen RC1 had no shear reinforcement. Four legged closed steel stirrups, with a 6 mm diameter were used to reinforce the SR1 specimen in cross displacement spanning 323 mm from the face of the column and 45 mm between layers. In the SR2 specimen, the same cross

arrangement was used in the positioning of the shear studs that consisted in 10 mm diameter bolts welded to a top and a bottom steel bar spaced 52 mm from each other. Two rails were positioned spanning 342 mm from each face of the column. The thin steel bands used to reinforce the RC3 specimen had a cross section of 30 mm by 3 mm and were similar to the ones tested by Kang [30].

The target shear ratio was 43 %, however, the actual value for the applied vertical load was not reported. The cyclic horizontal loading protocol, followed the pattern of fourteen increasing drift steps of three cycles per step, followed by increasing cycles until failure was achieved.

All the specimens with shear reinforcement presented a flexural failure, while the non-reinforced specimen failed by punching. The RC1 specimen failed for a drift of 1.8 %. Since no punching failure was achieved, no failure was considered, therefore, no ultimate drift was reported. Comparing the drift for the higher lateral load, the RC1 specimen reached 50 kN for 1.4 % drift and all the reinforced specimens reached the peak lateral load for 2.7 % drift, with 61 kN, 50 kN and 61 kN for SR1, SR2 and SR3, respectively. The SR2 and SR3 specimens were able to keep a lateral load over 40 kN for drifts up to 4.5 % and 8.0 %, respectively.

Polak, El Salakawy, Bu et al, 2004-2008

The use of post installed bolts as shear reinforcement is a proven technique as tested by Inácio [48] in centred monotonic punching tests. The strengthening of existing flat slab structures was the study subject of Polak [37], El-Salakawy [36], who strengthened an interior slab-connection with CFRP bands in the tensile surface and steel bolts, and Bu [49] by testing post installed steel bolts. The authors used a test setup that consisted in a variation of the one used by Ritchie [15], with the slab specimen upside down, as shown in Figure 2.12. The vertical load was applied by an actuator suspended in the top steel frame and the horizontal displacements were imposed by two horizontal actuators connected to the tips of the column. The specimen was secured against a square steel frame by two steel beams. Neoprene pads were placed between the specimen and the steel frames.

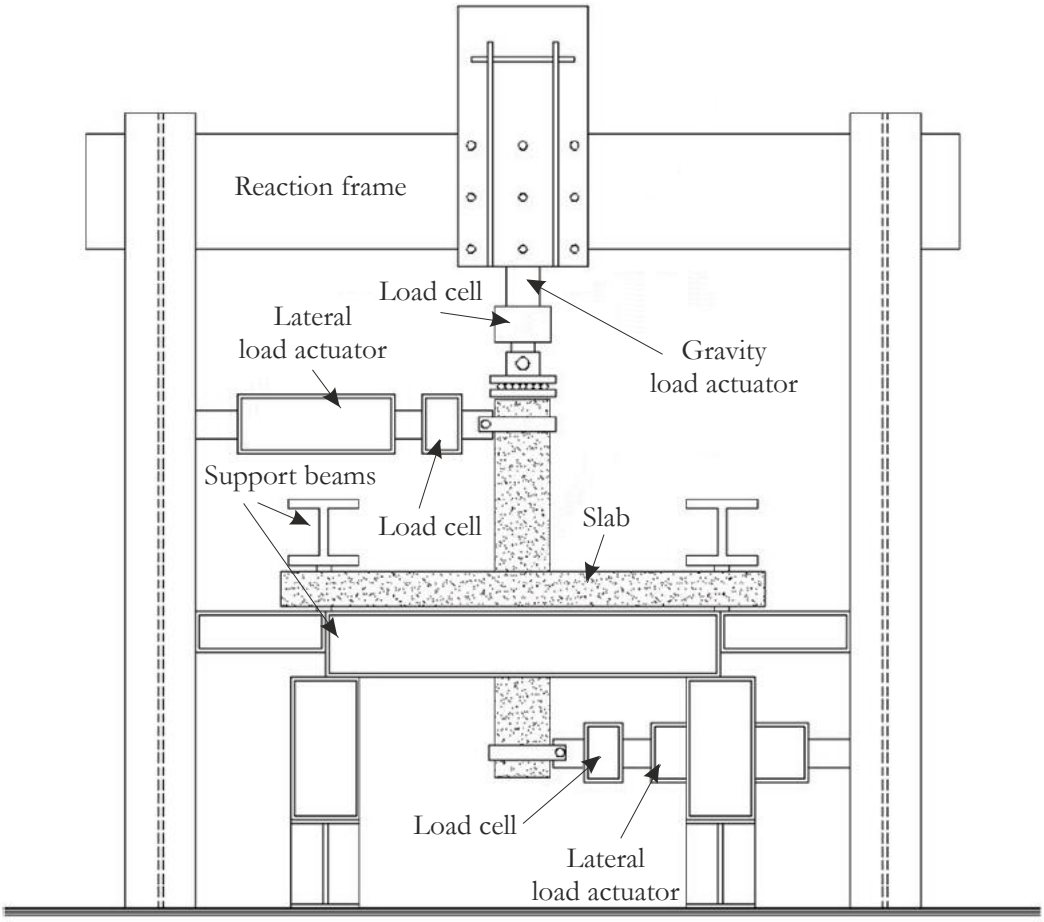

Figure 2.12: Test setup used by El-Salakawy (adapted from El-Salakawy [36]).

El-Salakawy [36] tested seven 1.54 m by 1.02 m edge connections with a thickness of 120 mm. Three specimens had a square 150 mm width hole in front of the column. The flexural reinforcement was not symmetric (0.75 % and 0.45 %), being the higher ratio in the horizontal loading direction at an effective depth of 90 mm. A square 250 mm width column with a total length of 1.52 m was placed in the centre of the longest edge of the slab, whose ends represented the inflection points of the column. The interior connections [49] had different dimensions, being those, 1.80 m squares with a thickness of 120 mm. The column was also different, having a square cross section of 200 mm width and the same 1.52 m length.

The flexural reinforcement, that had the same effective depth, was higher in the horizontal load direction, with a value of 1.3 % and 1.1 % in the transverse direction. Different reinforcement techniques were performed and combined, such as, stripes of CFRP or GFRP bonded to the surface of the slab and post installed steel bolts with several layouts. More information about the characteristics of the specimens, the type of carried on strengthening and failure modes is presented in **Table 2.7**.

Table 2.7: Characteristics of the specimens (adapted from Polak [37], El-Salakawy [36] and Bu [49]).

Slab	f_c (MPa)	Connection	Holes	Shear reinforcement	Vertical load (kN)	Failure mode
XXX	33	Edge	-	-	129	Punching
SF0	32		1	-	116	Punching
SX-GF	32		-	GFRP	136	Punching
SX-CF	32		-	CFRP	132	Punching
SX-GF-SB	40		-	GFRP+Bolts	159	Flexure
SH-GF	32		1	GFRP	141	Punching
SH-GF-SB	40		1	GFRP+Bolts	151	Flexure
SB1	44	Interior	-	-	*	Punching
SB2	41		-	Bolts	*	Pun/Flex
SB3	41		-	Bolts	*	Flexure
SB4	41		-	Bolts	*	Flexure
SB5	44		4	Bolts	*	Flexure
SB6	44		2	Bolts	*	Flexure
SW1	35		-	-	110	Punching
SW2	35		-	Bolts	110	Flexure
SW3	35		-	Bolts	110	Flexure
SW4	46		-	Bolts	160	Flexure
SW5	46			-	160	Punching
SW6	52		2	-	160	Punching
SW7	46		2	Bolts	160	Flexure
SW8	52		2	Bolts	160	Flexure
SW9	52		-	Bolts	160	Flexure

*not reported

From the obtained results, no cracking was reported until the horizontal drifts reached values in the order of 0.5 %. The specimens strengthened with CFRP or GFRP had the cracking delayed, resulting in higher stiffness, however, when used alone, those techniques did not affect the punching failure. The use of bolts led to lateral load increases ranging from 17 % up to 44 % according to the number of bolts used. The drift capacity was also increased up to 7.5 %. Strains from the instrumented shear bolts show that the ones farthest from the column had smaller contributions.

2.2 Experimental tests in multi-frame specimens

Performing experimental tests in multi-frame specimens allows researchers to overcome the difficulties replicating the accurate behaviour of the slab-column connections. The continuity of the multi-frame specimens overcomes the non-ideal boundary conditions of the simplified test setups. Because multi-frame tests have high demands regarding specimen costs and laboratory logistics, few tests were performed and found in the bibliography.

Durrani and Robertson, 1990-1995

Durrani [5] and Robertson [2], [3], [50] performed a series of tests in slab specimens with three columns. The specimen consisted in a two 2892 mm spans, in a total 6045 mm length slab with a width of 1980 mm and a thickness of 114 mm. Each specimen had two edge columns and one interior column. All the three columns were similar, having a square cross section of 254 mm width and a total length of 1537 mm. The columns had a hinged connection at both ends. The bottom hinges were fixed to the strong floor while the top ones were fixed to a steel beam which was connected to the horizontal actuator responsible for the horizontal loading.

The vertical load was applied by weights hanging on the specimens. An elevation view of the test assembly is shown in Figure 2.13. The reported effective depth was 96.8 mm for all specimens, however, the flexural reinforcement was different for both batches of specimens and is shown in Table 2.8, as well as the cylinder concrete compressive strength. The reported gravity load presented in Table 2.8 was distributed in the total area of the specimen, being the load in each column, measured by a load cell in the centre column and computed by equilibrium in the edge columns.

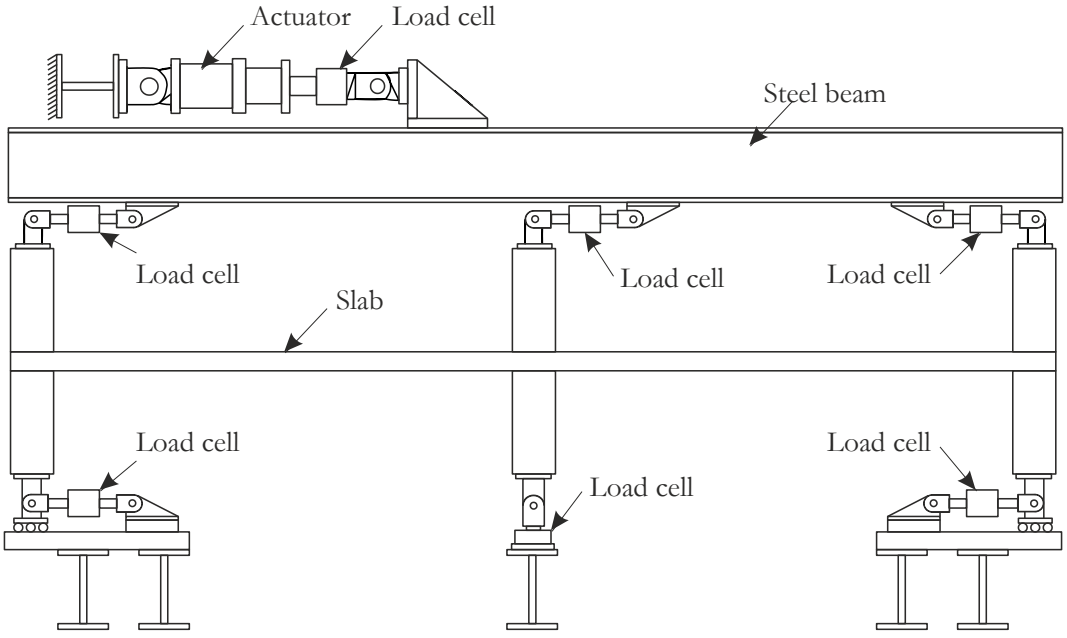

Figure 2.13: Test setup adapted from Robertson [50].

The tested variables in the first batch of specimens were the existence of beams or overhangs in the edge connections, the use of closed stirrups as shear reinforcement and the effect of the vertical load. In the second batch, bent up bars (inferior reinforcement that was bent up

at 45º to work as shear reinforcement) were used. A summary of the reinforcements used in each specimen is shown in **Table 2.8**.

Table 2.8: Characteristics of the specimens (adapted from. Durrani [5] and Robertson [2], [3], [50]).

Slab	f_c (MPa)	ρ (%)	Shear reinforcement	Vertical load (kN)
2C	33.0	0.83	-	53
3SE	44.0		Edge beam at the exterior connections	53
4S	43.9		Closed stirrups	53
5SO6	38.0		Overhang	53
6LL	32.2		-	121
7L	30.8		-	91
DNY-1	35.3	0.59	Bent up bars	160
DNY-2	25.7		Bent up bars	200
DNY-3	24.6		-	160
DNY-4	19.1		Edge beam at the exterior connections	160

After the application of the vertical load, increasing horizontal reversed drift steps were performed until the specimens reached failure. The tests showed that the drift capacity decreases with increasing shear ratio and that the regulations were non-conservative for shear ratios over 0.3. It was observed that the shear ratio influences the relative rotation between the column and the slab, at the connection, which increases the damage. All specimens without shear reinforcement failed by brittle punching. Shear reinforcement was effective to prevent punching failure and increased the drift capacity.

Dechka, 2001

Two three column specimens, similar to the ones tested by Durrani [5] and Robertson [2], [3], [50] were tested by Dechka [6]. The specimens were 10.00 m (each span measured 5.00 m) by 5.00 m with a thickness of 150 mm. The columns had a square cross section of 250 mm width and a total length of 3.00 m. Two vertical jacks with spreader beams were responsible for the vertical load, while two horizontal actuators applied symmetric horizontal displacements at the top and bottom edges of the columns, using two rigid beams connecting them as shown in Figure 2.14. Both specimens had shear studs in all the connections.

The S1 specimen was used to test three different solutions, with the spacing and the diameter of the studs as variables. The S2 specimens was strengthened with more studs per layer, reaching further from the face of the column. The specimens were tested under cyclic horizontal loading, after being loaded vertically, in increasing drift steps. The researchers concluded that when well detailed and shear reinforced, flat slabs may be used as primary structure in small buildings in seismic regions, however, regulations must be developed.

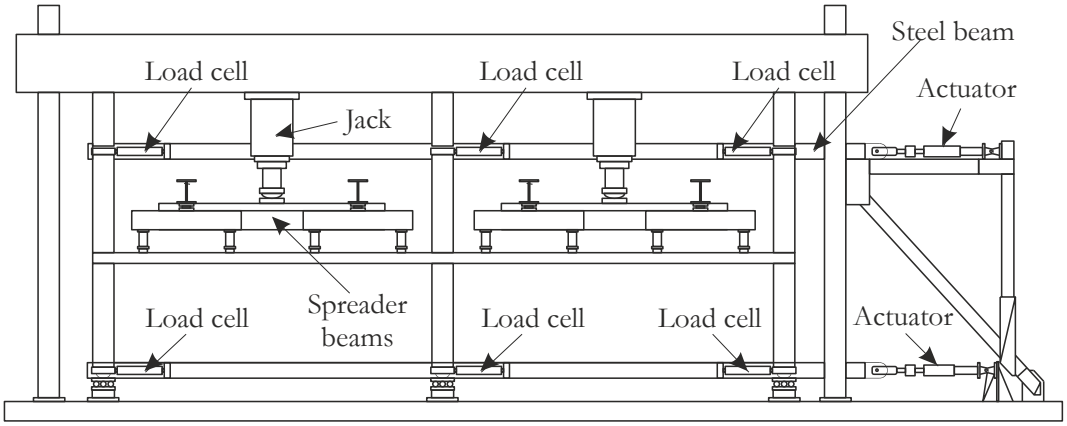

Figure 2.14: Test setup used by Dechka (adapted from Dechka [6]).

Hwang tested one single specimen that consisted in a 40 % reduced scale floor of a building with nine slab panels (three spans in each direction with four corner columns, eight edge columns and four interior columns). The bottom ends of the columns were pinned to the strong floor. The horizontal displacement was applied to the slab, this way, to reduce the axial compression in the specimen, the bottom columns were longer. The vertical load was applied using blocks on the top of the specimens. The longer spans measured 2743 mm and the shorter ones, measured 1829 mm, meaning that, the whole specimen had a total size of 8230 mm by 5486 mm with a slab thickness of 85 mm. The inferior portion of the columns were 1219 mm long and the superior portion was 305 mm. Several variables were tested, such as the column dimensions and rectangularity, flexural reinforcement and shear ratio. The lateral loading was applied in the two orthogonal directions (N-S and E-W). The protocol consisted in increasing sequences of vertical load, drift in the N-S direction and drift in the E-W direction.

The authors concluded that the geometry of the cross section of the column is determinant in the stiffness. Stiffness loss was observed for drifts from 0.5 % to 1.0 %. The specimen reached the 4.0 % drift step, which is the result of the low shear ratio (28 %) and small slab thickness. From this test, the author concluded that the connections with inferior continuous reinforcement bars passing through the column were able to withstand vertical load after punching failure.

Rha et al, 2014

Five 50 % scale four panel specimens were tested by Rha [8] in a test setup similar to the one used by Durrani [5] and Robertson [2], [3], [50]. The plan dimensions of the specimens were 5.50 m by 3.30 m with a thickness of 90 mm. The columns were 1.40 m long with a square cross section of 242 mm width. Three kinds of test were performed: centred punching tests, monotonic eccentric tests and cyclic reversed eccentric tests.

The vertical load was applied by hanging concrete blocks in the specimen. In the centred punching tests, the overload was applied by hydraulic jacks. Different flexural reinforcement ratios were used. The slabs subjected to centred punching, had different flexural ratios in both directions (0.78 % and 1.17 %) while the slabs subjected to lateral loading tests had the same ratio (1.17 %) in both directions at an effective depth of 70 mm. The lateral load was applied after the specimen was subjected to the vertical load (reported shear ratios from 29% to 44%). The cyclic horizontal displacement protocol consisted in increasing steps of two cycles until failure.

Punching failure of individual connections induced transient drops in the horizontal load that was recovered by force and moment distribution. The connections with more bottom reinforcement in the column region showed more ductility under horizontal loading.

2.3 Codes and standards

2.3.1 ACI 318 and ACI 421.2R

The ACI 318 [51] building code is used in more than thirty countries and is one of the most mentioned codes in the scientific publications. The approach of the ACI 318 code to punching shear consists in calculating the resistance of the slab to shear by integrating the shear stresses along the control perimeter. For slabs without shear reinforcement, the shear resistance is the smallest of the three values given by equation (2.1) that becomes determinative for rectangular columns with long cross-sections, equation (2.2) which becomes relevant for columns with large cross section areas when compared to the effective depth, and equation (2.3).

$$V_{c,\,ACI} = \frac{1}{6}\left(1 + \frac{2}{\beta_c}\right)\lambda\sqrt{f_{ck}}\,b_{0,\,ACI}\,d \tag{2.1}$$

$$V_{c,\,ACI} = \frac{1}{12}\left(2 + \frac{\alpha_s d}{b_{0,\,ACI}}\right)\lambda\sqrt{f_{ck}}\,b_{0,\,ACI}\,d \tag{2.2}$$

$$V_{c,\,ACI} = \frac{1}{3}\lambda\sqrt{f_{ck}}\,b_{0,\,ACI}\,d \tag{2.3}$$

where:

- $V_{c,\,ACI}$ is the ACI 318 value for the concrete contribution for the punching resistance
- β_c is the ratio of the longest over the shortest column width
- λ is a parameter that takes into account the type of concrete (1 for regular concretes)
- f_{ck} is the characteristic compressive strength of the concrete
- $b_{0,\,ACI}$ is the control perimeter of the punching failure zone calculated according to Figure 2.15
- d is the effective depth of the slab
- α_s takes into account the position of the column within the slab (40 for interior columns, 30 for edge columns and 20 for corner columns

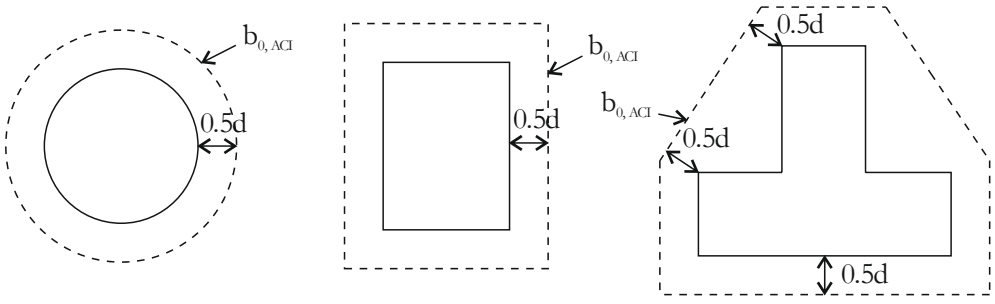

Figure 2.15: Punching control perimeter according to ACI 318 [51].

When shear reinforcement is required, the contribution of the shear reinforcement must be added to half of the contribution of the concrete, calculated previously. When stirrups, or similar shear reinforcement types, are used the contribution of the shear reinforcement can be calculated using equation (2.4).

$$V_{s,\,ACI} = \frac{A_{sw} f_{yt} (\sin\alpha + \cos\alpha) d}{s_r} \tag{2.4}$$

where:

$V_{s,\,ACI}$ is the provision for the shear reinforcement contribution in the punching resistance

A_{sw} is the sum of the effective area of the cross section of the shear reinforcement in a single perimeter around the column

f_{yt} is the characteristic value of the yield stress of the shear reinforcement

α is the angle between the shear reinforcement and the plane of the slab (top towards the column)

s_r is the distance between shear reinforcement perimeters

To calculate the punching resistance with stirrups as shear reinforcement, the parcel of the contribution of the concrete is reduced, as shown in equation (2.5)

$$V_{sr,\,ACI} = \frac{1}{2} V_{c,\,ACI} + V_{s,\,ACI} \tag{2.5}$$

This means that to achieve an increase in the punching resistance by using stirrup as shear reinforcement, a minimum cross section given by equation (2.6) must be used.

$$A_{sw} > V_{c,\,ACI} \frac{s}{2 f_{yt} (\sin\alpha + \cos\alpha) d} \tag{2.6}$$

Shear reinforcement is only allowed in slabs with an effective depth greater than sixteen times the diameter of the bar used for the shear reinforcement and greater than 150 mm. When shear studs are used, the reduction factor for the concrete parcel takes the value of 0.75. A verification regarding concrete crushing near the column must be made using equation (2.7) with the reduction factor ζ with a value of 0.5 for shear reinforced slabs.

$$V_{Crush,\,ACI} = \zeta \sqrt{f_{ck}}\, b_{0,\,ACI}\, d \tag{2.7}$$

Regarding shear reinforcement arrangement, shear reinforcement must be placed in a cross layout with both distances from the face of the column to the first layer and between layers, smaller than half of the effective depth. A punching failure outside the reinforced area needs to be taken into account, using equation (2.8) which is similar to the one used for the concrete parcel affected by the reduction factor Ø=0.75 (Chapter 21 from [51]) and computing the control perimeter ($b_{out,ACI}$) as suggested in Figure 2.16

$$V_{out,ACI} = \frac{1}{6} Ø \sqrt{f_{ck}}\, b_{out,ACI}\, d \tag{2.8}$$

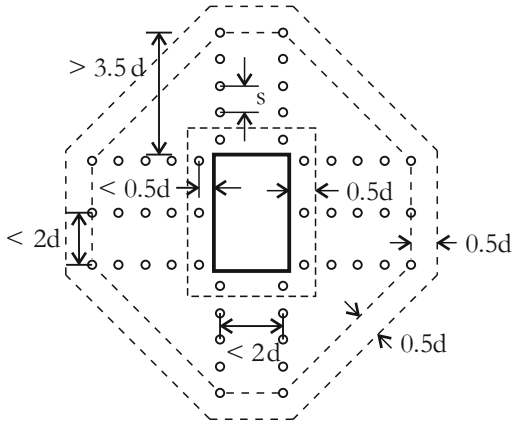

Figure 2.16: Punching control perimeter for shear reinforced slabs, according to ACI 421 [52].

When horizontal loads are applied to the structure, a parcel of the induced moment is, according to the code, transferred by bending from the column to the slab. This parcel is given by equation (2.9)

$$M_{f,\,ACI} = \gamma_f M_{sc} \tag{2.9}$$

with

$$\gamma_f = \frac{1}{1 + \frac{2}{3}\sqrt{\frac{b_1}{b_2}}} \tag{2.10}$$

where

- M_{sc} is the total moment to be transferred
- γ_f is the fraction of the total moment to be transferred by flexure
- b_1 is the dimension of the perimeter b_0 in the direction of the application of the horizontal loading
- b_2 is the dimension of the perimeter b_0 in the direction perpendicular to the application of the horizontal loading

The moment to be transferred by shear is then given by equation

$$M_{s,\,ACI} = 1 - M_{f,\,ACI} \tag{2.11}$$

Assuming a linear stress distribution along the critical perimeter b_0, the maximum shear stress ($\upsilon_{u,\,ACI}$) is given by the greatest absolute value resulting from equation (2.12)

$$\upsilon_{u,\,ACI} = \frac{V_{c,\,ACI}}{b_{0,ACI}d} \mp \frac{M_{s,\,ACI}c_L}{J_c} \tag{2.12}$$

where, for interior rectangular columns

c_L the distance from the centre of the column to the line of the control perimeter in the direction of the horizontal loading

J_c is the given by equation (2.13) with c_1 being the column dimension in the direction of the horizontal loading and c_2 the column dimension in the perpendicular direction

$$J_c = \frac{d(c_1+d)^3}{6} + \frac{(c_1+d)d^3}{6} + \frac{d(c_2+d)(c_1+d)^3}{2} \quad (2.13)$$

The final provision (V_{ACI}) is given by equation (2.14), with Ø=0.75

$$ØV_{ACI} = \upsilon_u b_{0,ACI} d \quad (2.14)$$

In seismic regions, recommendations from ACI 421 [52] must be taken into account. Flat slab structures without a complementary lateral force resisting system, that controls and limits the lateral displacements of the building, are not permitted to be used in seismic regions. When used in conjunction with the mentioned lateral force resisting system, the flat slabs must withstand the horizontal displacements without failure. There is no consensus for the allowed horizontal displacement ratio value, however, values from 0.7 % to 2.5 % are suggested. The design drift of the structure (the horizontal displacement between floors divided by the height of the column)is estimated using the procedures from ASCE/SEI 7 [53]. The approach taken by the ACI 421 consists in limiting the gravity shear ratio in function of the designed drift of the building.

Figure 2.17 defines three zones corresponding to different pairs of gravity shear ratios and horizontal drifts allowed by the resisting structure. The shear ratio is calculated by the ratio $V_u/ØV_{c,ACI}$ where V_u is the ultimate shear force transferred between the slab and the column.

If the design combination falls into Zones 1 and 3, a minimum shear reinforcement as given by equation (2.15) must be provided.

$$A_{sw} > \frac{\sqrt{f'_c} b_{0,ACI} s_r}{4 f_{yt}} \quad (2.15)$$

In cases where the combination stays in Zone 2, shear reinforcement, spanning to a minimum distance of four times the effective depth from the face of the column, must be provided, according to equation (2.4). The cross section area of the shear reinforcement must be higher than the value given by equation (2.16).

$$A_{sw} > \frac{7\sqrt{f'_c}\, b_{0,\,ACI}\, s_r}{24 f_{yt}} \tag{2.16}$$

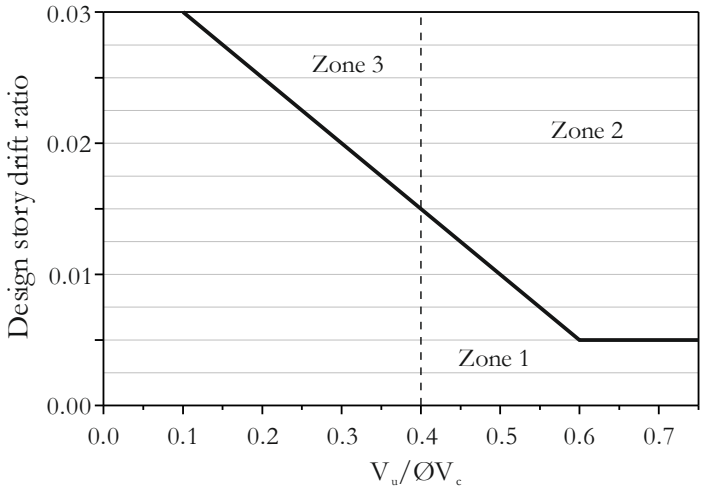

Figure 2.17: Requirement for shear reinforcement criterion [51][52].

2.3.2 Eurocode 2 - EN 1992-1-1

Eurocode 2 (EC2) [54] relies on an empirical formula designed to match the results from centred experimental punching tests. The punching capacity for slabs without shear reinforcement is given by equation

$$V_{c,\,EC2} = C_{Rd,\,c}\, b_{0,\,EC2}\, d\, k\left(100\rho_l f_{ck}\right)^{\frac{1}{3}} \geq 0.035 b_{0,\,EC2}\, d\, k^{\frac{3}{2}} f_{ck}^{\frac{1}{2}} \tag{2.17}$$

were

- $C_{Rd,c}$ is given by equation (2.18)
- $b_{0,\,EC2}$ is the control perimeter of the punching failure zone calculated according to Figure 2.18
- d is the average effective depth of the slab
- k is a factor that takes size effect into account given by equation (2.19), where d is in mm
- f_{ck} is the characteristic compressive strength of the concrete in MPa
- ρ_l is the weighted flexural reinforcement ratio of the slab given by equation (2.20)

γ_c is the partial safety factor for the concrete according to the standard (γ_c=1.5)

ρ_y is the flexural reinforcement ratio of the slab in the longitudinal direction

ρ_z is the flexural reinforcement ratio of the slab in the transversal direction

$$C_{Rd,\,c} = \frac{0.18}{\gamma_c} \tag{2.18}$$

$$k = 1 + \sqrt{\frac{200}{d}} \leq 2.0 \tag{2.19}$$

$$\rho_l = \sqrt{\rho_y \rho_z} \leq 0.02 \tag{2.20}$$

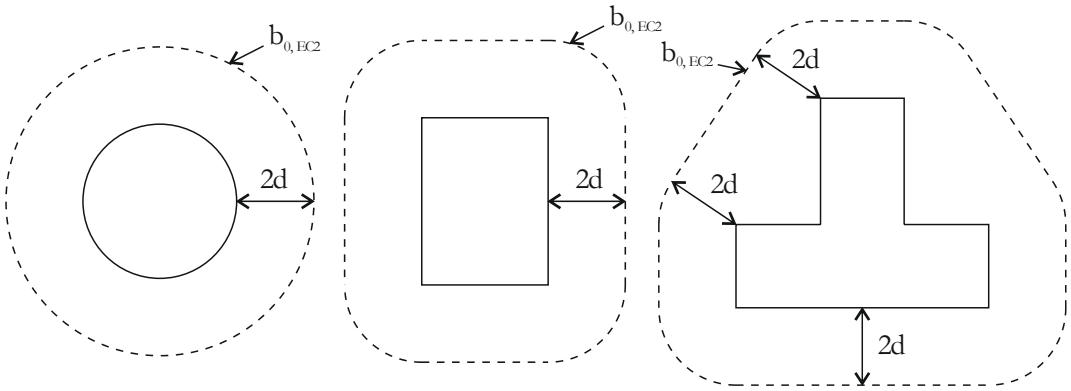

Figure 2.18: Punching control perimeter according to EC2 [54].

In the cases were shear reinforcement is required, the concrete contribution to the resistance is reduced and the contribution given by the shear reinforcement is added,

$$V_{sr,\,EC2} = 0.75V_{c,\,EC2} + 1.5A_{sw}f_{ywd,ef}\frac{d}{s_r}\sin\alpha \tag{2.21}$$

were

$V_{sr,\,EC2}$ is the EC2 punching resistance for slabs with shear reinforcement

A_{sw} is the sum of the effective area of the cross section of the shear reinforcement in a single perimeter around the column

$f_{ywd,ef}$ is the effective stress in the shear reinforcement given by equation (2.22), with d in mm, and is limited by the characteristic value of the yield stress of the shear reinforcement (f_{yt})

α is the angle between the shear reinforcement and the plane of the slab (top towards the column)

s_r is the distance between shear reinforcement perimeters

$$f_{ywd,ef} = 250 + 0.25d \leq f_{yt} \quad (2.22)$$

Concrete crushing near the column must be verified using the general method used for shear, presented in equation (2.23)

$$V_{Crush,\ EC2} = 0.4\upsilon_{cr} f_{cd} b_{col} d \quad (2.23)$$

where

υ_{cr} is the reduction factor of the compression resistance for cracked concrete under shear

f_{cd} is the design concrete compressive strength

b_{col} is the control perimeter, equal to the column perimeter for interior columns

Punching failure outside the reinforced area is given by equation (2.24), which is analogous to equation (2.17), considering a control perimeter outside the reinforced area (b_{out}) calculated following the guidelines from Figure 2.19.

$$V_{out,\ EC2} = C_{Rd,\ c} b_{out,\ EC2} d\ k\left(100\varrho_l f_{ck}\right)^{\frac{1}{3}} \quad (2.24)$$

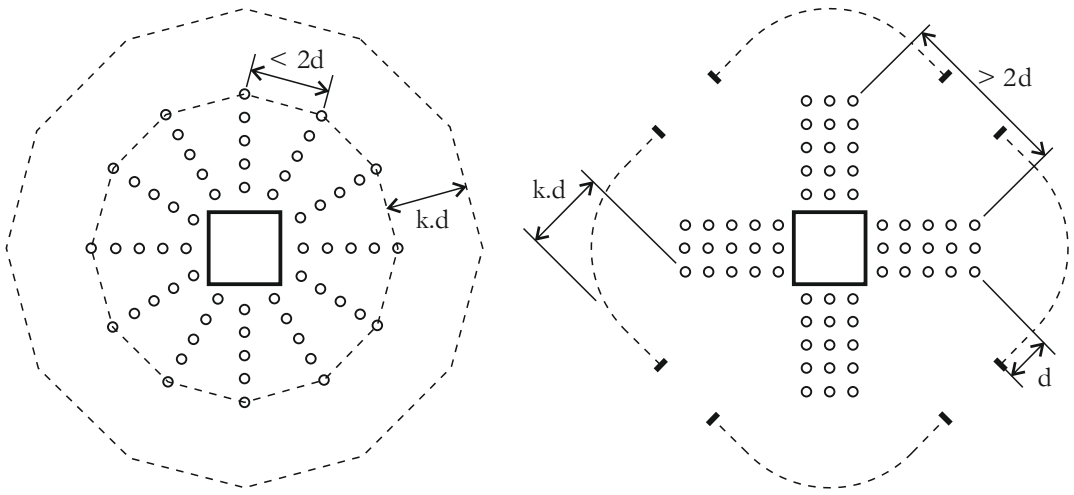

Figure 2.19: Punching control perimeter and shear reinforcement detail guidelines according to EC2 [54].

Eccentric bending moments in the column region are taken into account by the computation of a factor (β), given by equation (2.25) in the case of eccentricity along a single axis and by equation (2.26) in case of eccentricity in both axis. This factor increases, by multiplication, the design shear load.

$$\beta = 1+k_c \frac{M_{Ed}}{V_{Ed}} \frac{b_{0,\,EC2}}{W_1} \tag{2.25}$$

$$\beta = 1+1.8 \sqrt{\left(\frac{M_{Ed,y}}{V_{Ed} b_y}\right)^2 + \left(\frac{M_{Ed,z}}{V_{Ed} b_z}\right)^2} \tag{2.26}$$

where

k_c is a factor that takes into account the ratio of the dimensions of the column and is given by Table 2.9.

M_{Ed} is the design unbalanced moment in the column region (along the respective axis)

V_{Ed} is the design shear force

$b_{0,\,EC2}$ is the control perimeter

$$W_1 = \int_0^{b_{0,\,EC2}} e_L \; dl \tag{2.27}$$

e_L is the distance parallel to the eccentricity from each point of the control perimeter to the bending moment action axis

b_y is the maximum dimension of the control perimeter in the direction of the application of the horizontal loading

b_z is the maximum dimension of the control perimeter in the direction perpendicular to the application of the horizontal loading

Table 2.9: Values for the k_c parameter.

c_1/c_2	≤ 0.5	1.0	2.0	≥ 3.0
k_c	0.45	0.60	0.70	0.80

The safety is then verified by equation (2.28), being V_{Rd} the design resistance of the slab, according to EC2.

$$\beta V_{Ed} \leq V_{Rd} \tag{2.28}$$

Neither EC2 [54] nor EC8 [55] provide specific details for the design of flat slabs under seismic actions, however, it is referred that flat slabs must not be used as primary lateral resistant structures.

2.3.3 Model Code 2010

The approach taken by the Model Code 2010 (MC2010) [56] regarding punching in flat slabs is based in the Critical Shear Crack Theory (CSCT) developed by Muttoni [57][58]. The CSCT is a mechanical model, contrary to the usual empirical formulations, designed to overcome the limitations of the empirical approach and give control over the parameters involved in the resistance of flat slabs to punching. This theory is based in the premise that punching resistance is a function of parameters such as: the critical crack width; the stress state of the flexural reinforcement; the concrete strength; the slab and column dimensions. The critical crack width, the effect of the aggregate interlock and the stress state of the flexural reinforcement can be estimated as functions of the rotation of the slab at the vicinity of the column. Results from experimental tests were used to plot the normalized dispersion of the punching resistance as a function of slab rotation and to compute the trend line (Figure 2.20) presented in equation (2.29).

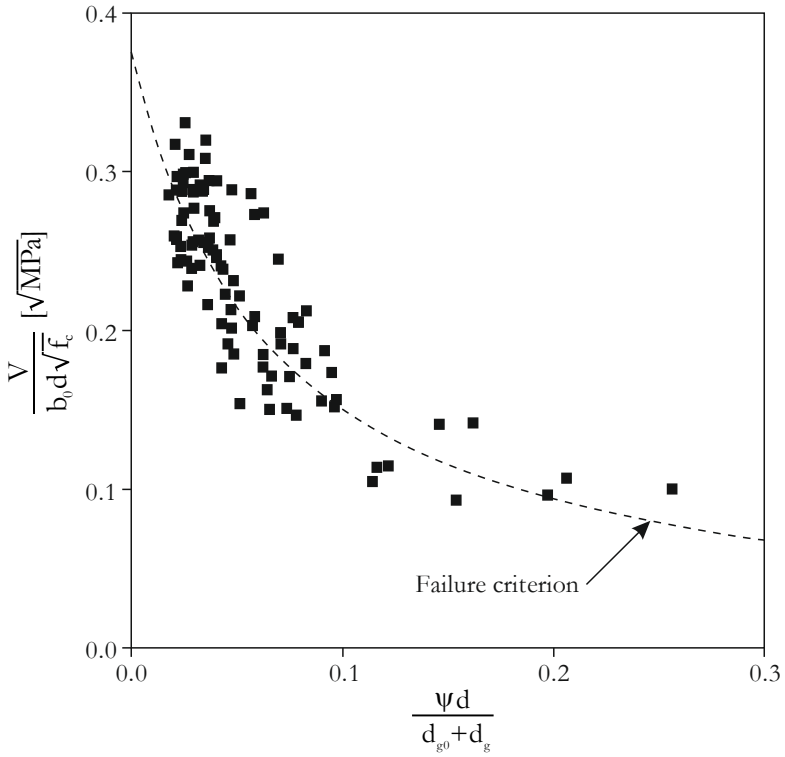

Figure 2.20: Punching resistance as a function of slab rotation [57].

$$\frac{V_R}{b_0 d\sqrt{f_c}} = \frac{\frac{3}{4}}{1+15\frac{\psi d}{d_{g0}+d_g}} \tag{2.29}$$

where

V_R	is the punching resistance of the slab without shear reinforcement
b_0	is the control perimeter as defined by Muttoni [57] defined in Figure 2.21
f_c	is the average concrete compressive strength in cylinders
d_{g0}	is a reference aggregate size equal to 16 mm
d_g	is the maximum dimension of the aggregates
ψ	is the rotation of the slab

The value of d_v (Figure 2.21) is the average distance from the centre of the flexural reinforcement to the base of the punching cone, or to the base of the shear reinforcement in the case of quantification of the punching resistance outside the shear reinforcement zone, as defined in section 7.3.5 in MC2010 [56].

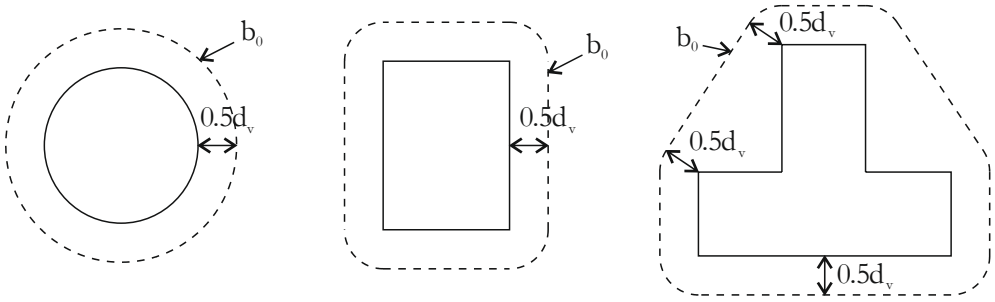

Figure 2.21: Control perimeter as suggested by Muttoni, [57] adopted by MC2010 [56].

The relation between the shear force (V) and the rotation of the slab (ψ) is defined by a quadrilinear expression, however, by neglecting the effect of the reinforcement tension stiffening and the concrete tensile strength, a simpler bilinear relation is achieved. By combining equation (2.29) with the one of the mentioned shear-rotation equations, and solving the resulting equation iteratively, a punching shear prediction may be computed.

For design purposes assuming a parabolic deformation of the slab, the rotation of the slab is given by equation (2.30)

$$\psi = 1.5 \frac{r_s f_y}{d\, E_s} \left(\frac{V}{V_{flex}} \right)^{\frac{3}{2}} \tag{2.30}$$

where

r_s is the distance from the centre of the column to the counter-flexure point

f_y is the average yield strength of the flexural reinforcement

E_s is the modulus of elasticity of the flexural reinforcement

V is the shear force

V_{flex} is the shear force associated to the flexural failure of the slab

Based in the CSCT, the MC2010 takes the design shear concrete resistance as

$$V_{c,\,MC2010} = k_\psi \frac{\sqrt{f_{ck}}}{\gamma_c} b_{0,\,MC2010}\, d_v \tag{2.31}$$

with

$$k_{\psi} = \frac{1}{1.5+0.9k_{dg}\,\psi\,d} \leq 0.6 \tag{2.32}$$

and

$$k_{dg} = \frac{32}{16+d_g} \geq 0.75 \tag{2.33}$$

where

d_v is the average distance from the centre of the flexural reinforcement to the base of the punching cone

$b_{0,\,MC2010}$ is the control perimeter according to MC2010 [56] (Figure 2.21)

The rotation of the slab (ψ) can be computed in four levels of approximation with increasing precision and complexity:

The Level I of Approximation is used for regular slabs analysed using an elastic model and without considering bending moment redistribution, the rotation is given conservatively by equation (2.34)

$$\psi = 1.5\frac{r_s f_{yd}}{d\,E_s} \tag{2.34}$$

The Level II of Approximation takes into account moment redistribution. Values for the average distributed bending moment and design flexural strength per unit of length must be computed in a slab strip of a width given by equation (2.35), for both reinforcement directions. The rotation is then calculated using equation (2.36)

$$b_s = 1.5\sqrt{r_{s,\,x}\,r_{s,\,y}} \tag{2.35}$$

$$\psi = 1.5\frac{r_s f_{yd}}{d\,E_s}\left(\frac{m_{sd}}{m_{Rd}}\right)^{1.5} \tag{2.36}$$

where

$r_{s,x}$ is the distance from the centre of the column to the counter-flexure point in the x direction

$r_{s,y}$ is the distance from the centre of the column to the counter-flexure point in the y direction

m_{sd} is the average bending moment, per unit of length

m_{Rd} is the average design flexural strength per unit of length

In the Level III of approximation, the values of r_s and m_{sd} must be calculated using a linear elastic model. The width of the strip in which m_{sd} and m_{Rd} are considered, is calculated using equation (2.35). The rotation is then calculated using equation (2.37).

$$\psi = 1.2 \frac{r_s f_{yd}}{d\, E_s} \left(\frac{m_{sd}}{m_{Rd}} \right)^{1.5} \tag{2.37}$$

The Level IV of approximation is the most precise and demands a non-linear analysis to compute the rotation of the slab (ψ), taking into account all the effects that are relevant to a precise result, such as cracking, tension-stiffening, concrete tensile strength, etc.

In the cases where shear reinforcement is required, its contribution to the overall punching capacity is given by equation (2.38).

$$V_{sr,\,MC2010} = \sum A_{sw}\, \sigma_{swd} \sin\alpha \geq 0.5 V_{Ed} \tag{2.38}$$

with

$$\sigma_{swd} = \frac{E_s \psi}{6} \left(1 + \frac{f_{bd}}{f_{ywd}} \frac{d}{\varnothing_w} \right) \leq f_{ywd} \tag{2.39}$$

where

$V_{s,\,MC2010}$ is the MC2010 provision of the shear reinforcement contribution in the punching resistance

A_{sw} is the sum of the cross section areas from all the steel reinforcement that efficiently contribute to punching resistance (well anchored and crossing a 45º crack)

σ_{swd} is the stress in the shear reinforcement

f_{bd} is the design bond strength calculated as suggested in section 6.1.3.2 from MC2010. A design value of 3 MPa may be used for corrugated reinforcement bars

$Ø_w$ is the diameter of the shear reinforcement

In the presence of shear reinforcement, the usual additional verifications must be made. Punching failure outside the reinforced area must be verified using equation (2.31) with the control perimeter ($b_{0,\,MC2010}$) calculated according to Figure 2.22.

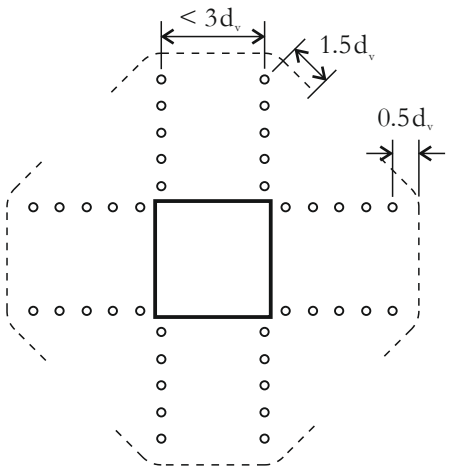

Figure 2.22: Control perimeter outside the shear reinforced area as from MC2010 [56].

The crushing resistance of the compressed concrete strut is computed using equation (2.40).

$$V_{crush,\,MC2010} = k_{sys} V_{c,\,MC2010} \leq \frac{\sqrt{f_{ck}}}{\gamma_c} b_{0,\,MC2010}\, d_v \qquad (2.40)$$

where k_{sys} takes the following values as referred in MC2010 [56]:

2.0 when no detailed data is known and the shear reinforcement is detailed according to MC2010

2.4 for stirrups with sufficient development length at the compression face of the slab and bent (no anchorages or development length) at the tension face

2.8 for studs with a diameter of heads larger or equal than 3 times the stud bar diameter

The MC2010 approaches the presence of unbalanced moments in the slab-column connection the same way it approaches other non-uniform stress distributions. The control perimeter is, in those cases considered to be equal to a reduced perimeter ($b_{1,\,red}$) to be

calculated according to the specifications from the code. In the presence of unbalanced bending moments, an eccentricity coefficient (k_e) must be calculated using

$$b_0 = k_e \, b_{1,\,red} \tag{2.41}$$

$$k_e = \frac{1}{1+\frac{e_u}{b_u}} \tag{2.42}$$

where

e_u is the eccentricity of the shear force relative to the centroid of the control perimeter

b_u is the diameter of circle with an area equal to the area inside the control perimeter

2.4 Final remarks

Some work has been done in the subject of flat slabs under seismic actions. In the last decades, experimental work has increased, giving researchers more data to develop better analytical models and regulation codes. However increasing in number, the amount of experimental tests in slab-column connections under vertical and cyclic horizontal loading is small when compared to the hundreds of existing results on flat slabs under centred punching, which allowed to compute the ruling regulation codes. Also, the inconsistency of results presented by the scatter showed in Ramos [59] makes it difficult to compute mathematical approximations. The dispersion in the results is less pronounced in tests using multi frame specimens, which are rare due to costs and logistics. As referred before, researchers have been making efforts to develop simplified test setups to ease and make it less expensive the experimental tests on flat slabs under combined vertical and horizontal loading. Improvements in the simplified test setups have been made since Hanson [1] to Robertson [13], however some limitations are still present. The free rotation of the borders perpendicular to the loading direction, implies that the inflection point is stationary at mid-span which is not ideal as referred by Robertson [50]:

> "The assumption that the point of contraflexure in the slab is stationary at midspan is invalid for almost all practical situations. An appreciation of the point of countraflexure is essential for the correct interpretation of results obtained from individual connection tests which make this assumption".

The elements that support the specimen, even in the cases that are adjusted at specific times during the test are keen to absorb vertical forces as referred by Cheng [31].

Several methods were used to apply vertical loading to the specimens, such as loading the surface with weights (which may make it difficult to reach significant shear ratios) and jacks or tendons (which make it difficult to maintain the loading constant due to slab degradation and the movement inherent to the test nature).

The scale factor is also an important factor in the wide scatter of the experimental results, as specimens that were small in thickness, may result in slabs with higher flexibility, leading to an unreal drift capacity.

The motivation to this work was to develop a test setup for simplified slab-column connection specimens that solves the main problems inherent to the simplified test setups and test several slab specimens with the developed test setup to be compared between then and also with the ones reported in the bibliography.

Chapter 3

Description of the Experimental Campaign

3.1 Development of the test setup

3.1.1 Analysis and conceiving of the test setup elements

The complexity inherent to replicate the deformed shape in simplified test setups is due to the fact that, in the case of flat slabs subjected to vertical and lateral loading, the boundary conditions are dependable of the response of the remainder structure. The boundary conditions in specimens of partial structures are crucial to obtain results, both in experimental tests and numeric models. Consequently, researchers take huge efforts developing test apparatus in order to replicate the behaviour of the real structure. The case study of this dissertation is flat slabs subjected to both vertical and lateral loads, thus, a typical multi story building, as shown in Figure 2.1, was considered.

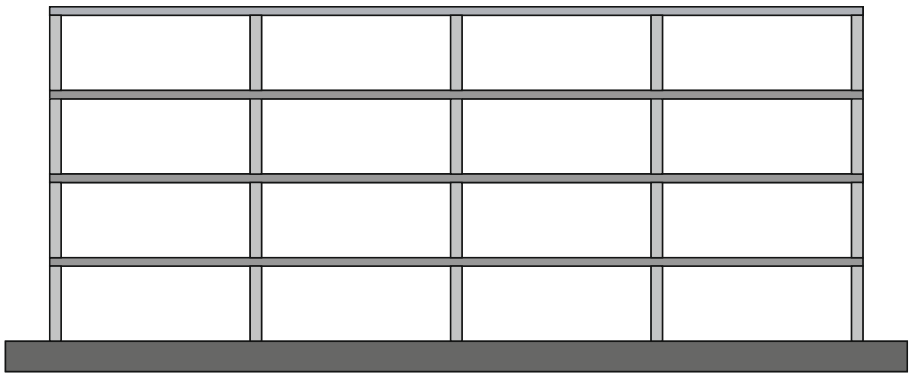

Figure 3.1: Scheme of elevation of a typical flat slab structure.

Henceforward, an interior slab-column connection from a middle floor will be considered, as the following observations do not apply to edge and corner columns, as well as the bottom and top floors. When vertical loads alone are acting in the structure, the interior slab panels present a symmetric behaviour with reference to the column, with theoretical elastic inflection points at 22 % of the span length between columns, as seen in Figure 3.2.

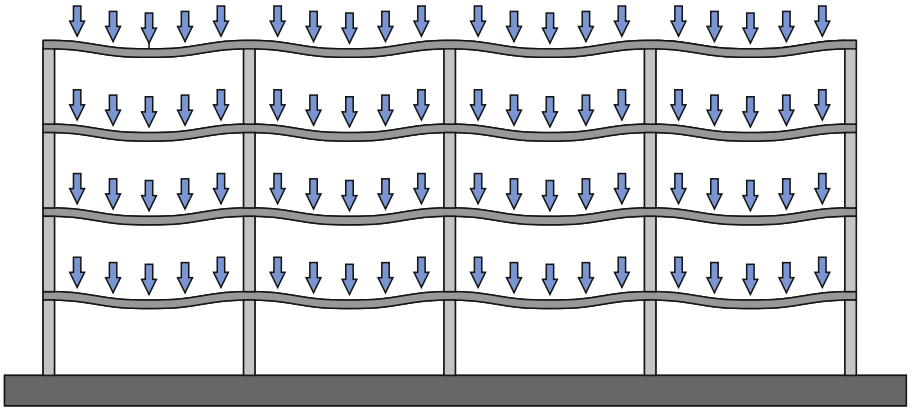

Figure 3.2: Scheme of a typical flat slab structure under vertical loading.

In a real reinforced concrete (RC) structure, the position of the inflection points depends on the cracking state of the structure and the ratio between stiffness for positive and negative bending moments and is considered to be somewhere between 0.20 and 0.25 of the span. Under vertical load, the mid-span between columns deflects vertically and, the deflection increases with the magnitude of the load, the degradation and the stiffness loss of the slab, mostly keeping the symmetry. In this particular case, the mid-span movement is strictly vertical and the positioning of the inflection points varies very little, making those points strategic places to truncate the structure, to design the simplified test specimens.

When a horizontal load is added to the structure, the deformed shape, as presented in Figure 3.3, is no longer symmetrical. The magnification in Figure 3.3 shows that the vertical displacements in the mid-span points are equal, however, the rotations of the mid-spans are anti-symmetrical. Those vertical displacements and rotations are at every instant, dependent of the stiffness of the rest of the structure that is connected to the considered truncated specimen. Because an interior slab-column connection is being considered, the truncated portion can be replicated in both orthogonal directions to complete the structure. At every time, the rotation in the left edge of the truncated specimen is equal in magnitude and direction to the rotation in the right edge (θ_b in Figure 3.3) and the bending moments are symmetrical. The vertical displacements (δ_b in Figure 3.3) are equal in magnitude and direction. Those displacements and forces are a result of the equilibrium between the stiffness of the slab to positive and negative bending moments.

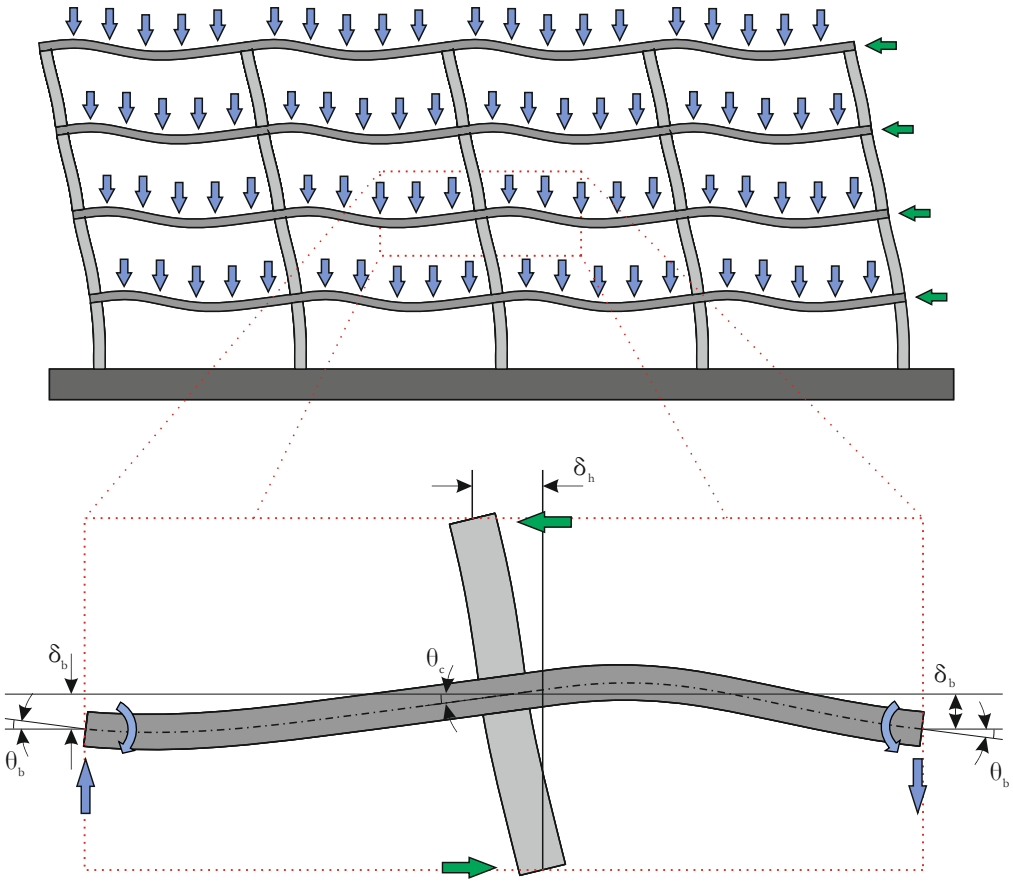

Figure 3.3: Scheme and detail of a typical flat slab building under vertical and horizontal loading.

The adopted principle in the development of the test setup consisted in transferring the rotations and vertical displacements and, consequently, transverse forces and bending moments between both borders in real time. By doing this, the test setup simulates the structure continuity by mimicking the influence of the remaining structure in the free edges of the specimen. This real time transfer must be as passive as possible in order to simulate the real internal stresses of the real structure while avoiding the introduction of additional external forces.

The compatibilization of rotations at the free edges of the test specimen was already performed with positive results by Soares [44] therefore, a similar approach was taken. Double pinned rigid steel struts connected to rigid steel profiles monotonically connected and hanging from the borders of the test specimen, as depicted in Figure 3.4.

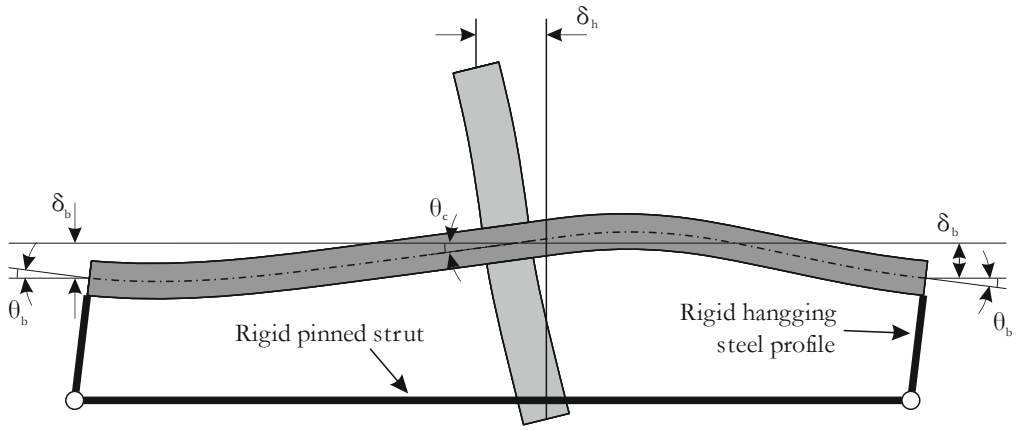

Figure 3.4: Scheme and detail of the rotation compatibilization system.

The adopted system keeps, in the left and right edges, the rotation that results of the equilibrium state of the stiffness of both sides of the slab. Each side of the specimen acts on the other one as it was in the remaining structure that was truncated out.

Regarding the vertical displacements, a system consisting in two seesaw elements was designed to keep the vertical displacements equal and yet, at the same time, dependable on each other, as schematized in Figure 3.5.

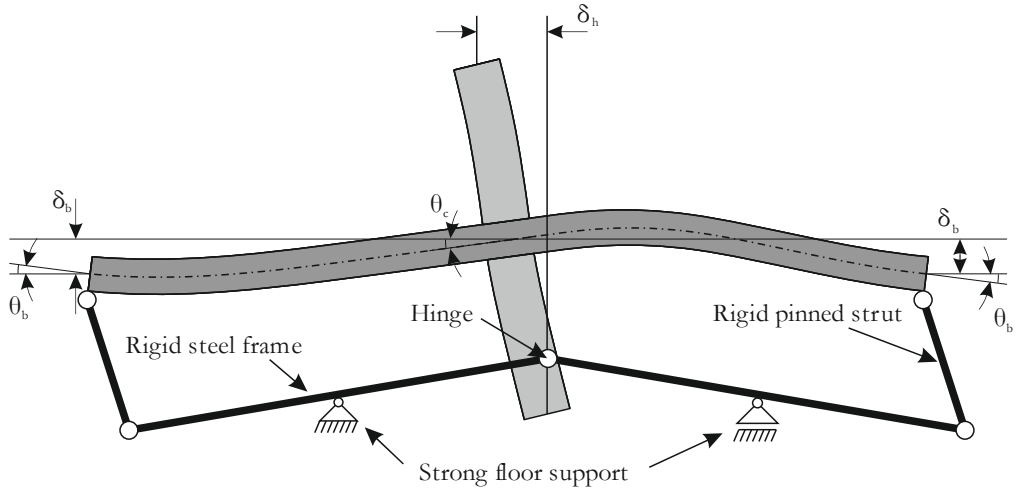

Figure 3.5: Scheme and detail of the vertical displacement compatibilization system.

When a horizontal load with a direction from right to left is applied to the test specimen, without vertical restrictions at the borders, the left side will move down and the right side will move up. Using the proposed system as vertical restriction will ensure that both right and left borders will move the same and those deflections will result, once more from the equilibrium state of both sides of the specimen.

The vertical load applied to the test specimen must be constant throughout the test, which is easily accomplished by placing weights on the top of the tested slab, as used in some tests described previously. However, for higher loads it is not practical to use this method due to the size of the required weights. The usage of tendons anchored to the strong floor was also observed in previous testes but, as reported by the authors, it is hard to keep a constant loading in the slab due to the lateral movement of the specimen. The vertical displacement compatibilization system made it impossible to apply the punching load directly in the base of the column, because it would allow equal vertical displacements. The adopted solution consists in using four spreader beams to distribute the total load by eight equidistant points to resemble an area uniformly distributed load. Four similar hydraulic jacks were used, one per spreader beam, all sharing the same hydraulic hose and connected to a load maintainer machine. The force applied by the hydraulic jacks in each pair of top spreader beams was applied via steel tendons through a larger steel profile, supported by a corbel, at the side of the bottom column. The reaction force was then applied directly to the bottom column, instead of to the strong floor. This way, the whole system moved along with the test specimen using the load maintainer device to keep the vertical load constant. A representation of the vertical load system can be seen in Figure 3.6.

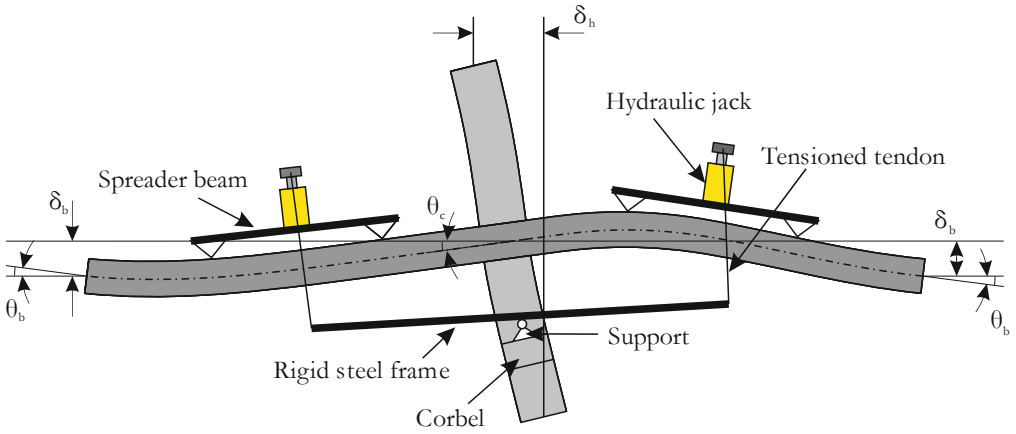

Figure 3.6: Scheme and detail of the vertical load system.

3.1.2 Design of the test specimens

A prototype office building with multiple floors and regular equidistant spans was pre-designed. From the resulting prototype building, an interior slab-column connection, from one of the middle floors, was considered. In this study, the horizontal drifts were intended to be applied in one direction only, therefore, for the previously stated premises to

be applicable, the test specimen must be truncated at mid-span, in the axis of the horizontal drift direction. Due to laboratory area restrictions, the specimens had to be reduced to a 2/3 scale and had the edges parallel to direction of the horizontal action, truncated at an approximately 22 % of the span length. The shortening of the span in the transversal direction will introduce an asymmetry in the vertical loading, but it should not influence significantly the stiffness of the specimen to lateral drifts since, as reported in previous studies, the moment transfer takes place in the close proximity of the column. The transversal width of the specimen matches approximately the position of the zero bending moment line, avoiding the need of using moment restricting boundary conditions. The resulting test specimens ended up measuring 4150 mm x 1850 mm x 150 mm.

The specified actions for office buildings from Eurocode 1 were taken into account and the flab slab was designed following the Eurocode 2 specifications. Because the specimens were to be subjected to horizontal loads, eventually, positive moments could occur in the vicinity of the column, therefore, no curtailment of the bottom reinforcement was made, however, curtailment of the top reinforcement was made at the mid-span area (edge of the test specimen). The design clear cover was 20 mm and the average effective depth of the reinforcement was 118 mm for all specimens with the higher effective depth in the direction of the horizontal loading. The resulting top reinforcement closer to the column had a ratio of 0.96 %. The top and bottom reinforcement are detailed in Figure 3.7. Two steel half-columns, prestressed to the slab , were used, as it was proven to be effective by Stark [34]. Using steel columns had several advantages, namely, it is easier to cast and assembly the specimens. To allow the connection of the steel column to the concrete slab specimen, four holes were left in the centre, during the cast process, as well as twenty holes in each North (N) and South (S) edges to connect the rotation and displacement compatibilization systems of the test setup and four holes for the steel tendons responsible for the vertical load to pass through (Figure 3.8).

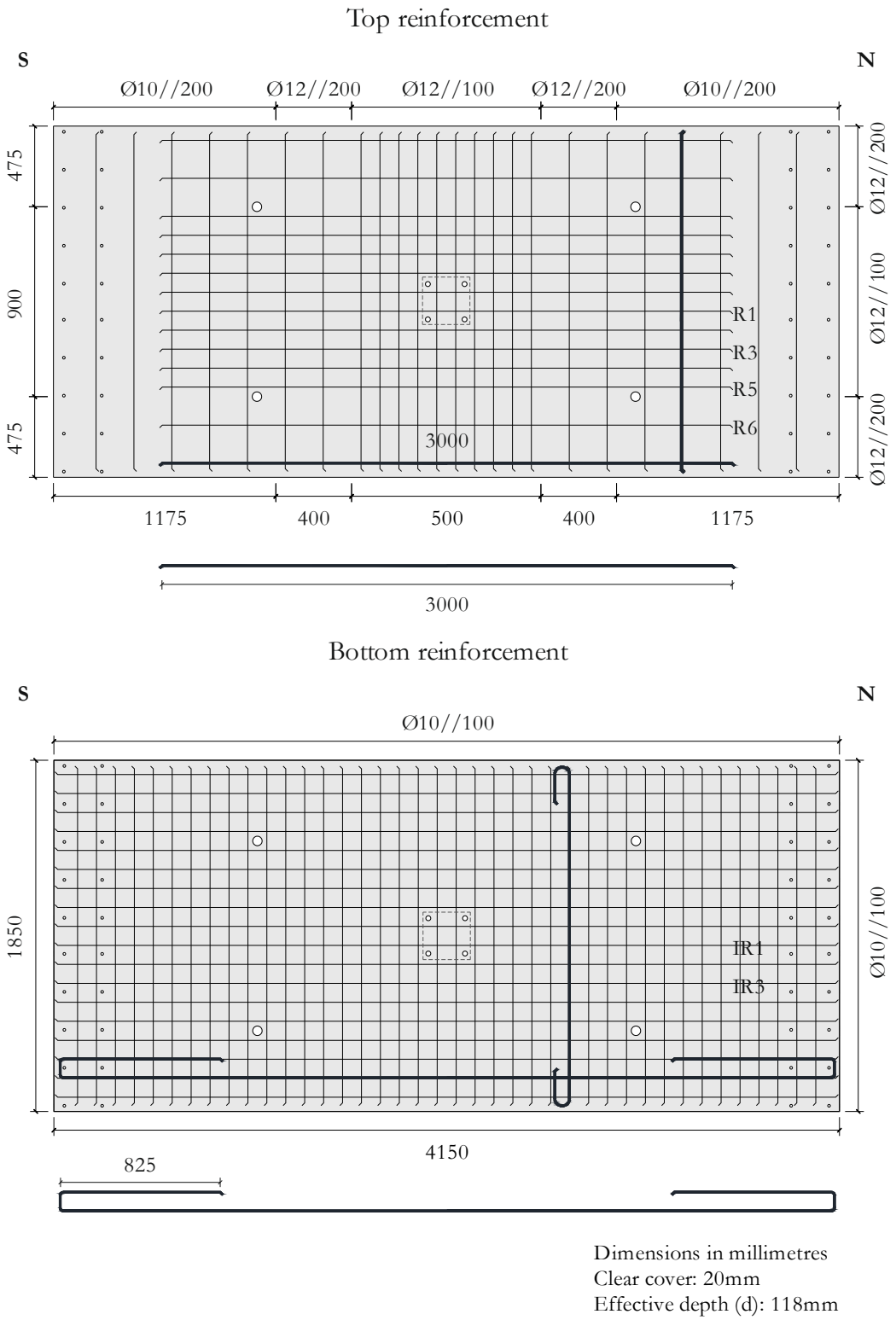

Figure 3.7: Flexural reinforcement detail.

Figure 3.8: Fabrication of the test specimens.

3.1.3 Design of the test setup

A pre-design of the test setup was performed using a finite element software. The boundary restriction elements needed to be as stiff as possible for the test setup to work as intended. A linear elastic finite element model was used, since the steel frames were intended to be

kept under linear elastic regime. Regarding the concrete elements, considering linear elastic behaviour resulted in a conservative underestimation of the stiffness of the steel elements.

The rotation compatibilization system schematized in Figure 3.4 comprised two similar steel structures in each side of the column, which had three main elements: the pinned strut that will be under compression, the hanging elements that will be under bending and the torsion resistant block that connects the hanging elements to the slab. The vertical elements, due to size restrictions, were made of HEM120 steel profiles. The pinned struts consisted in SHS100 profiles with a wall thickness of 6.3 mm to which a nut and a threaded end was added to allow for length adjustment. The steel element that connected the hanging HEM120 profiles to the concrete slab consisted in a RHS150×100×10 profile welded to a 10 mm thick steel plate with an area of 1850×200 mm². A similar steel plate with the same dimensions was used at the top of the slab to spread the prestress force used to fix the steel elements to the concrete slab. The prestress was applied by forty M12 steel bolts of class 10.9. The connection between the RHS profile and the inferior rectangular plate was also reinforced with 10 mm gussets spaced of 200 mm and placed right next to the prestress holes. A load cell and a hydraulic jack were added to each strut to allow for monitoring and controlling the force in both struts. The definitive rotation compatibilization system is shown in Figure 3.9 and a detailed view of the struts, load cells and hydraulic jacks is presented in Figure 3.10.

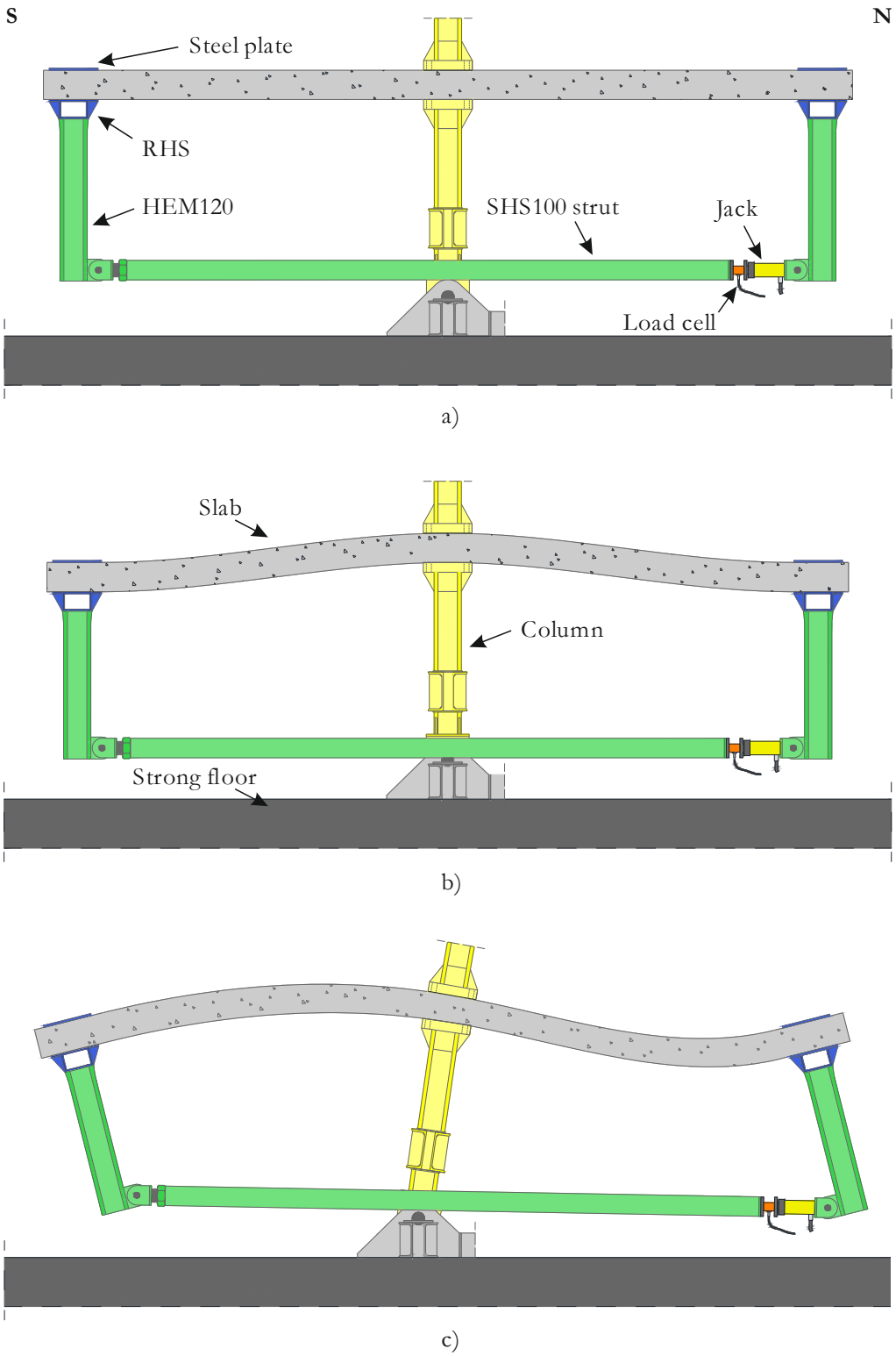

Figure 3.9: Scheme and detail of the rotation compatibilization system. a) Unloaded specimen; b) Vertically loaded specimen; c) Vertical and horizontally loaded specimen.

Figure 3.10: Detail of the struts with the load cells and hydraulic jacks.

The vertical displacement compatibilization system, as schematized in Figure 3.5, consisted in two seesaw-like elements hinged together and with the ends connected to the slab by double pinned struts. The seesaw elements were designed to be rigid under bending, therefore IPE360 steel frames, with shear strengthening in the supports, were used. For the double-pinned struts, similar SHS100 steel profiles that were used in the struts of the rotation compatibilization system were used. The double-pinned struts were connected to the same RHS steel frame used to anchor the rotation compatibilization system to the slab. Two of these systems were used, one in each side of the column. The supports responsible for the rocking of the seesaw elements were prestressed to the strong floor. The complete details of the vertical displacement compatibilization system are presented in Figure 3.11.

All the spreader beams as well as the corbel were made of two UPN profiles welded together in the webs using steel plates to keep between them a void wide enough to pass the steel tendons.

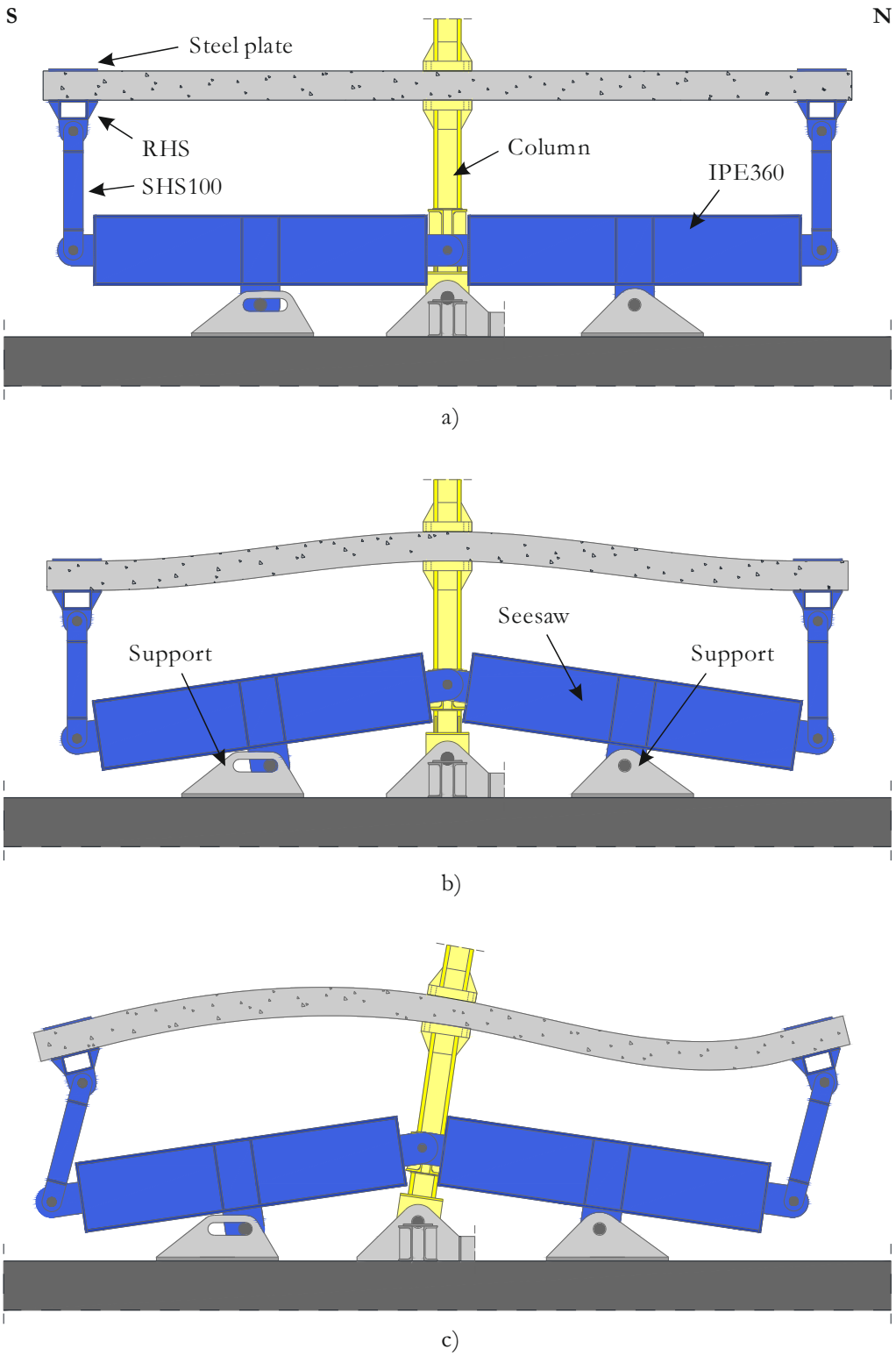

Figure 3.11: Scheme and detail of the vertical displacement compatibilization system. a) Unloaded specimen; b) Vertically loaded specimen; c) Vertical and horizontally loaded specimen.

The elements of the vertical loading system did not need to be rigid, therefore, they were designed to perform under linear elastic regime for the aimed loads. The vertical load was

applied in eight points in the surface of the slab, two load points by each top spreader beam. Each top spreader beam had a dedicated hydraulic jack and a load cell. All hydraulic jacks were connected together and controlled by an electronic controlled hydraulic pump with load maintainer capabilities. The vertical load system is represented in Figure 3.12.

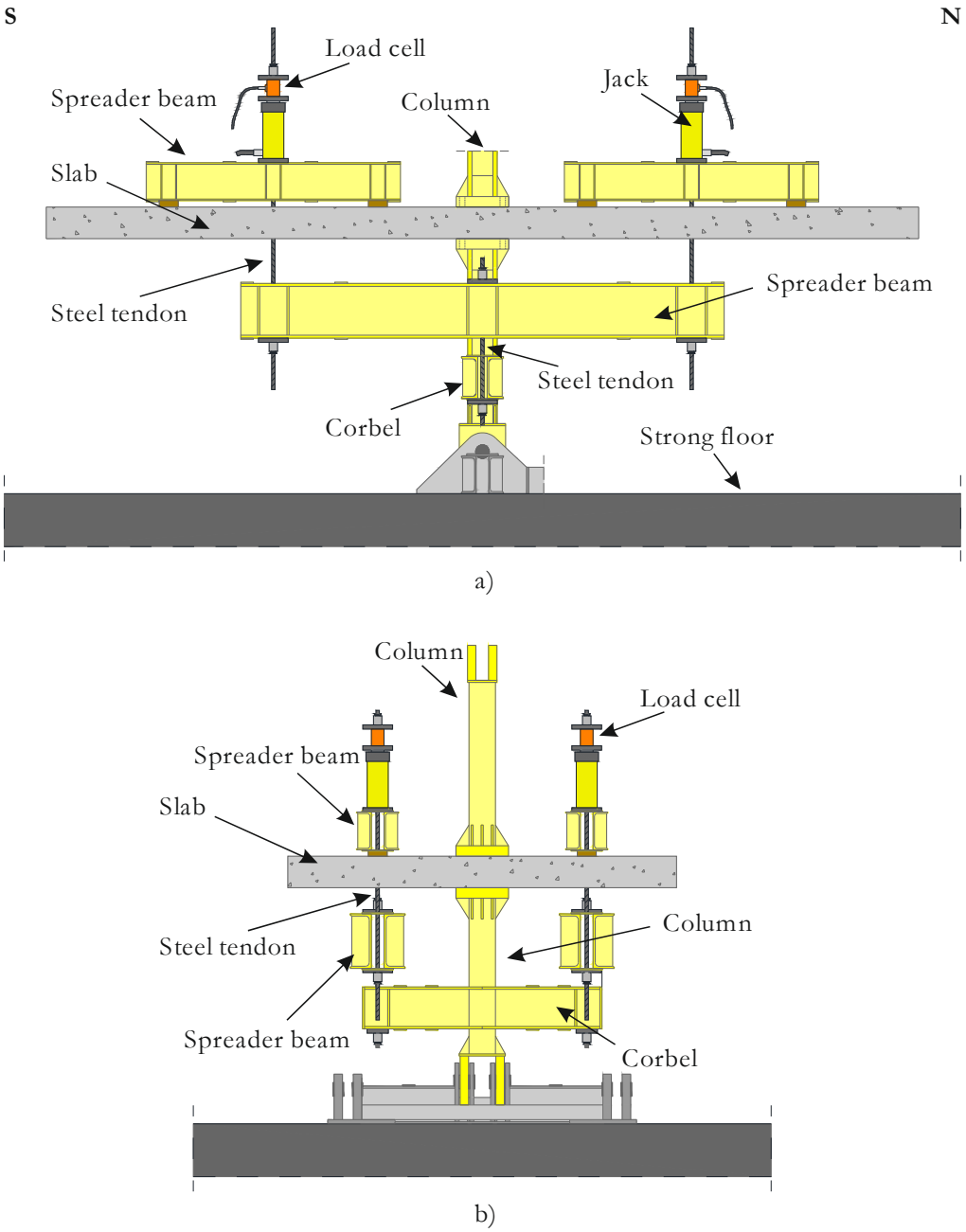

Figure 3.12: Scheme and detail of the vertical load system. Unloaded specimen. a) Side view; b) Front view.

The column consisted in two HEM120 steel profiles, each one welded to 50 mm thick steel plates with an area of 250×250 mm². The connection between the HEM120 profile and the steel plate was reinforced with gussets. The support in the bottom end of the lower column

had two bearings (Figure 3.12b) in order to withstand moments in the transverse direction and keep the setup stable. The hinged supports in the ends of the columns were 2000 mm away from each other and represented the middle of the column in the prototype building, where the bending moments due to horizontal loading is expected to be zero. The three referred systems work in conjunction to form the whole test setup which is showed, with the test specimen in place, in Figure 3.13 as well as the connection of the test setup to the edge of the slab. Figure 3.14 shows how the different systems fit together.

Figure 3.13: Perspective of the test setup.

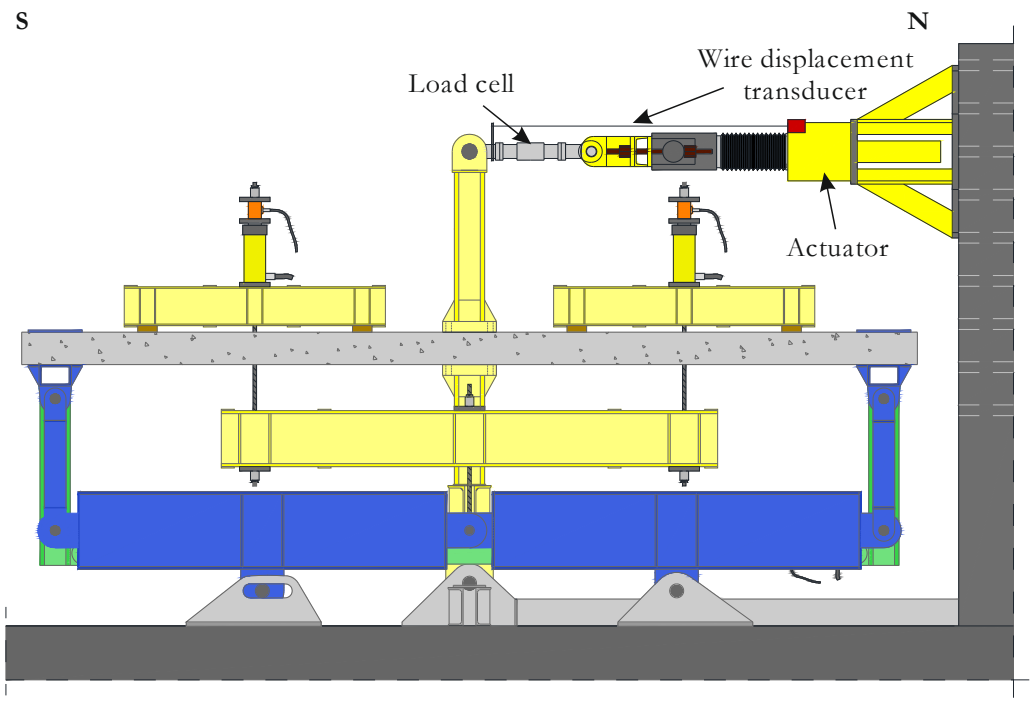

a)

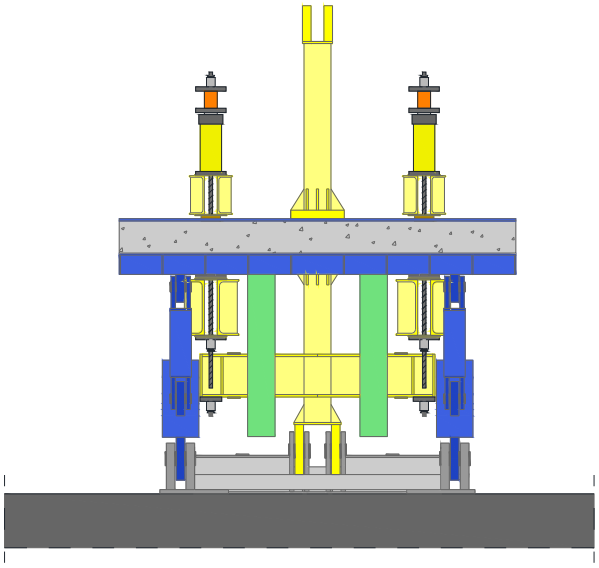

b)

Figure 3.14: Scheme and detail of the complete test setup. Unloaded specimen. a) Side view; b) Front view.

The top of the column is connected to a displacement actuator, which is anchored to the shear wall of the laboratory. The column and the vertical displacement compatibilization system are hinged to steel supports that are prestressed against the strong floor and to the shear wall.

All steel profiles and plates were made of S355 steel and all the hinges in the test setup used NSK roller bearings to ensure friction free movement. The bearings were chosen according to the loads measured in each hinged joint in the linear elastic numeric model.

3.2 Test specimens and materials

The goal of this experimental work was to focus on the behaviour and response of flat slabs under vertical and horizontal cyclic loading, varying the shear ratio, and the arrangement and type of shear reinforcement. Eleven specimens were cast to be tested as follow

MLS	Monotonic centred punching until failure.
E-50	Gravity load of 50% of the shear capacity of the slab plus unidirectional and increasing monotonic eccentricity until failure.
C-50	Gravity load of 50% of the shear capacity of the slab plus reversed and increasing cyclic eccentricity until failure.
C-40	Gravity load of 40% of the shear capacity of the slab plus reversed and increasing cyclic eccentricity until failure.
C-30	Gravity load of 30% of the shear capacity of the slab plus reversed and increasing cyclic eccentricity until failure.
C-50 BR	Gravity load of 50% of the shear capacity of the slab plus reversed and increasing cyclic eccentricity until failure. Three layers of post-installed steel shear bolts in radial arrangement.
C-50 BC	Gravity load of 50% of the shear capacity of the slab plus reversed and increasing cyclic eccentricity until failure. Three layers of post-installed steel shear bolts in cross arrangement.
C-50 STR1	Gravity load of 50% of the shear capacity of the slab plus reversed and increasing cyclic eccentricity until failure. Three layers of small section steel stirrups.
C-50 STR2	Gravity load of 50% of the shear capacity of the slab plus reversed and increasing cyclic eccentricity until failure. Three layers of steel stirrups.
C-50 STR3	Gravity load of 50% of the shear capacity of the slab plus reversed and increasing cyclic eccentricity until failure. Five layers of small section steel stirrups.

C-50 STR4 Gravity load of 50% of the shear capacity of the slab plus reversed and increasing cyclic eccentricity until failure. Five layers of steel stirrups.

All specimens were intended to be similar, in all aspects except the variables to be tested. The designed reinforcement shown in Figure 3.7 was used in all slabs. The measured effective depths for each specimen can be seen in Table 3.1

Table 3.1: Effective depth of the top flexural reinforcement.

Specimen	d (mm)
MLS	118
E-50	118
C-50	118
C-40	119
C-30	118
C-50 BR	118
C-50 BC	118
C-50 STR1	117
C-50 STR2	119
C-50 STR3	119
C-50 STR4	118

During cast, voids were left in the locations where the pass through holes would be, as seen in Figure 3.7. Four holes of a diameter of 30 mm were left for the fastening of the column. At each border, twenty 16 mm diameter holes were left to anchor the test setup. Four 34 mm holes were left for the steel tendons of the vertical load system.

Post installed steel bolts were used in two specimens (C50-BR and C-50 BC) as shear reinforcement. The reinforcement ratio was intended to be similar to the one used in the C-50 STR3, therefore, three class 8.8 M10 bolts were used. For the calculations of the reinforcement ratio, the threaded zone nominal cross section was considered. Two arrangements were tested: a radial arrangement, and a cross arrangement, similar to the ones used in the slabs reinforced with stirrups. Both the radial and cross displacements were detailed following the EC2 specifications and are shown in Figure 3.15.

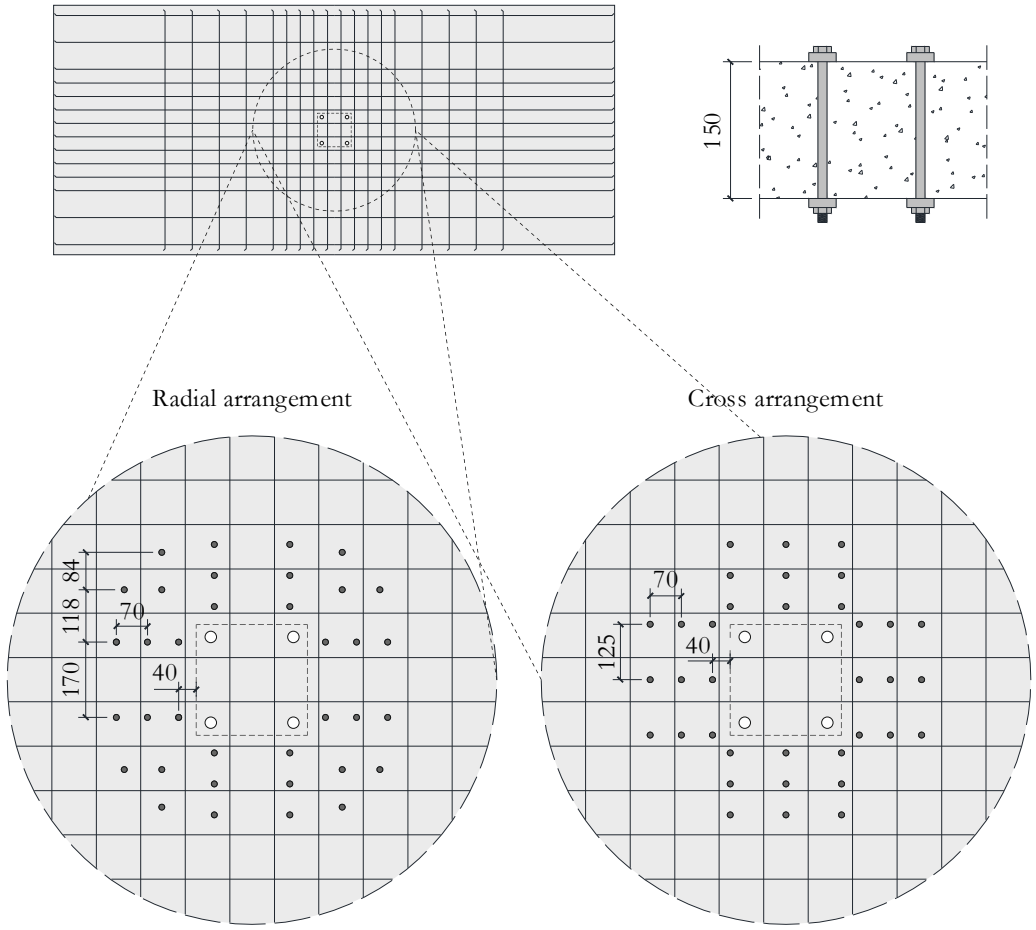

Figure 3.15: Arrangement and details of the post installed shear bolts. Dimensions in millimetres.

The arrangement of the shear bolts in the specimen C-50 BR is shown in Figure 3.16.

Figure 3.16: Detail of the Shear bolts in the C-50 BR slab.

Steel stirrups as shear reinforcement were used in four specimens (STR). For the detailing of the shear reinforcement, variations were made in the amount of steel reinforcement in each layer and in the number of used layers. Two different ratios of shear reinforcement were used. It was assumed that the shear reinforcement was not required to resist the vertical loads, being added with the sole purpose to increase drift capacity and ductility. A higher ratio was also tested to prevent punching failure inside the shear reinforced zone. These ratios were tested in a three layer configuration as detailed in Eurocode 2 (EC2) [54] and in

a five layer configuration to prevent failure outside the shear reinforced area. The stirrups were arranged in four legs per layer in each side of the column in a total of sixteen legs per layer. The smaller shear reinforcement ratio was obtained by using 4.5 mm diameter reinforcement bars. The higher shear reinforcement ratio resulted from a combination of two legs of 6 mm reinforcement bars (outer legs) and two legs of 8 mm reinforcement bars (centre legs). Information on the arrangement and the details of the stirrups are presented in Figure 3.17.

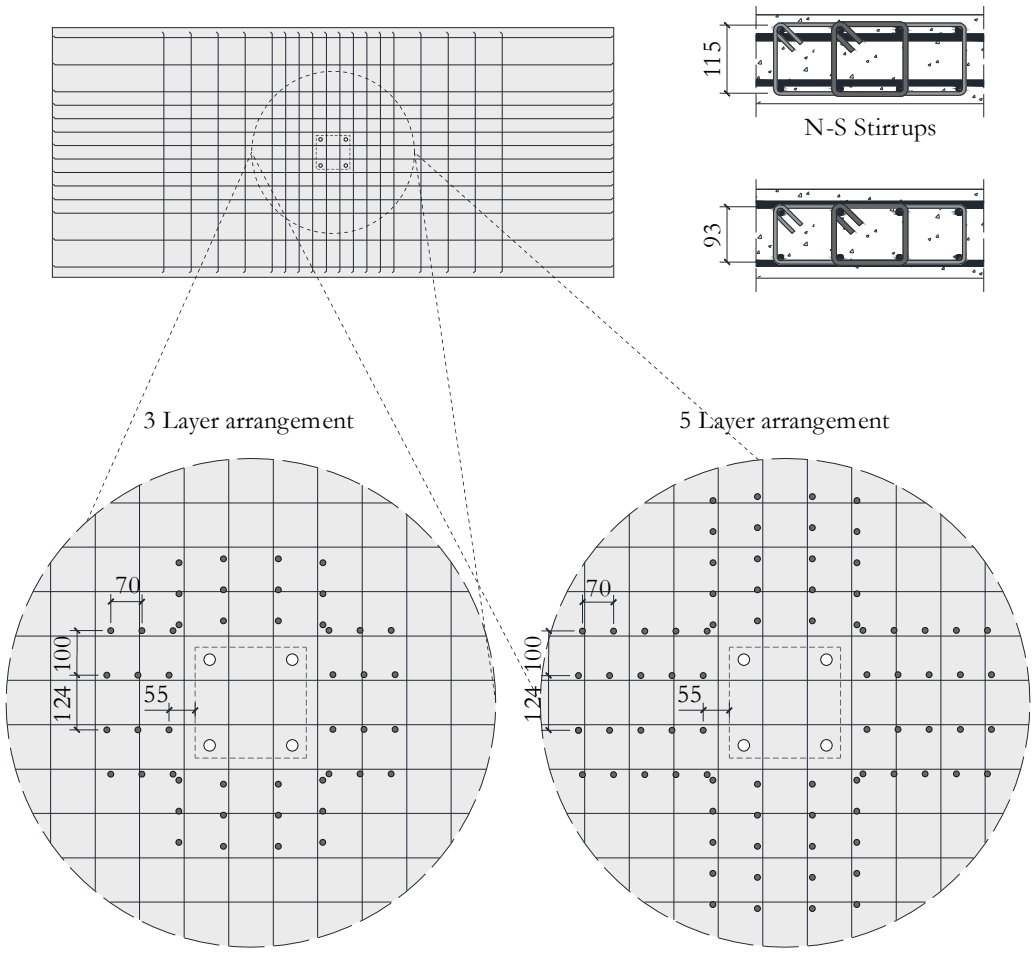

Figure 3.17: Arrangement and details of the stirrups. Dimensions in millimetres.

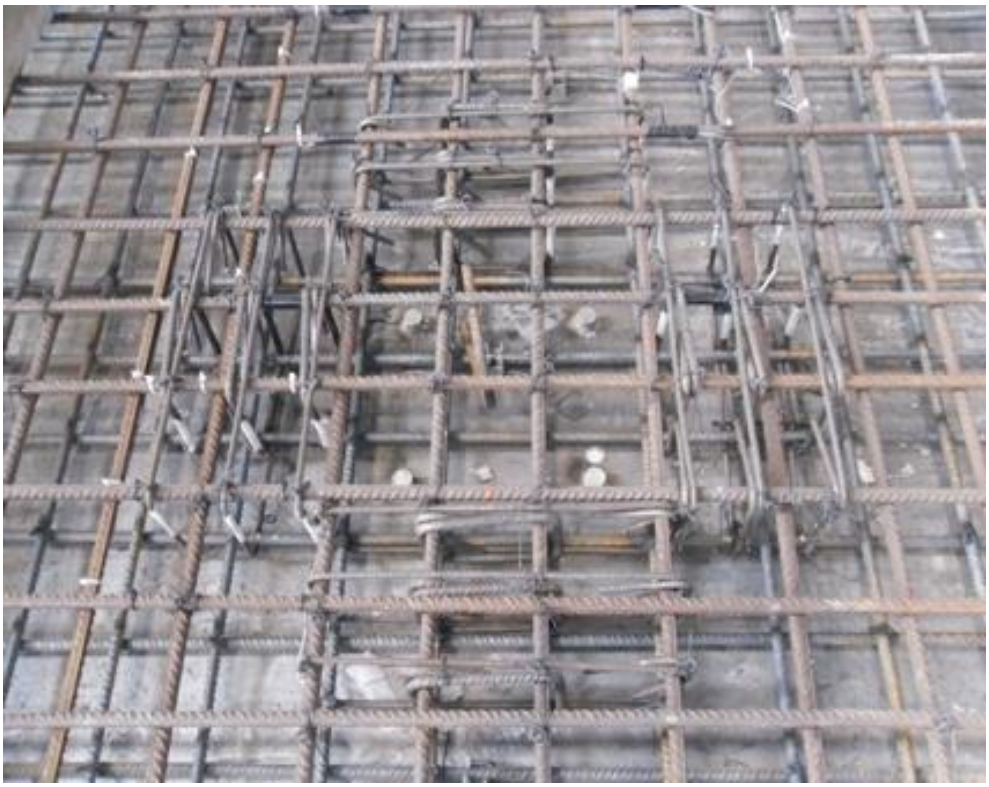

Figure 3.18: Positioning of the stirrups in the C-50 STR2.

Tensile tests were performed in samples of the flexural reinforcement, the stirrups and the shear bolts to evaluate the yield stress (f_y) and the yield strain (ε_y) and the Young modulus (E). The results are presented in Table 3.2. The 4.5 mm bars were A500ER steel bars. All the other reinforcement bars were regular A500 SD steel bars and the bolts used as shear reinforcement were class 8.8 M10 steel bolts. The measured modulus of elasticity was 200 GPa.

Table 3.2: Reinforcement characterization.

Designation	Diameter (mm)	f_y (MPa)	ε_y (%)
Flexural	10	523.9	0.26
Flexural	12	544.9	0.27
Stirrups	4.5	543.3	0.27
Stirrups	6	538.0	0.27
Stirrups	8	533.5	0.27
Class 8.8 M10 bolt	8.6 (threaded zone)	826.5	0.41

To characterize the concrete, six 150 mm side cubes and twelve 300 mm long and 150 mm diameter cylinders were cast, for each slab. Concrete mean compressive strength (f_c) and mean splitting tensile strength ($f_{ct,sp}$) were determined by tests on the cylinders while the cubes were used to measure the cube compressive strength ($f_{c,cube}$) as summarised in Table 3.3.

Table 3.3: Concrete characterization.

Specimen	f_c (MPa)	$f_{c,cube}$ (MPa)	$f_{ct,sp}$ (MPa)
MLS	31.6	34.5	2.9
E-50	55.1	56.7	3.8
C-50	52.4	48.6	2.9
C-40	53.1	53.1	4.2
C-30	66.5	64.2	4.2
C-50 BR	57.6	59.6	3.5
C-50 BC	58.8	59.6	4.1
C-50 STR1	53.1	55.2	3.7
C-50 STR2	52.5	56.2	3.6
C-50 STR3	49.2	47.1	4.2
C-50 STR4	44.4	43.7	3.6

3.3 Test instrumentation and procedures

3.3.1 Instrumentation

The test data was acquired using three computers and several HBM data-loggers (Quantum X and Spider 8 models).

As stated previously, each one of the struts from the rotation compatibilization system had a 200 kN load cell (Figure 3.9) to monitor the force in the strut and, consequently, the magnitude of the bending moment in the edge of the specimen (mid-span of the prototype slab).

200 kN load cells were also used in series with the each one of the four hydraulic jacks responsible for the application of the gravity load (Figure 3.12).

The mechanical actuator was equipped with a 500 kN load cell and a wire linear displacement transducer (WLDT), showed in Figure 3.14, used to measure the horizontal load and imposed displacement, respectively.

Along the centre North-South (N-S) and East-West (E-W) axis of the specimens, eighteen TML® linear displacement transducers (LDT) were placed according to the arrangement displayed in Figure 3.19. The LDTs were suspended in a rigid steel beam that was fastened to the base plate of the top half-column. This way, the instrumentation moved along with the specimen during the test. All LDTs have a maximum range of 100 mm except for D6 to D11, D16 and D17 that have a maximum range of 50 mm. For higher drifts it was observed that some transducers (D1, D2, D3, D12, D13 and D14) ran out of range which led to the need of substitute them by six Variohm® wire LDT. Variohm® wire LDTs were used in the tests of the specimens C-50 STR1, C-50 STR2, C-50 STR3 and C-50 STR4.

An extra LDT was used to measure the horizontal displacement of the slab. Those results were used to help in the synchronization of the readings between the different computers, as well as a redundant verification of the horizontal displacement.

Two Variohm® biaxial inclinometers were used at the edges, attached beneath the RHS steel frame, in the same positions as LDTs D1 and D14, to measure the rotation of the borders along the test.

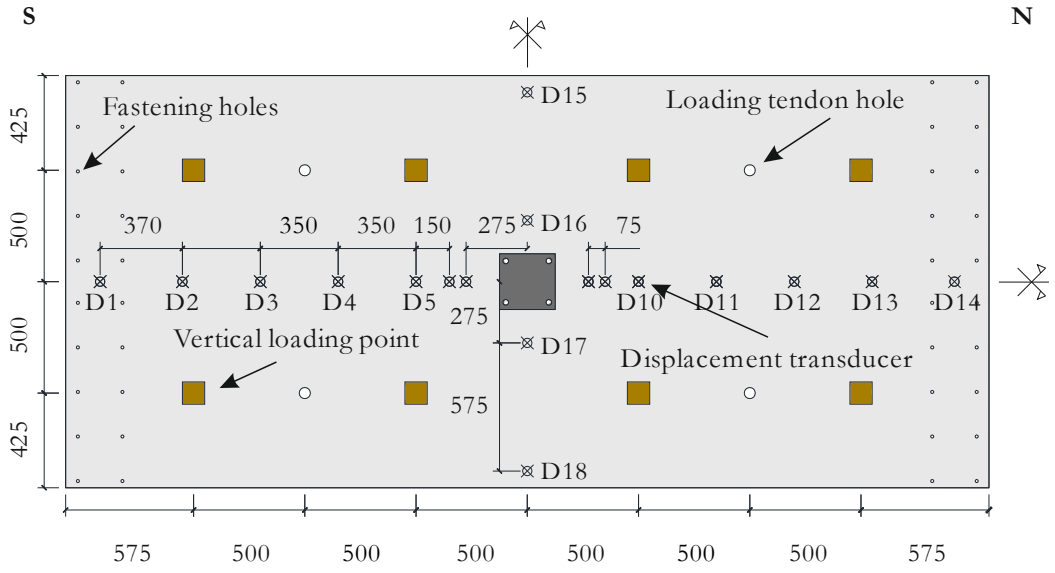

Figure 3.19: Arrangement of the displacement transducers and loading points. Dimensions in millimetres.

The two types of LDT devices used in the experimental tests can be seen in Figure 3.20. The strain gauge LDTs were placed in an acrylic plate to ensure a flat contact surface. The wire LDTs were connected to a steel hook glued to the surface of the slab with epoxy resin.

Figure 3.20: Strain gauge LDT and wire LDT.

Four top flexural reinforcement bars were instrumented with strain gauges in two points each, as showed in Figure 3.21. The instrumented points were 50 mm far from the face of the column in the N-S direction and two strain gauges per point were used. Due to the symmetry of the specimen, only the East side of the slab was instrumented.

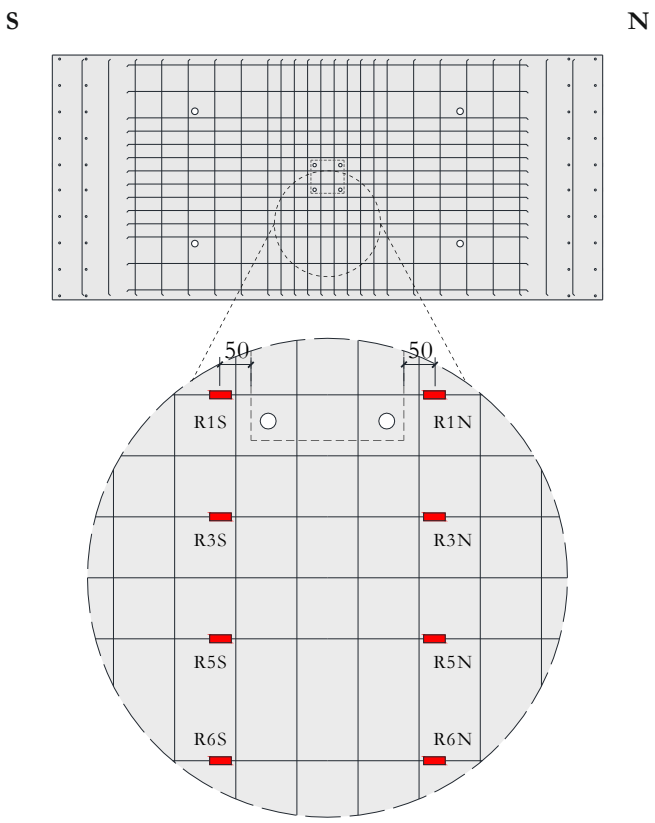

Figure 3.21: Instrumentation of the top flexural reinforcement. Dimensions in millimetres.

In the C-50 STR specimens, the bottom flexural reinforcement bars were also instrumented, on four measuring points, two in the column region and two in the border of the specimen, as shown in Figure 3.22. The strain gauges placed in the column region had a location analogous to the ones used in the top reinforcement (50 mm from the face of the column) while in the South border, the measuring points range 120 mm from the position of the theoretical mid-span of the prototype slab.

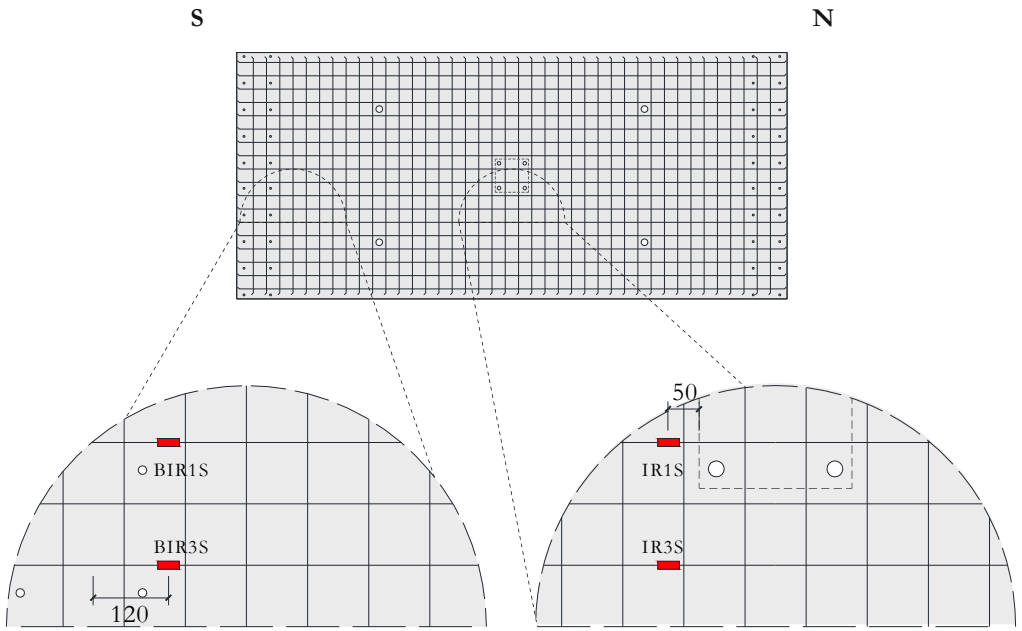

Figure 3.22: Instrumentation of the bottom flexural reinforcement. Dimensions in millimetres.

Strain gauges were also used to measure strains in the shear reinforcement. Figure 3.23 shows the arrangement of the instrumented stirrups and shear bolts. All specimens had instrumented shear reinforcement in both North and South. Due to data logger input channel limitations, a single strain gauge was used per stirrup leg or shear bolt.

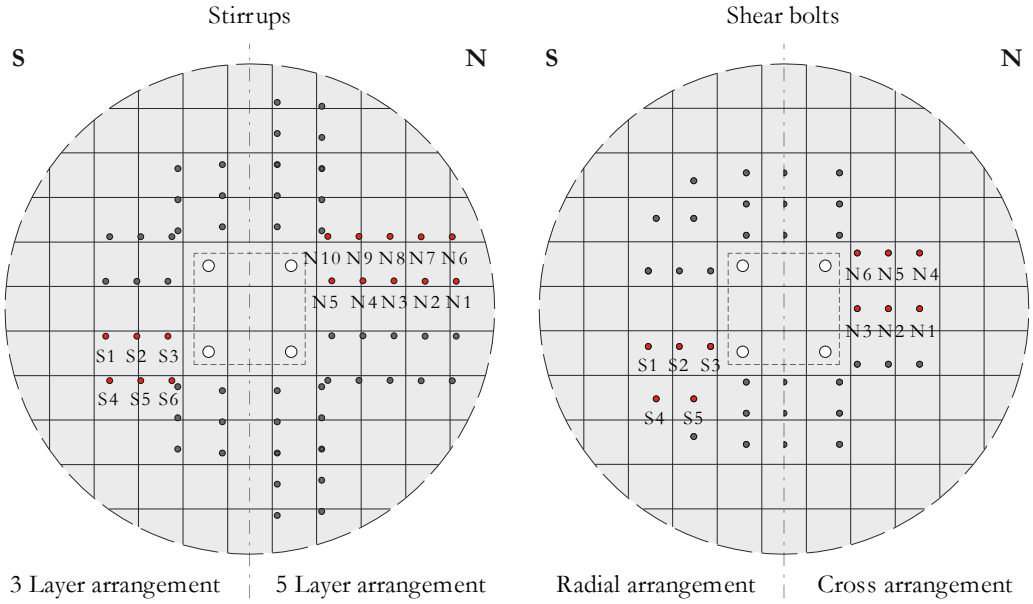

Figure 3.23: Instrumentation of the shear reinforcement.

3.3.2 Test assembly

Part of the test setup consisting in the floor supports, the rotations and vertical displacement compatibilization systems, the bottom half-column and the two inferior spreader beams of the vertical loading system were assembled in the laboratory. The inferior half-column was kept in the vertical position by a removable strut and the spreader beams were laid on the corbel of the column. The RHS profiles to be anchored to the borders of the slab were kept in the ideal position for fastening (slightly higher than the plate of the column) by four steel supports.

Figure 3.24: Test setup ready for the test specimen.

The specimens were suspended by a crane in four points over the previously assembled elements of the test setup. Forty class 10.9 M12 bolts were used to gradually fasten the RHS profiles to the slab with a torque of 170 Nm. The prestress force in the bolts was designed to keep the bolts in elastic regime while providing a solid anchorage.

With the specimen suspended in the crane and part of the test setup suspended in the slab, the length of the struts of the rotation compatibilization system was adjusted using the dedicated hydraulic jacks, while monitoring the load cells. As soon as a force reading appeared in the load cells, the hydraulic hoses were closed from the pump in order to keep the achieved state. Both jacks shared common hoses to ensure equal forces in both struts.

Next, the four supports were removed and the specimen was laid on top of the base plate of the inferior half-column. The reading in the load cell from the struts showed an increase due to the self-weight of the specimen plus the hung elements of the test setup.

The top half-column was then placed in position and fastened by means of four 8.8 class M24 steel rods. The interface between the concrete and the base plate of the top half-column was evened with a thin layer of Hilti® RE500® epoxy resin and the voids in the holes of the slab, where the rods pass through, were filled with BASF® MasterFlow® 765 grout. Before the grout and the epoxy set, each one of the four rods were fastened until the target pre-load of 244 kN was achieved, resulting in a compressive stress of 15.6 MPa in the concrete between the base plates of both half-columns. The pre-load was designed to prevent the disconnection of the column from the surface of the slab in the occurrence of the maximum horizontal force allowed by the column.

Figure 3.25: Assembly of the column.

The supporting frame with the displacement transducers was then attached to the base plate of the top half-column followed by the precise positioning of all the transducers (Figure 3.19).

Solid steel plates with an area of 180×180 mm² and a thickness of 50 mm were placed in the loading points with the top spreader beams laid on top of them as shown in Figures 3.12, 3.14 and 3.19. The hydraulic jacks and the load cells were placed on the top of the spreader

beams, followed by the installation of the steel tendons used to apply the vertical load. To finalize the test assembly the top of the column was connected to the horizontal actuator and the strut that kept the inferior half-column in the vertical position was removed.

The C-50 BR and C-50 BC had post-installed bolts as shear reinforcement. The holes in the slab had a diameter of 12 mm to accommodate both the bolts and the wires of the strain gauges. The bolts were put after the assembly of the specimen in the test setup and before the application of the vertical load, while self-weight only was acting on the specimen. The bolts had two 30 mm diameter, 10 mm thick washers to prevent concrete crushing under the bolt and to ensure adequate anchorage. A dynamometric wrench was used to prestress all the bolts to a quarter of their nominal strength (160 MPa for 8.8 class bolts). To confirm the torque, a previously calibration was carried out by wrenching several bolts gripping a load cell.

3.3.3 Test protocols

In this experimental campaign, three different kinds of tests were performed, therefore, different protocols were used.

The MLS specimen was tested by increasing the vertical load until failure was reached. Because the goal was a centred punching failure, the top of the column was not connected to the horizontal actuator, in this test, to avoid eccentricity due to asymmetries in the specimen and the loading inherent to experimental tests. The load was applied at a rate of 18.6 kN/min, one eighth in each load point, until punching failure.

For both the eccentric and cyclic tests, the vertical load was first applied until the target shear ratio was reached. Then, the vertical load was maintained by the load maintainer hydraulic pump. To quantify the vertical load to be applied in the specimens with eccentric and cyclic tests, according to the chosen shear ratio (V_{exp}/V_{norm}), the expected punching capacity of the specimens was extrapolated using the experimental result of the MLS specimen. For the extrapolation, equation (3.1) was used.

$$V_{norm} = V_{MSL,exp} \left(\frac{f_c}{f_{c,MLS}} \right)^{0.41} \tag{3.1}$$

where:

V_{norm} is the expected extrapolated punching load capacity for each slab;

$V_{MSL,exp}$ is the experimental punching capacity of the MLS specimen;

$f_{c,MLS}$ is concrete mean compressive strength of the MLS slab;

Although the shear capacity also depends on the effective depth of the flexural reinforcement, because the measured effective depths was very similar between specimens, the contribution of this parameter was neglected. The parameter 0.41 was proposed by Mamede et al. [60], based in a potential regression analysis that showed that the punching capacity depends on average on the concrete strength to the power of 0.41 ($f_c^{0.41}$). This value lies between the one presented by EC2 [54] (1/3) and the one recommended by the MC2010 [56] and ACI [51] (1/2). A summary of the addressed test parameters is presented in Table 3.4.

Table 3.4: Details of the experimental tests.

Specimen	V_{norm} (kN)	V_{exp} (kN)*	Average A_{sw} (mm²/Layer)	Layers
MLS	-	323.4	-	-
E-50	406.3	212.7	-	-
C-50	397.9	203.4	-	-
C-40	400.0	167.4	-	-
C-30	438.9	131.3	-	-
C-50 BR	413.8	220.2	697.0	3 Radial
C-50 BC	417.2	222.3	697.0	3 Cross
C-50 STR1	419.8	209.9	254.5	3 Cross
C-50 STR2	429.1	215.7	628.3	3 Cross
C-50 STR3	405.7	202.3	254.5	5 Cross
C-50 STR4	391.8	195.9	628.3	5 Cross

*Load measured during the test. May differ from the target load due to equipment tolerances.

The experimental tests with eccentricity were performed in two phases. The first phase consisted of the vertical load application until the shear ratio target load for each specimen was reached and kept constant throughout the test. The shear ratio was considered to be the ratio between the applied vertical load and the punching capacity of the slab without shear reinforcement. The protocol to impose the vertical loading was changed for the two last specimens (C-50 STR3 and C-50 STR4) to optimize the function of the rotation compatibilization system. With the added capability to read the inclinometers and the load

cells from the struts in real time during the test by using an extra data logger, it was possible to actively keep the rotations at the borders equal, by means of the hydraulic jacks attached to the compressed struts. This allowed the rotation compatibilization system to perform at its full potential.

In the second phase, a horizontal displacement was imposed at the top of the column. The monotonically eccentric loaded slab specimen (E-50) was tested under constant vertical loading, with a target shear ratio of 50%, and monotonically increasing horizontal displacement. The vertical load was applied at a 15kN/min rate until the aimed value. Once vertically loaded, the horizontal displacement protocol for the eccentric test consisted in an increasing imposed horizontal displacement at the top of the column, of about 1.2 mm/min in the N-S direction.

The specimens tested under reversed cyclic eccentricity, followed the same protocol for the application of the vertical load. The horizontal displacement was imposed at a speed of 9 mm/min for drift steps up to 3.0% and 18 mm/min for higher drift steps, following the protocol shown in Figure 3.26, consisting in sets of three complete cycles for each drift step up to 3.5%. In the subsequent drift steps, of 4.0% and 4.5%, the cycles were reduced to two and one cycle respectively. From this point until the end of the test only one cycle was applied.

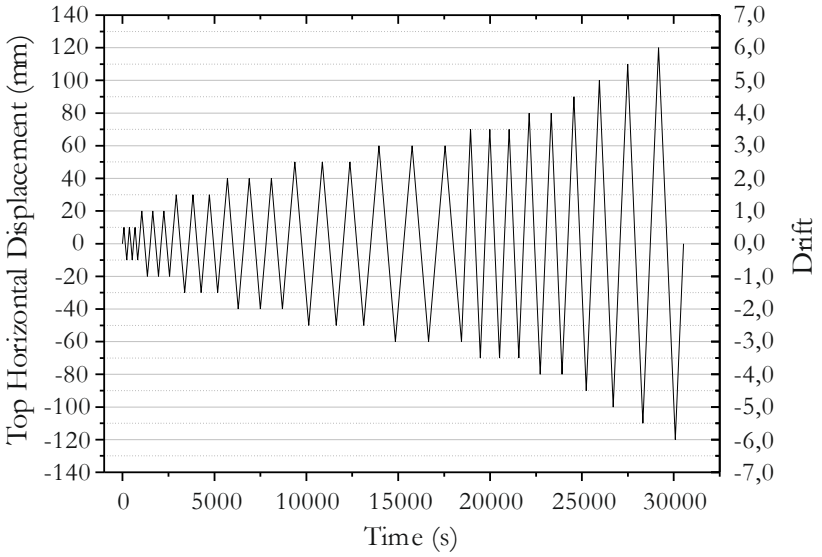

Figure 3.26: Cyclic horizontal displacement protocol.

The adopted failure criterion consisted of a drop to 80% of the maximum horizontal load for a new peak in either drift direction. If a specimen completes the imposed displacement protocol without verifying the failure condition, a non-failure is assumed. For post failure

behaviour purposes, the tests were stopped when a horizontal load of under 30% of the maximum load was achieved. The failure criterion adopted in the cyclic tests is presented in Figure 3.27.

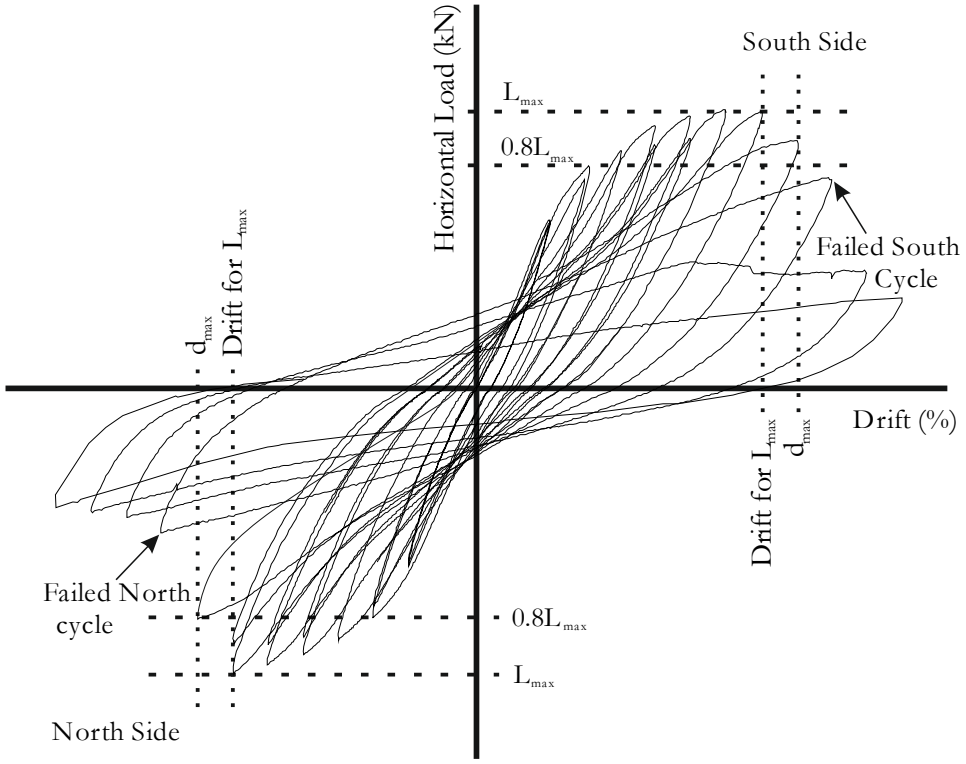

Figure 3.27: Failure criterion for the cyclic tests.

Chapter 4

Experimental Test Results

In this chapter, the results of the experimental campaign are presented and discussed. The MLS specimen will be the first to be addressed, followed by the E-50 specimen. The cyclically tested specimens will be next presented, grouped according to the tested variables following the order in which they were tested. Thus, the specimens without shear reinforcement, the specimens with post-installed steel bolts as shear reinforcement and the ones reinforced with stirrups will be respectively grouped and discussed.

4.1 Tests without horizontal displacement

4.1.1 Specimen MLS

In the first tested specimen the vertical loading was monotonically applied until punching failure. The failure load of this specimen was used to compute the punching capacity of all the following specimens, as well as to test the behaviour of the test setup under vertical load.

Failure mode

The failure of the specimen occurred for a vertical load of 323.4 kN, including the slab and the equipment self-weight. The post failure saw cut of the specimen (Figure 4.1) shows a typical punching failure with a symmetric inclination of the punching cracks, close to 45º. The extended damage on the right hand side of the picture, was the result of the blade impact during cuting.

Figure 4.1: Saw cut of the MLS specimen.

Vertical deformation

Figure 4.2 presents the longitudinal deformed shape of the slab, for different load steps along the test. The stiffness loss is visible as equal load steps lead to increasing displacement increments. It is also visible that the specimen has positive bending moment at the borders as intended and, therefore, bending moment redistribution capacity. The outlines also show that the opposite borders present the same vertical displacement, which means that the vertical displacement compatibilization mechanism of the test setup worked as designed.

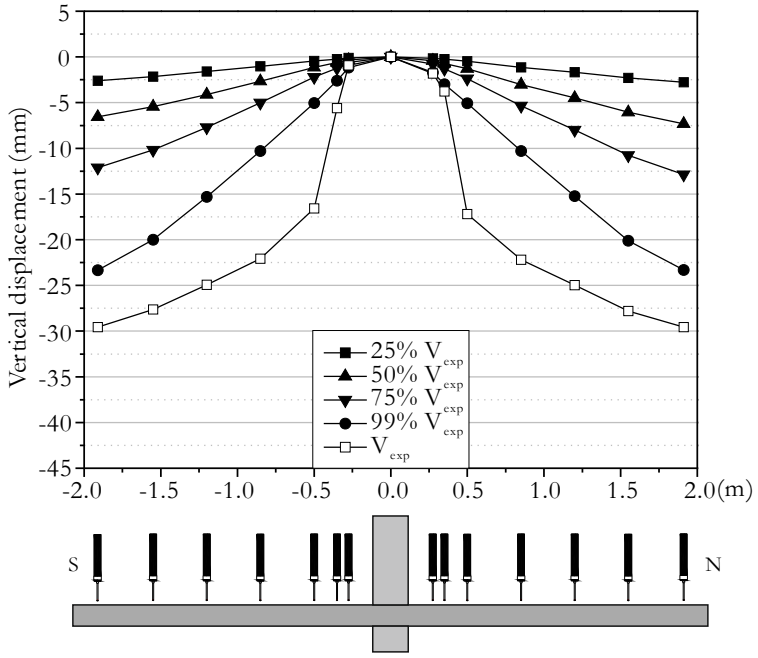

Figure 4.2: Vertical deformation of the MLS specimen.

Flexural reinforcement strains

The evolution of the strains measured at the top longitudinal flexural reinforcement, presented in Figure 4.3, show that yielding occurred only for the reinforcement bars within the column width (R1S and R1N), however, other bars from the flexural reinforcement yielded after punching. The computed yielding strain, based on the rebars tensile tests performed, is represented by a dashed horizontal line. The longitudinal rebars nearest the column presented the higher strain values, as expected, since the higher bending moments are also in the vicinity of the column. The flexural reinforcement strains also corroborate the previously hinted symmetric behaviour.

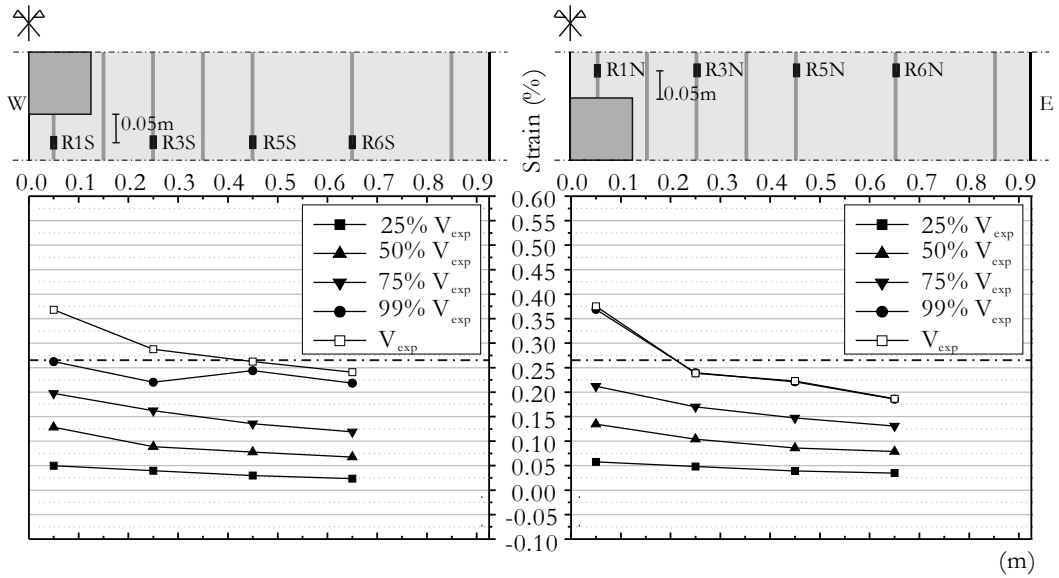

Figure 4.3: Strains in the top flexural reinforcement of the MLS specimen.

4.2 Specimens tested with horizontal eccentricity

The test protocol used for the following specimens consisted, as stated in the previous chapter, in two stages. In the first stage the vertical load was applied until the target value was reached, according to the test protocol of each specimen. The second stage consisted in the imposition of horizontal displacements at the top of the column, in the N-S axis. Two different protocols were used to apply the horizontal displacement. The E-50 specimen was tested under increasing monotonic eccentricity, while all the remaining specimens followed the cyclic test protocol presented in the previous chapter.

4.2.1 Specimen E-50

The E-50 specimen was tested under vertical loading and monotonically increasing eccentricity. The horizontal displacement was applied in the S direction.

Failure mode

The specimen presented a punching failure as shown in the saw cut depicted in Figure 4.4. It was assumed that failure was achieved when the horizontal load presented a sudden decrease, since the failure criteria can be subjective for this kind of tests.

The saw cut in Figure 4.4 shows flexural cracks closer to the column in the N side only, because at the S side, the horizontal load decreased the moment due to the vertical load, while increasing the moment at the N side. The shear cracks were symmetric, however the slab presented more damage in the N side.

Figure 4.4: Saw cut (S-N) of the E-50 specimen.

The load-drift chart in Figure 4.5 shows that specimen E-50 presented a continuous decrease of stiffness throughout the test until punching failure was reached, which occurred for an inter-story drift of about 1.8 %. The failure was brittle and abrupt even under a constant shear ratio of 50 %.

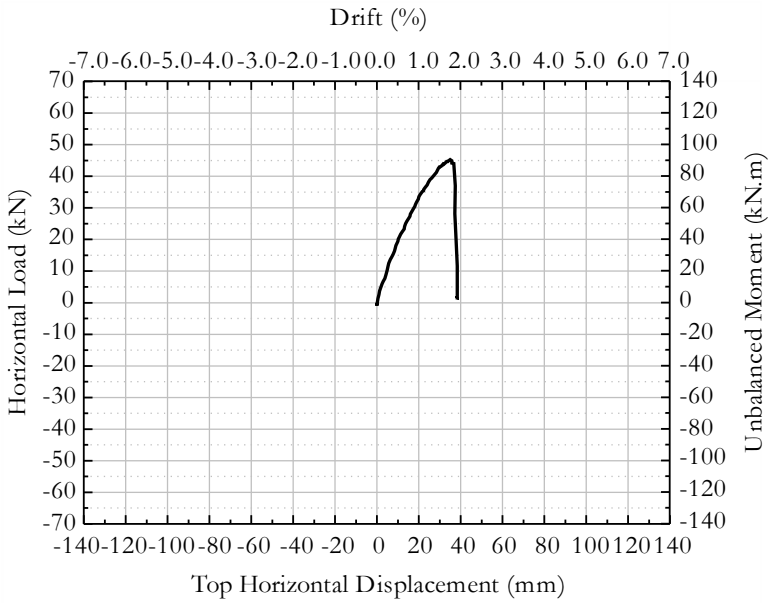

Figure 4.5: Load vs drift chart of the E-50 specimen.

Vertical deformation

The displacement transducers positioned along the N-S and E-W axis of the slab, show the evolution of deformation during the test. Figure 4.6 represents the deformed slab shape along the centre axis in the N-S direction, for the vertical load application phase (0.0 % drift) and different horizontal drift steps. The increasing vertical displacement shows the effect of the horizontal loading in the damaging of the slab by an increasing deformation under

constant vertical load. The deformed profiles also show a discontinuity point in the deformed shape of the slab, due to the wide bending cracks next to the column, at the greater negative bending moment side (N). This is consistent with the observed yielding of the reinforcement.

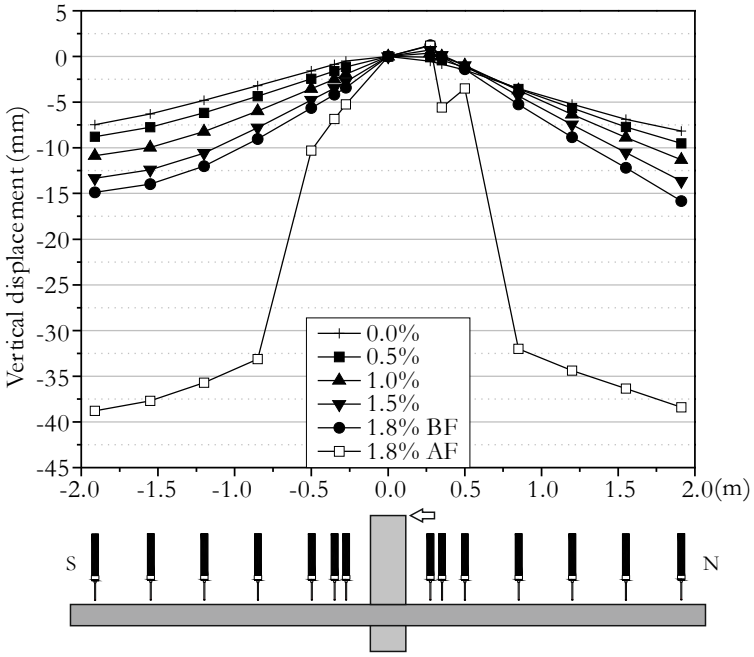

Figure 4.6: Vertical displacement of the N-S axis of the E-50 specimen.

Vertical displacement data was also used to compute the approximate equation of the deformed shape of the specimen, along the N-S axis, for each side of the column. This data was then used to compute the position of the inflection points in the same axis for each instant of the test. These results are shown in the chart from Figure 4.7. When only the vertical load is applied there are two inflection points close to 24% of the span of the slab, which is close to the theoretical inflection point location. When the horizontal displacement is applied in the S direction, the inflection point from the S side moves towards the column, while the other one (N side) moves slightly in the mid span direction. The N side inflection point movement is small and it is caused by the cracking and corresponding stiffness loss in the N side of the column. When the drift reaches about 1.7%, the S side inflection point position is coincident with the column and stays fixed for drifts beyond. This phenomenon is due to the cracking in the column region which causes a local discontinuity in the curvature of the slab.

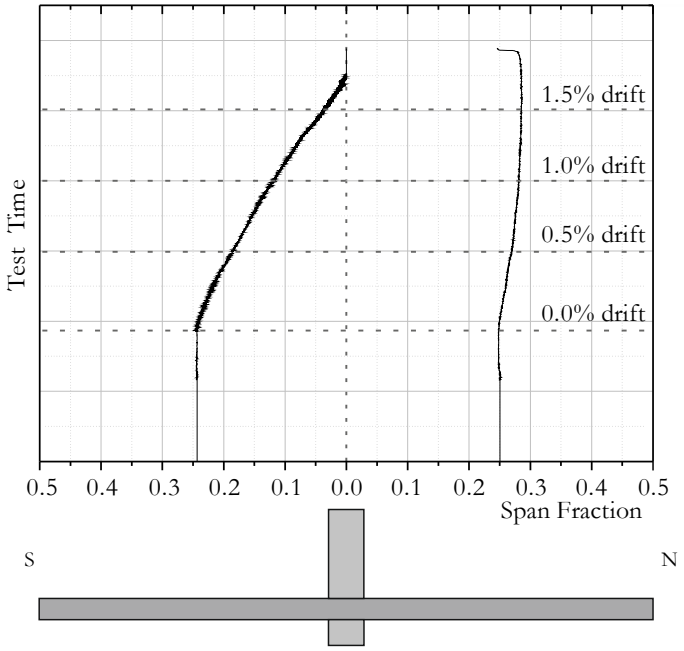

Figure 4.7: Position of the zero moment point in the N-S axis of the MLS specimen.

Flexural reinforcement strains

In the first loading stage (vertical loading), when the target load was reached, cracks due to the negative bending moment with a radial pattern and origin in the column were observed, however the wider ones are in the East-West direction. The higher the vertical load, the wider the cracks, though no instrumented flexural reinforcement yielded at that stage, as can be observed in Figure 4.8. The longitudinal rebars nearest the column presented the higher strain values, as expected, since the higher bending moments are also in the vicinity of the column.

In the second stage, when the horizontal displacement was applied in the S direction, the negative bending moment increased in the N side and decreased in the S side. The effect of the unbalanced moment is more visible in the proximity of the column. Most of the reinforcement bars farther from the column present a small strain variation with the horizontal load throughout the tests, while the ones closer to the column were highly influenced by the eccentricity. The rebar closer to the centre of the column reached the yielding strain (horizontal dashed line) close to the 1.0 % drift mark. As the drift increased, more reinforcement bars yielded, however the development of a full flexural negative yield line was not achieved.

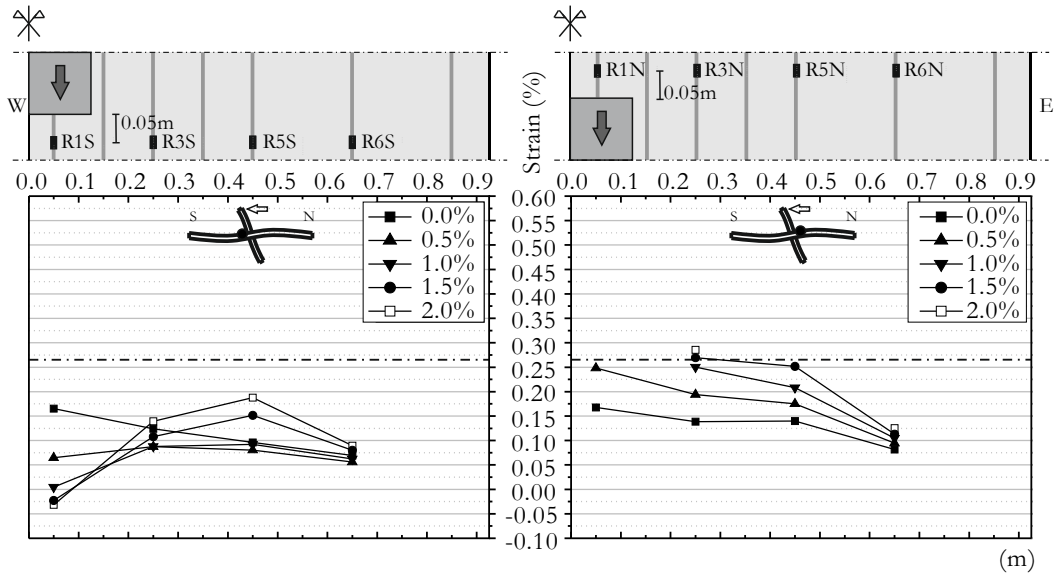

Figure 4.8: Strains in the top flexural reinforcement of the E-50 specimen.

As the test progressed, the top bending cracking stabilized and bottom cracks close to the edges started to be noticed, showing moment redistribution capability of the slab specimen.

4.2.2 Specimens C-50, C-40 and C-30

All specimens discussed in this section followed the cyclic test protocol. In the first stage, the vertical load was applied until the target value was reached. The second stage consisted in eccentric loading by imposing cycling horizontal displacements at the top of the column, resulting in an eccentric punching load.

Failure modes

All specimens presented in this section, failed by punching as shown in Figures 4.9, 4.10 and 4.11. It was assumed that failure was achieved when the previously discussed failure criterion (Chapter 3) was matched.

The C-50 specimen (Figure 4.9) shows a more symmetric failure when compared to the slabs tested with smaller shear ratios, C-40 (Figure 4.10) and C-30 (Figure 4.11). This can be explained by the fact that the less the shear ratio, the more cycles the specimen was subjected, leading to more degradation of the concrete in the punching region.

Figure 4.9: Saw cut (N-S) of the C-50 specimen.

Figure 4.10: Saw cut (N-S) of the C-40 specimen.

Figure 4.11: Saw cut (N-S) of the C-30 specimen.

A top view of the failure of the C-50 specimen is shown in Figure 4.12.

Figure 4.12: Top view of the failure of the C-50 specimen.

The hysteretic charts from the cyclically loaded specimens shown in Figures 4.13, 4.14 and 4.15, show an almost linear progression both for loading and unloading during the 0.5% drift cycles. No major stiffness loss is observed as the horizontal load grows almost linearly with the drift. For drifts over 0.5%, stiffness loss is visible for all specimens which indicates the existence of an asymptotic value for the horizontal load. A slight narrowing can be noted from the first cycle of each drift value to the following ones.

The C-50 specimen reached a maximum horizontal load of 37.4kN for a drift of 1.1%. Punching failure occurred for the second cycle of the 1.0% drift step for a -0.9% drift.

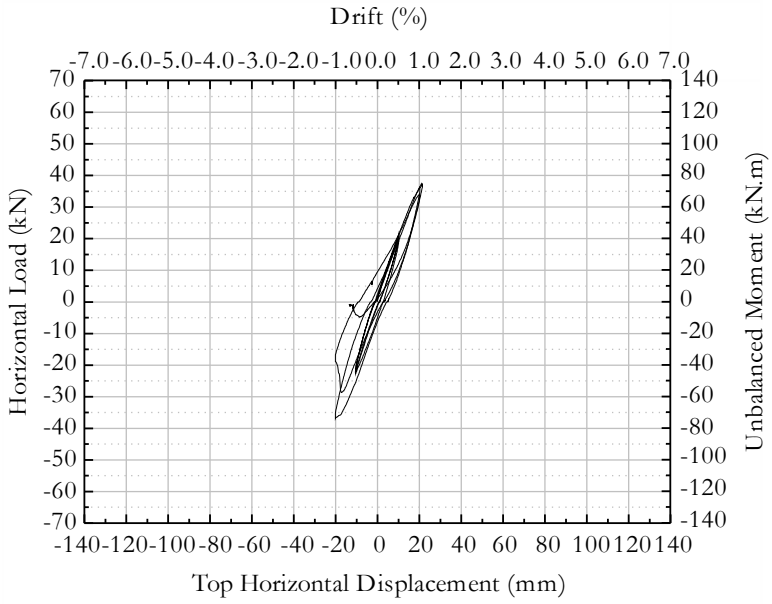

Figure 4.13: Hysteretic chart of the C-50 specimen.

A maximum horizontal load of 51.4kN was achieved by the C-40 specimen for a corresponding drift of 1.5% and punching failure took place during the first cycle of the 2.0% drift step. The failure occurred while reaching the 2.0% drift mark for the first time, for a 1.2% drift.

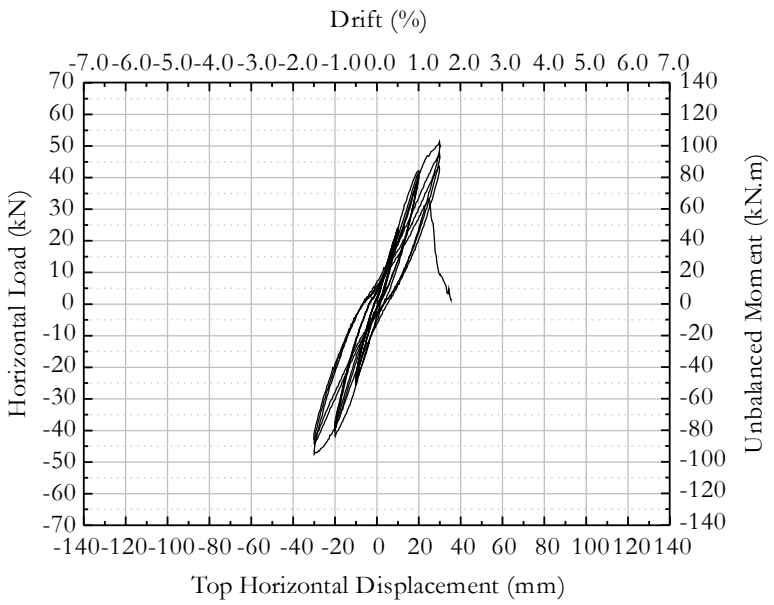

Figure 4.14: Hysteretic chart of the C-40 specimen.

The C-30 specimen presented a maximum horizontal load of 60.8kN for a drift of 2.0% and reached punching failure during the second cycle of the 2.0% drift step for a -1.9% drift. It was observed that the decrease of shear ratio resulted in higher horizontal displacements, and subsequently higher horizontal loads. All data is summarized in Table 4.1.

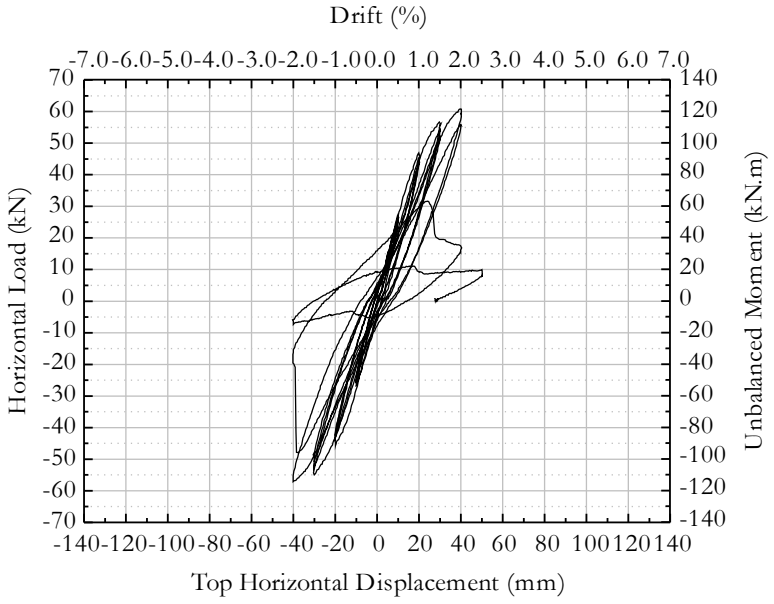

Figure 4.15: Hysteretic chart of the C-30 specimen.

Vertical deformation

Figures 4.16, 4.17 and 4.18 present the vertical deformation in the N-S axis, throughout the test. As shown in Figure 4.16, for consecutive cycles within the same drift, some stiffness loss was observed. The same phenomenon was observed for all the slabs tested under cyclic horizontal loading, however, for clarity reasons, all cycles are showed for the slab C-50 only. For the remaining slabs, the deformed configuration is only represented for the first load cycle of each horizontal drift value. It is also visible that vertical deformation at failure depends on the vertical load applied to the specimen. The deformed profiles also show a discontinuity point in the deformed shape of the slab, next to the column, at the greater negative bending moment side, as corroborated by the reinforcement yielding and observed cracking (to be discussed ahead).

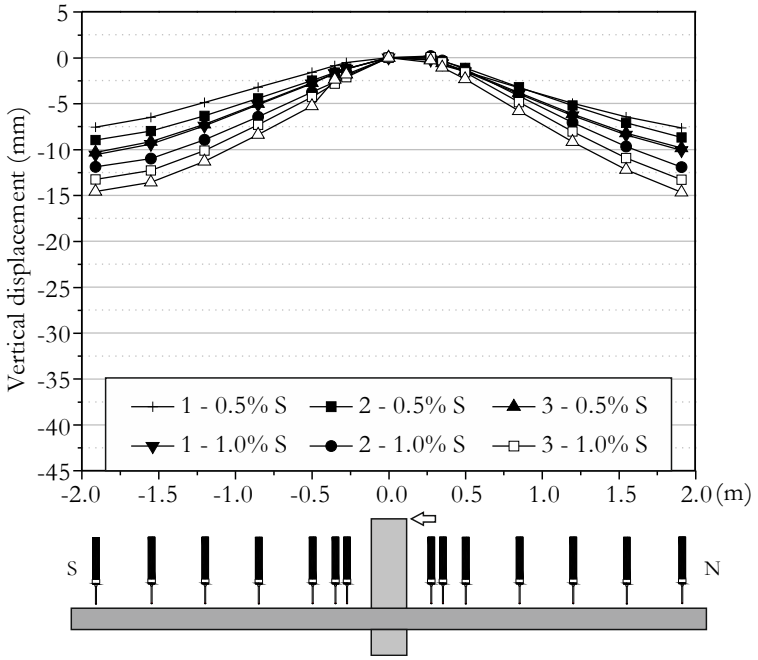

Figure 4.16: Vertical displacement of the N-S axis of the C-50 specimen.

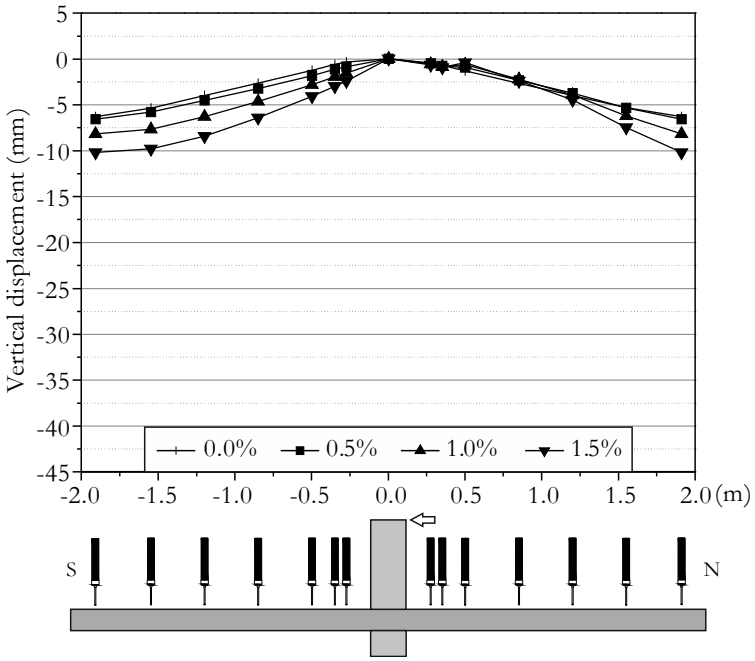

Figure 4.17: Vertical displacement of the N-S axis of the C-40 specimen.

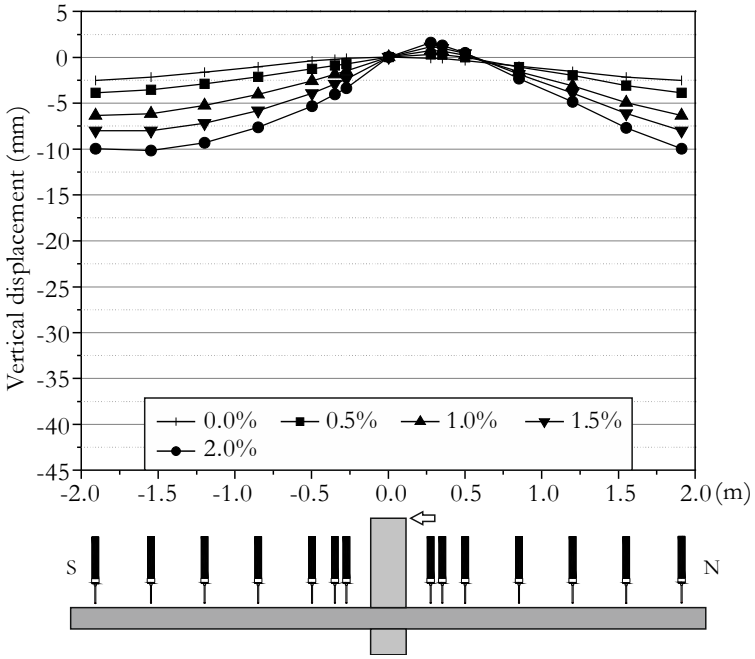

Figure 4.18: Vertical displacement of the N-S axis of the C-30 specimen.

The position of the inflection point in the N-S axis for the C-50 and C-30 specimens, obtained from the vertical displacement data, is displayed in Figures 4.19 and 4.20, respectively. Due to problems in the acquired data, it was not possible to compute the deformed shape of the C-40 specimen. Both C-50 and C-30 specimens show a similar behaviour. In the end of the vertical load imposition, the zero moment point is close to the theoretical value, as expected. With the application of the horizontal displacement in the

South (S) direction, the inflection point in the S side approaches the column while the one in the N side moves slightly away from the column. Once the horizontal displacement is reversed, the S side inflection point moves towards the 24% span position while the N side inflection point moves in the direction of the column. The movement of the inflection point is more pronounced with high drifts and low shear ratios because in those conditions the moment due to the vertical load loses magnitude when compared to the horizontal loading induced bending moment. The inflection point movement can also be seen in the longitudinal outlines.

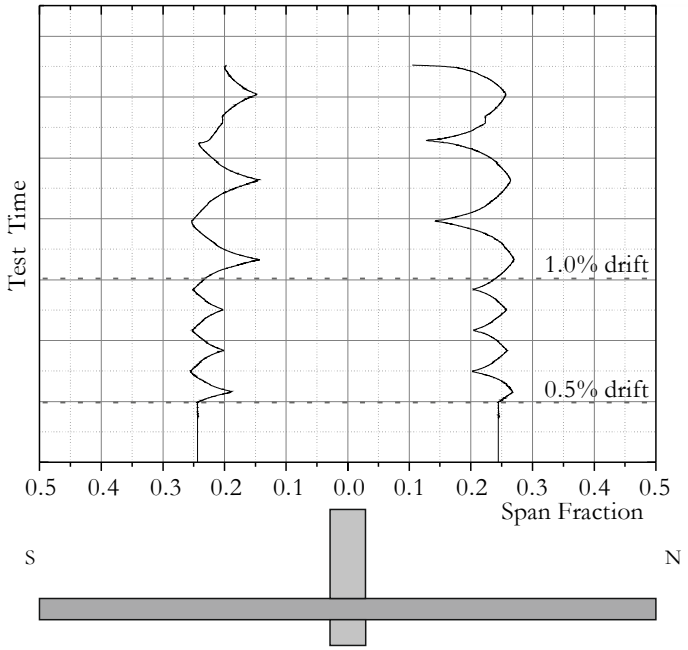

Figure 4.19: Position of the zero moment point in the N-S axis of the C-50 specimen.

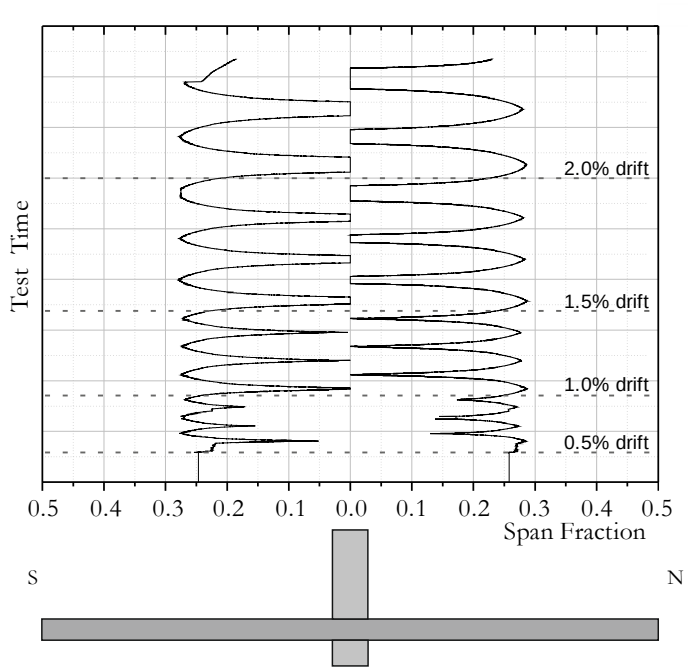

Figure 4.20: Position of the zero moment point in the N-S axis of the C-30 specimen.

Flexural reinforcement strains

The information provided by the strain gauges from to the top longitudinal reinforcement is displayed in Figures 4.21, 4.22 and 4.23. For the specimens tested under combined vertical and horizontal cyclic displacements, the results are only presented for one of the sides of the column, and for both horizontal drift directions, for clarity reasons. It was chosen the side with more data available, since some of the strain gauges were damaged before or during the test.

For the vertical load, the strains in the flexural reinforcement are proportional to the vertical load value (shear ratio), however, no instrumented flexural reinforcement yielded at that stage, as may be observed in Figures 4.21 to 4.23. The longitudinal reinforcement bars nearest the column presented the highest strain values, as expected, since the higher bending moments are also in the column vicinity.

When the displacement is applied in the N-S direction, the negative moment is increased at the N side and decreased at the S side. Displacement imposition in the S-N direction has the opposite effect, as shown in Figures 4.21 to 4.23 where strains at the top rebars are almost symmetrical under vertical load only, but they assume opposite tendencies under eccentric loading. The effect of the unbalanced moments is more visible in the proximity of the column. Most of the reinforcement bars farther from the column present a small strain variation with the cyclic load throughout the tests, while the ones near the column were

severely influenced by the eccentricity. In all of the cyclic tested specimens, the reinforcement bar in the column alignment reached the yielding strain (horizontal dashed line) for higher drift ratios (about 1.0 %), however, the development of a full flexural negative yield line was not achieved in none of the specimens. Also, as the test progressed, the top bending cracking stabilized, and bottom cracks close to the edges started to be noticed, showing moment redistribution capabilities of the slab specimens. R3, R5 and R6 strains from Figures 4.21 to 4.23 also show that lower vertical loads allow the unbalanced moment to be transferred by a wider area surrounding the column.

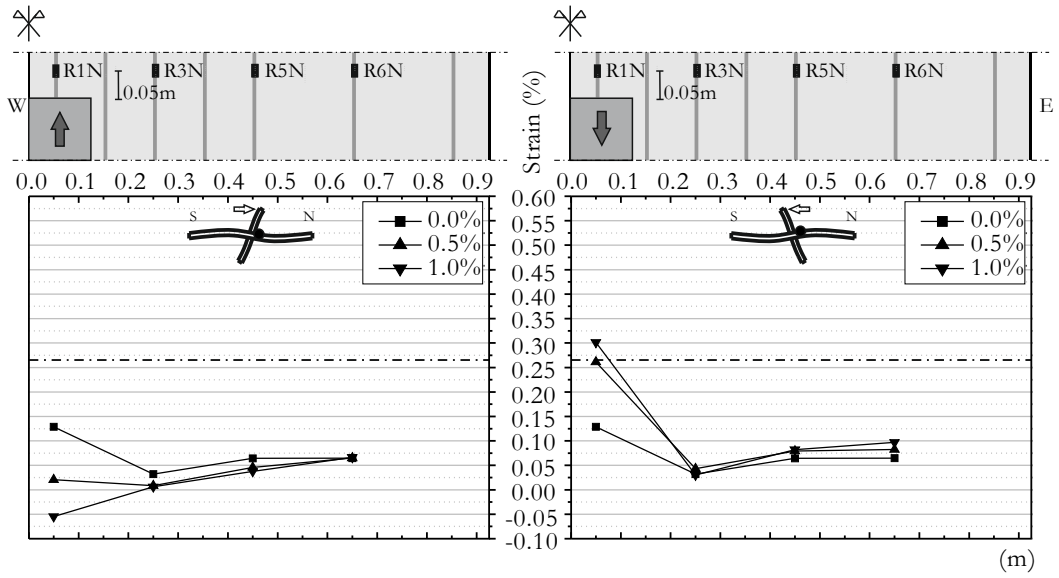

Figure 4.21: Strains in the top flexural reinforcement of the C-50 specimen.

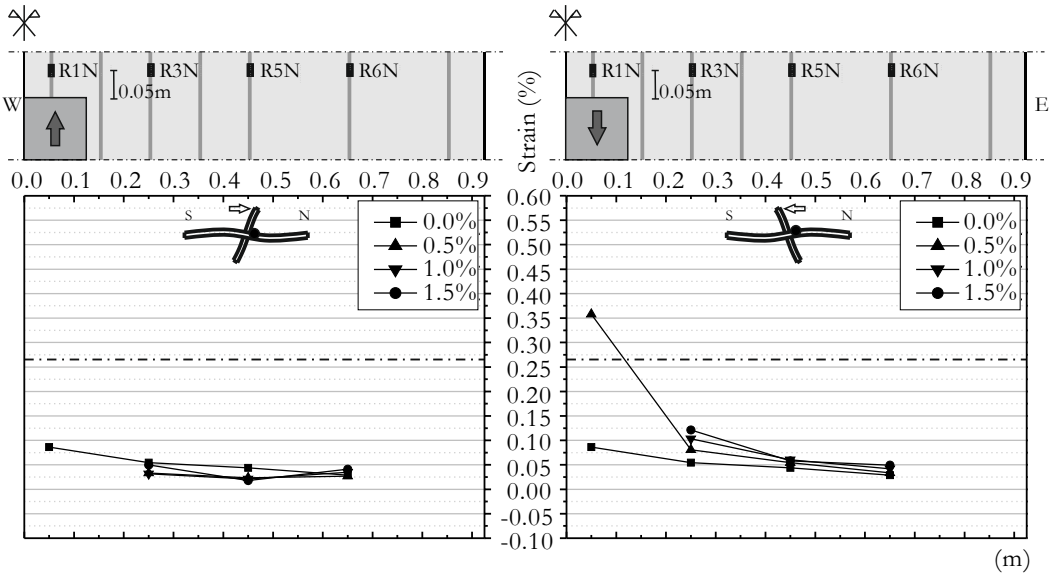

Figure 4.22: Strains in the top flexural reinforcement of the C-40 specimen.

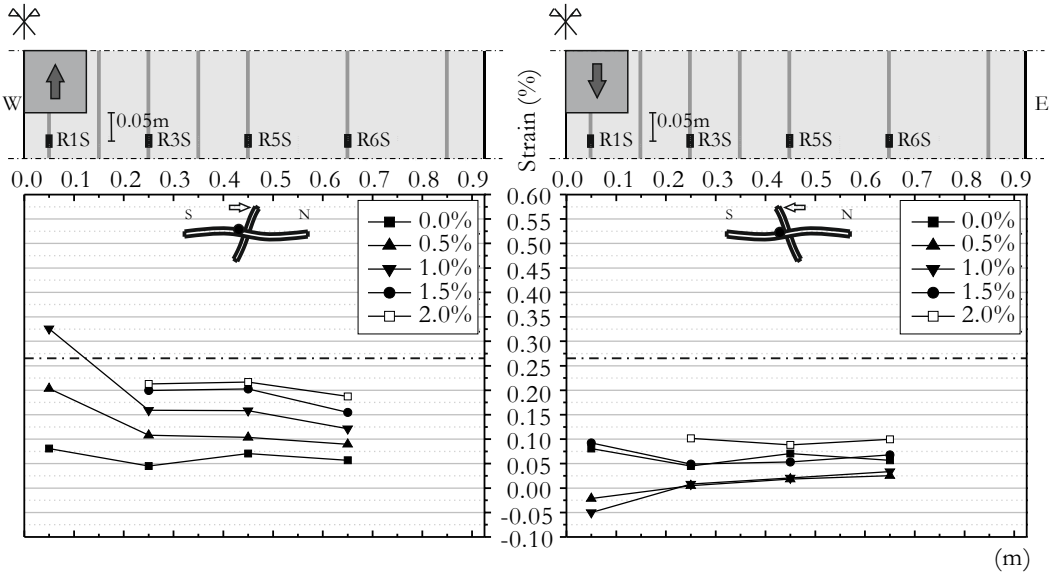

Figure 4.23: Strains in the top flexural reinforcement of the C-30 specimen.

4.2.3 Specimens C-50 BR and C-50 BC

The C-50 BR and C-50 BC, consisting in the specimens strengthened with post-installed shear bolts, were tested following the same procedure as the previously referred cyclic tests.

Failure modes

The saw cuts depicted in Figures 4.24 and 4.25, suggest that the typical punching failure was avoided. Instead, a kind of plastic hinge was formed due to progressive slab degradation in the region of the column.

For the target gravity load, both specimens presented flexural cracking in the top surface in the vicinity of the column. At the N and S edges, where the mid span of the slab was simulated, smaller flexural cracks were visible at the bottom surface.

The imposition of the cyclic horizontal displacement at the top of the column followed the already referred protocol, starting in the South (S) direction. This action unbalanced the bending moment at the slab column connection, increasing the negative bending moment in the N side while decreasing it in the opposite side of the column. Imposed displacements in the North (N) direction had a symmetric behaviour.

Similar failure modes were achieved for both tested specimens. Figures 4.24 and 4.25 show that both failure zones are constricted to an area close to the slab column connection. C-50 BR presented a slightly wider failure zone with the damaged area presenting a slight slant from the vertical plane. This is a localized damage that happened in between the bolts. The second tested specimen, C-50 BC, had the bolts closer to each other in the N-S axis (three lines of three bolts), leading to less visible damage in the saw cut alignment. The failure occurred by concrete crushing in the area surrounding the slab column connection due to the combined action of vertical and cyclic horizontal forces. Those actions slowly deteriorate the concrete by cyclically opening and closing the main flexural cracks that appeared right next to the column. Once the concrete was damaged the mechanisms needed to resist shear forces were no longer possible, as well as the moment transfer from the column to the slab. The shear bolts were effective in preventing a typical punching failure.

Figure 4.24: Saw cut (N-S) of the C-50 BR specimen.

Figure 4.25: Saw cut (N-S) of the C-50 BC specimen.

The hysteretic graphs (Figures 4.26 and 4.27) show that both bolt strengthened specimens present a similar hysteretic behaviour. C-50 BC performed better, achieving 1.0% more maximum horizontal drift (although, marginally) and a slightly higher maximum horizontal load. The loss of horizontal load was more drastic in the C-50 BR resulting in a lower energy dissipation capacity.

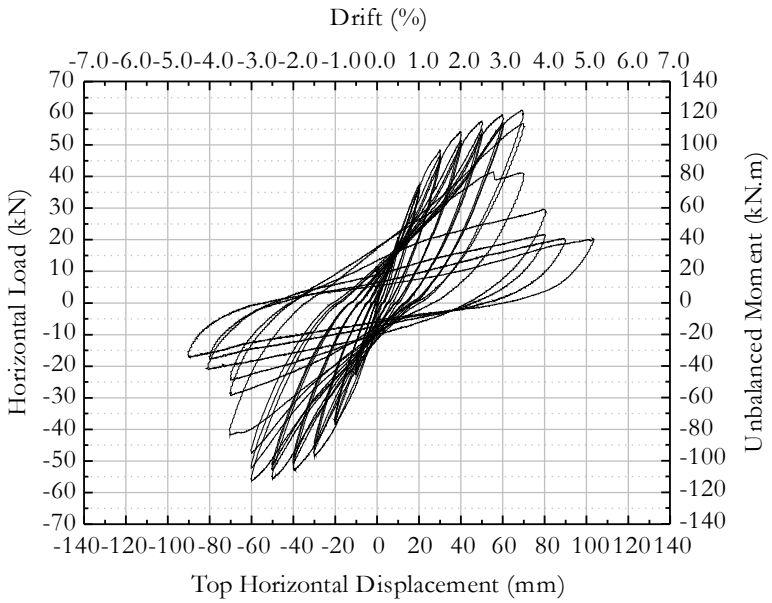

Figure 4.26: Hysteretic chart of the C-50 BR specimen.

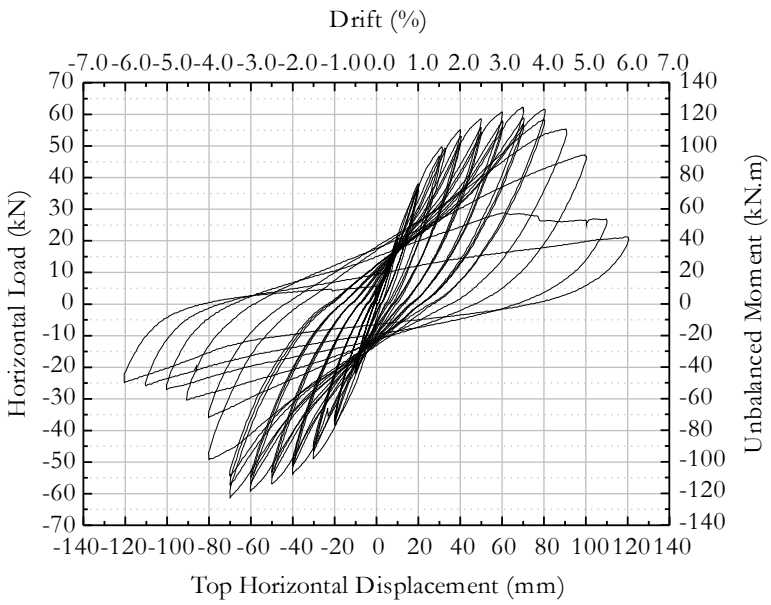

Figure 4.27: Hysteretic chart of the C-50 BC specimen.

The post failure pictures from Figures 4.28 and 4.29 show the surface damage of both specimens and puncture from the shear bolts. The better performance from C-50 BC is due to the closer distance between the bolts in the orthogonal directions and the fact that the outer bolt lines (bolts 4, 5, 6 and their symmetric) were positioned right next to the longitudinal reinforcement bars (Figure 3.15), preventing the bolts from penetrating through the damaged concrete. Failure information is compiled in Table 4.1.

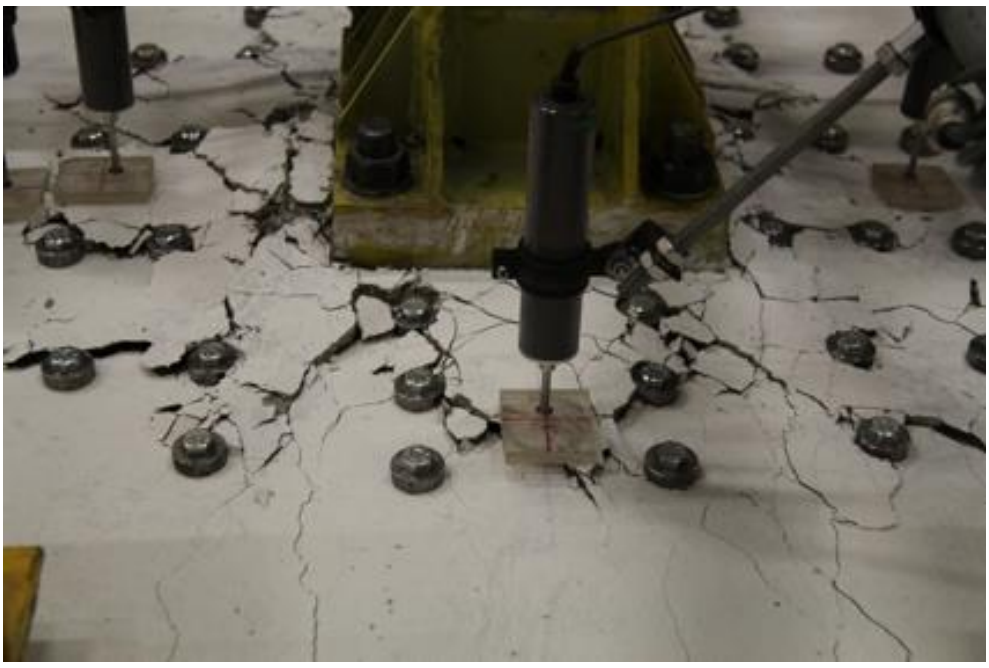

Figure 4.28: Post failure at the vicinity of the column of the C-50 BR specimen.

Figure 4.29: Post failure at the vicinity of the column of the C-50 BC specimen.

Vertical deformation

The displacement transducers placed along the N-S axis allowed to monitor the vertical deformation of that axis during the test. Because the achieved drifts were higher than anticipated, the maximum range of the available transducers was insufficient to measure those displacements for drifts higher than 3.0% and 2.5% for specimens C-50 BR and C-50 BC, respectively. The obtained data is shown in Figures 4.30 and 4.31. Longitudinal outlines for the vertical load only (0.0% drift) and for the combined action of vertical and horizontal loads are shown, for every first South peak of each drift step. Both C-50 BR and C-50 BC show a similar behaviour in the shown drift range, presenting similar vertical deformations for the same steps, which corroborates the data from the hysteretic charts from Figures 4.26 and 4.27.

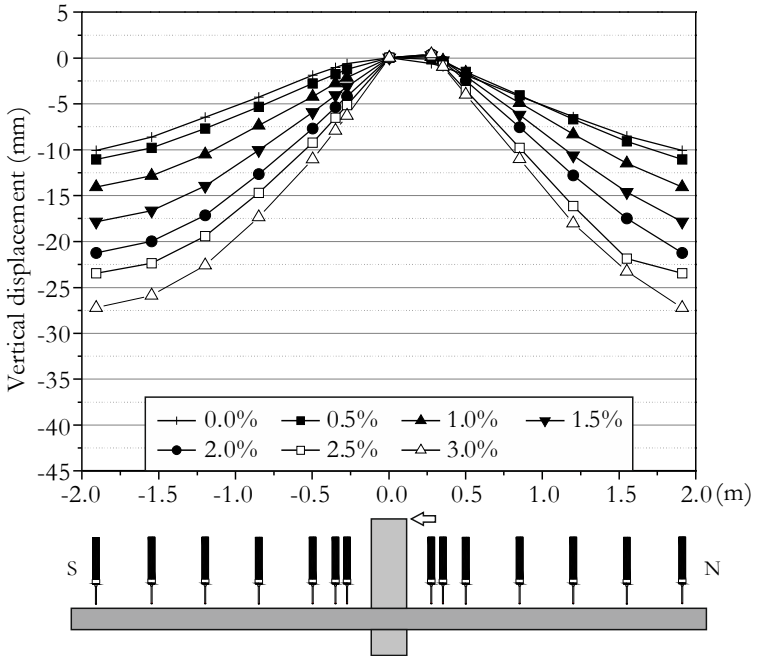

Figure 4.30: Vertical displacement of the N-S axis of the C-50 BR specimen.

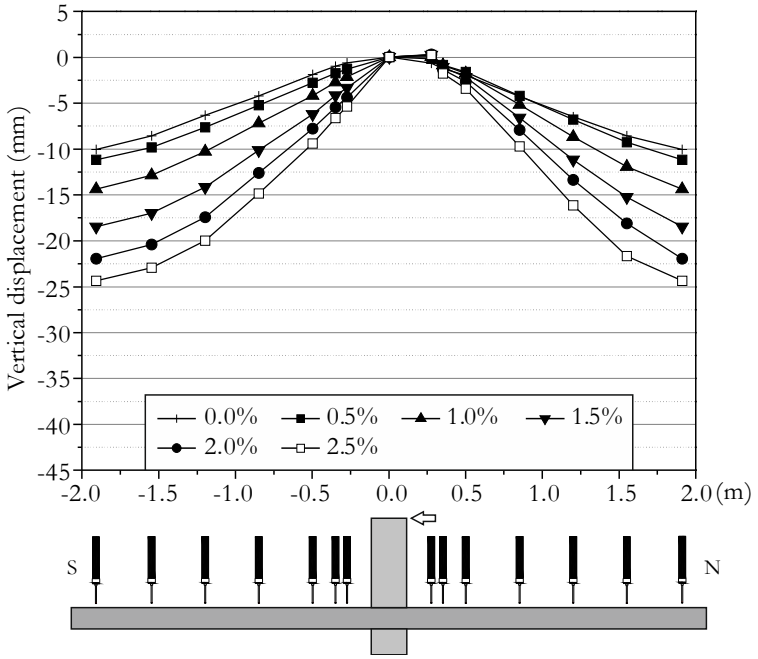

Figure 4.31: Vertical displacement of the N-S axis of the C-50 BC specimen.

The information from the vertical displacement transducers was used to calculate the position of the inflection lines in the N-S axis. Usable information was only attained for drift cycles up to 2.0% and 2.5% for C-50 BR and C-50 BC, respectively. Figures 4.32 and 4.33 show that, for both specimens, North and South inflection lines were at about 25% of the total span of the slab, which is a good approximation for the theoretical value of 22% of the total span. Once more, a very similar behaviour is shown for both specimens. Throughout

the test, the inflection lines move according to the application of the imposed horizontal displacements, justifying the appearance of bending cracks in the bottom surface of the specimen from the mid-span to the quarter-span section, as shown in Figure 4.34. For drift steps higher than 2.0% the inflection lines reached the column, which suggests a bending moment inversion due to the moment induced by the horizontal load being larger in magnitude than the negative bending moment in the slab due to the gravity load. This phenomenon results in different signal of the moments in both sides of the column.

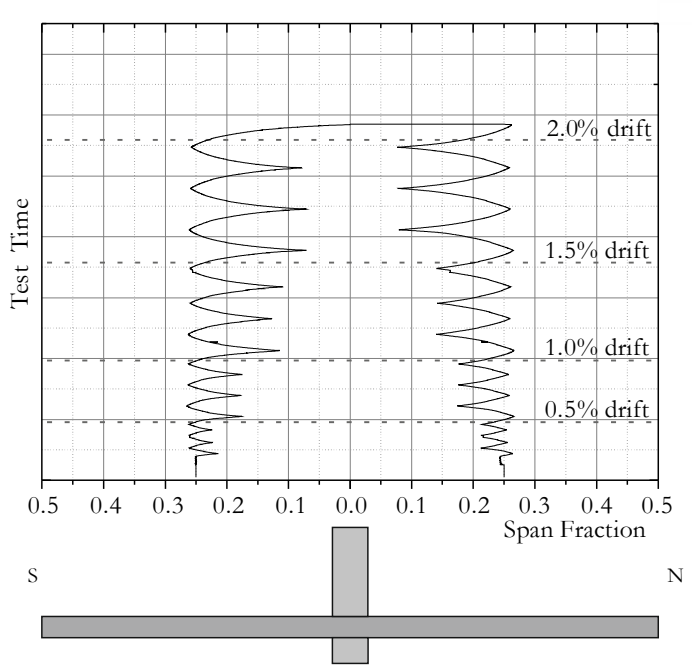

Figure 4.32: Position of the zero moment point in the N-S axis of the C-50 BR specimen.

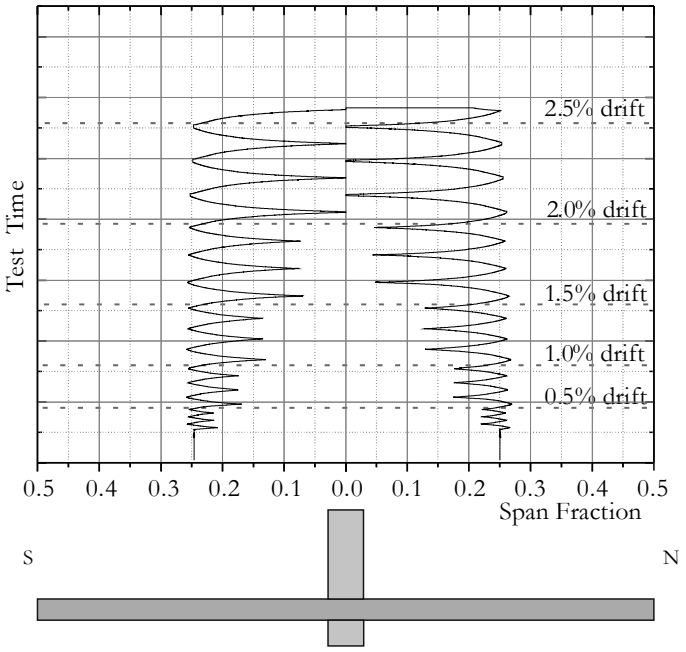

Figure 4.33: Position of the zero moment point in the N-S axis of the C-50 BC specimen.

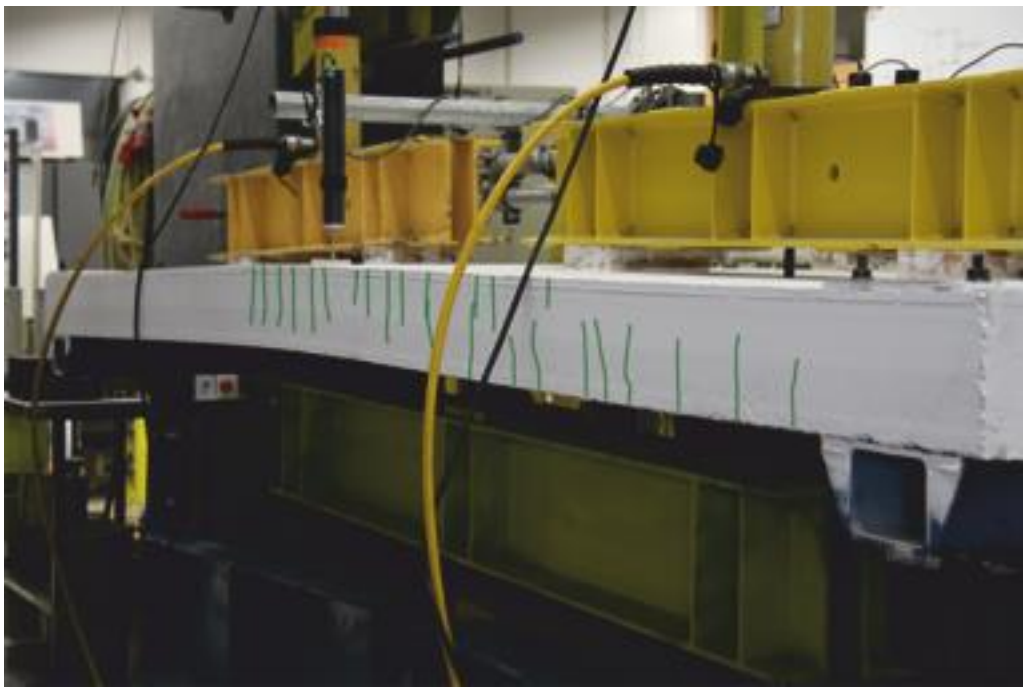

Figure 4.34: Bending cracks at the bottom side of the C-50 BR specimen.

Flexural reinforcement strains

Figures 4.35 and 4.36 show the strains in the South instrumented longitudinal reinforcement bars for the gravity load only, as well as for the first peaks in each North and South drift

steps. The strain gauge pair that was placed in the R1S position in specimen C-50 BC failed making it impossible to retrieve information. Both specimens presented similar strains for the gravity load only (0.0% drift) with the reinforcement bars closer to the column presenting higher strains, though, without yielding. The instrumented reinforcement bar closer to the column was the most susceptible to the cyclic horizontal action, as expressed by the amplitude of the opposed peaks. This effect gradually decreases with the increase of the distance from the column. The most stressed instrumented reinforcement bar from C-50 BR yielded for the first drift step. For the 1.5% drift step, the same bar reached compression when the imposed displacement was in its direction. As the test progressed, the strain gauges progressively failed, however, it was possible to see that almost all instrumented reinforced bars yielded for the last measured drift step (1.5%). Those results suggest that for further drift steps, all reinforcement bars in the East-West axis yielded.

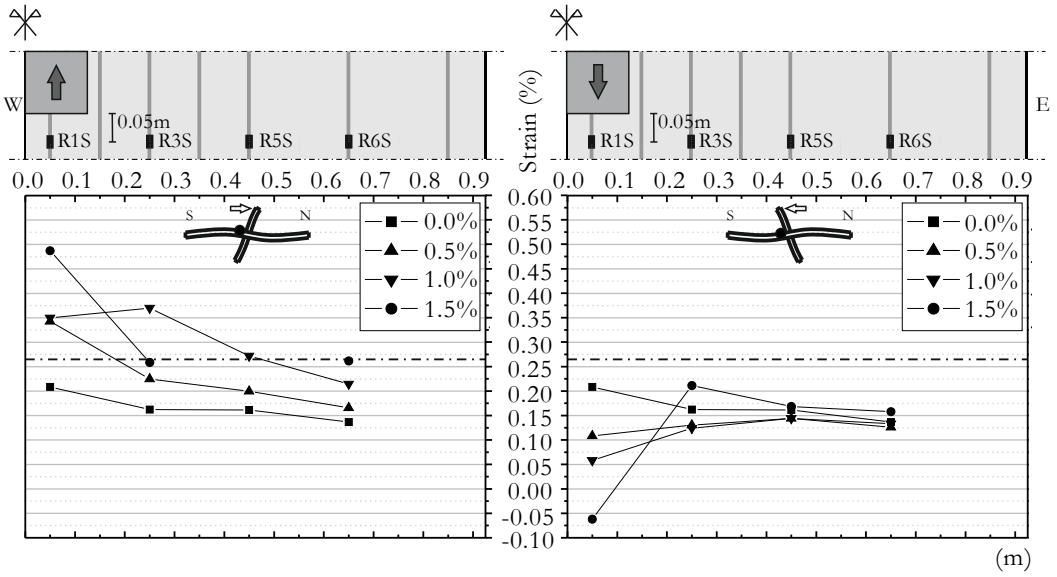

Figure 4.35: Strains in the top flexural reinforcement of the C-50 BR specimen.

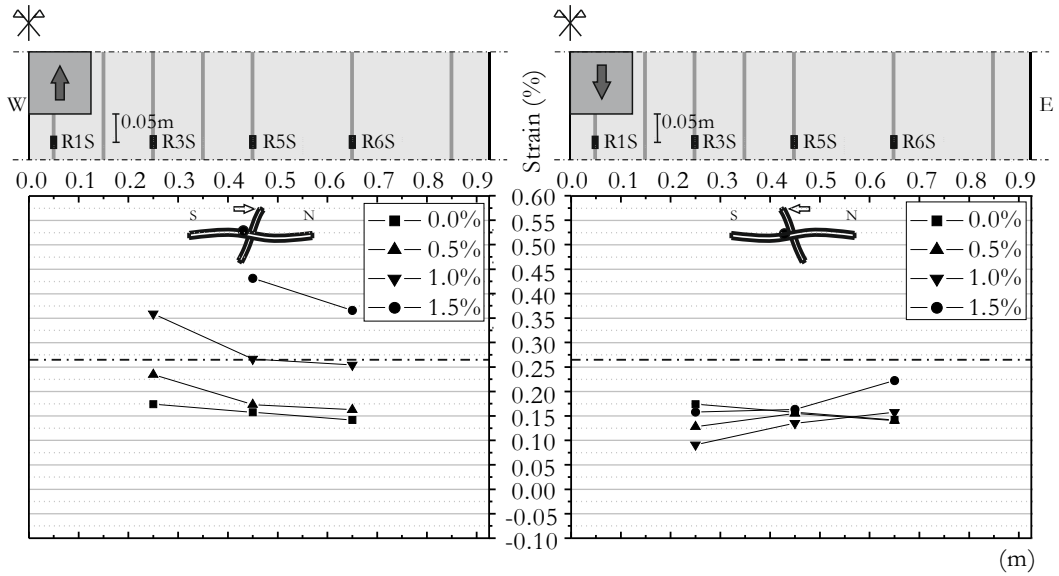

Figure 4.36: Strains in the top flexural reinforcement of the C-50 BC specimen.

Shear reinforcement strains

As depicted in Figure 3.23, two lines of bolts from each side of the column were instrumented in the tested specimens. For a better comparison, variations in strain from the initial strain corresponding to the initial prestress of 160 MPa per bolt are presented in Figures 4.37 and 4.38. Because the holes were not injected, the bolts were anchored only by the extremities, hence, the measured strains are constant along the length of the bolt.

As expected, the bolts at the side of the column, contrary to the imposed displacement, presented a significant increase in strain while, in some cases, the bolts in the opposite side of the column show some decompression. The S3 bolt from C-50 BR appeared to show decompression throughout the test, however, this may be the result of the strain gauge getting loose from the bolt surface. Both C-50 BR and C-50 BC behaved similarly with the bolts near to the corner of the column (S5 and N5 for C-50 BR and S6 and N6 for C-50 BC) presenting the higher strain variations than the ones closer to the N-S axis (S3 and N3). In the C-50 BR, the first layer of bolts is the one that depicts the higher strain variations, with the remaining layers staying almost constant throughout the test. For the C-50 BC, the first layer is also the most strained, although, the second layer is also mobilized. This specimen depicted a more even strain distribution.

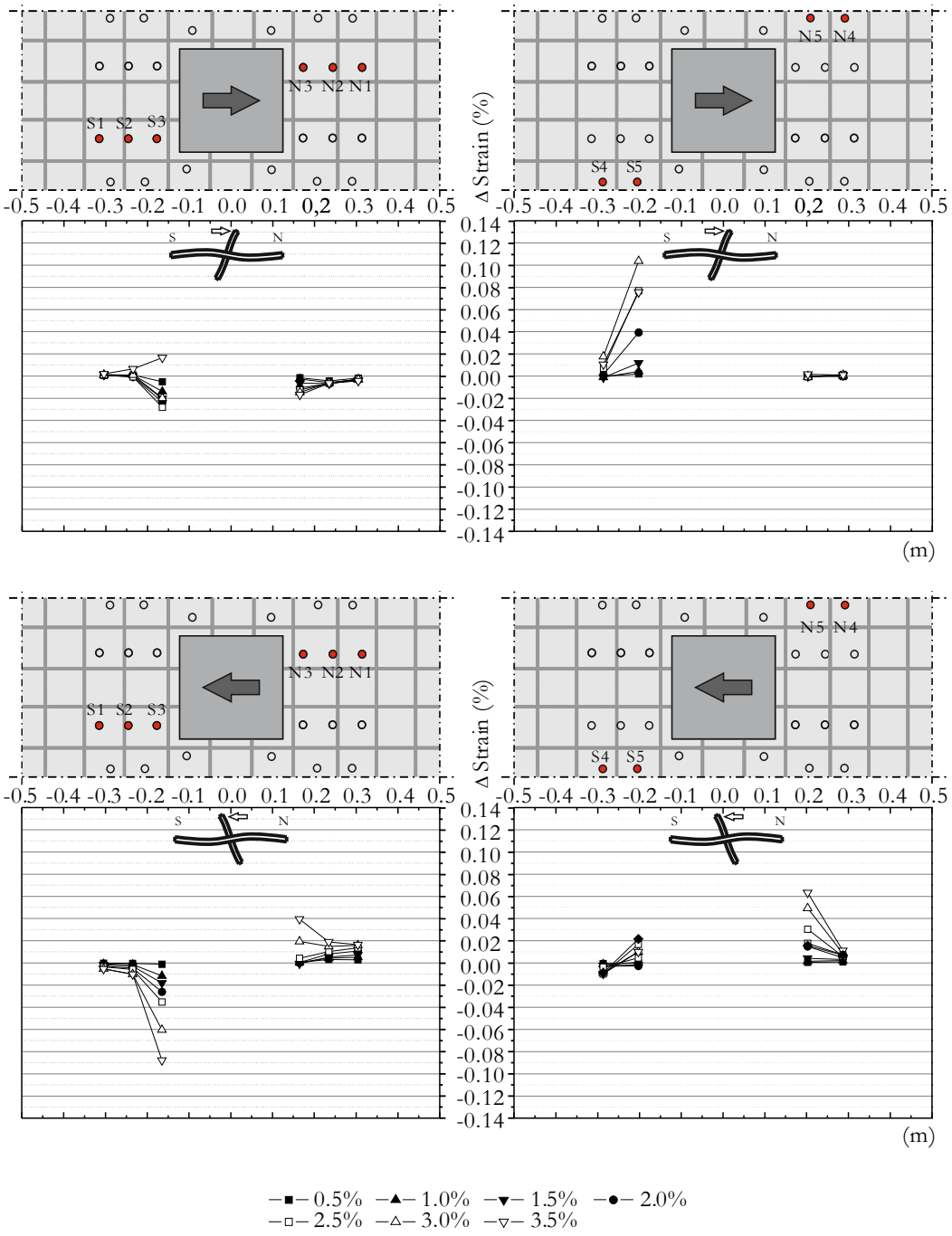

Figure 4.37: Strains in the shear reinforcement bolts of the C-50 BR specimen.

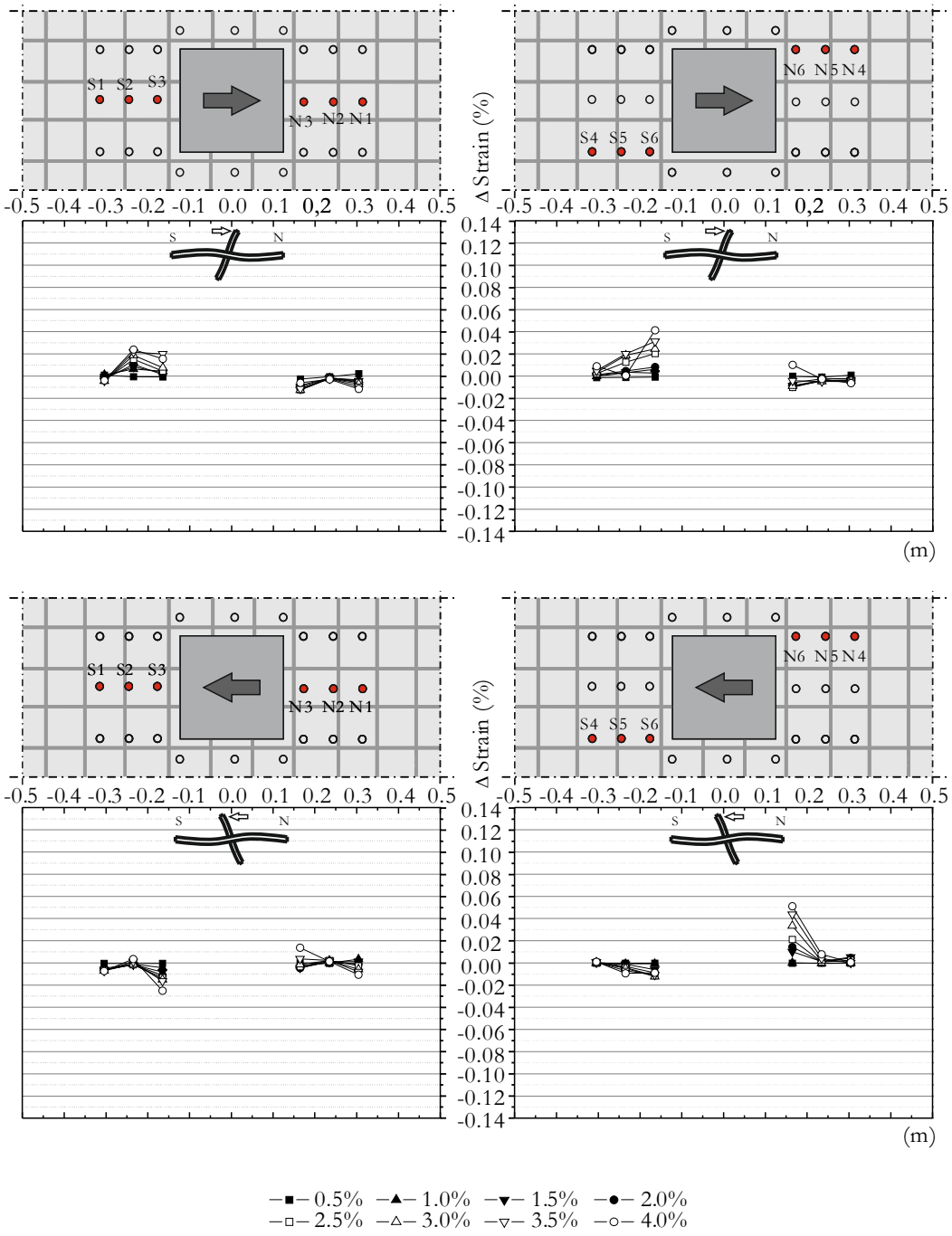

Figure 4.38: Strains in the shear reinforcement bolts of the C-50 BC specimen.

The small strain variation in the second layer and the high strain variations of the first layer from both specimens suggests that no shear crack was formed and all the damage was contained in the vicinity of the column, which corroborates the analysis of the saw cuts from Figures 4.24 and 4.25.

4.2.4 Specimens C-50 STR1, C-50 STR2, C-50 STR3 and C-50 STR4

The specimens presented in this section were tested using the same protocol used in the other cyclically tested specimens, consisting in the application of a vertical load that was kept constant, followed by the imposition of increasing reversed horizontal displacements at the top of the column. The first imposed displacement was in the South (S) direction, increasing the negative bending moment in the North (N) side of the column and decreasing it in the South side. This effect was reversed when a North direction displacement was imposed.

Failure modes

All specimens presented a punching failure except the C-50 STR4, where a plastic hinge was formed. All specimens presented top flexural cracking in the column region for the target vertical load and small cracks in the lower side at the North and South edges due to positive bending moment. Since all specimens were subjected to similar vertical loads, the cracking pattern was also similar.

From the specimen saw cuts shown in Figures 4.39, 4.40, 4.41, and 4.42 different failure modes were observed. Both C-50 STR1 and C-50 STR2 (Figures 4.39 and 4.40, respectively) failed by punching, outside the zone where the shear reinforcement was located. In Figure 4.39 a diagonal shear crack crossing the stirrups can also be observed. These results suggest that an interior failure was imminent, however the failure surface is clearly outside the stirrup zone. The higher cross section of the stirrups in the C-50 STR2 specimen was more efficient at controlling shear cracking, preventing the opening of the interior shear crack. Specimen C-50 STR3 (Figure 4.41) failed by punching inside the shear reinforced area as the smaller shear reinforcement ratio was unable to prevent the punching failure where some stirrups failed. The final test specimen, C-50 STR4 (Figure 4.42), presented failure by concrete crushing in the slab-column connection. In this case, the amount of shear reinforcement combined with the higher number of layers, were able to prevent the typical punching failure.

Figure 4.39: Saw cut (N-S) of the C-50 STR1 specimen.

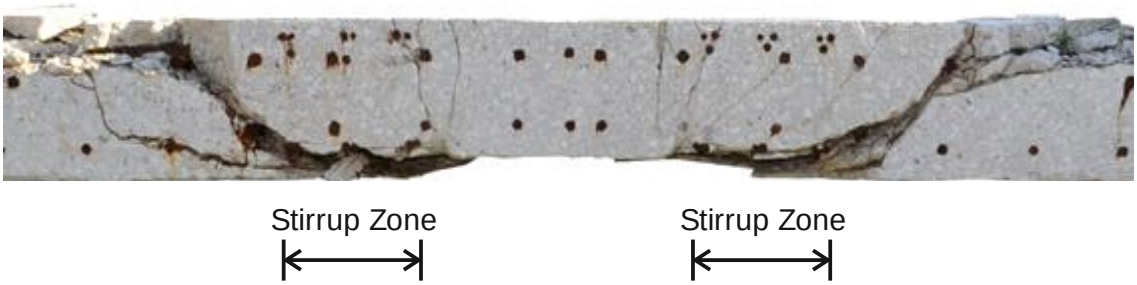

Figure 4.40: Saw cut (N-S) of the C-50 STR2 specimen.

Figure 4.41: Saw cut (N-S) of the C-50 STR3 specimen.

Figure 4.42: Saw cut (N-S) of the C-50 STR4 specimen.

The saw cuts from Figures 4.41 and 4.42 show that, due to manufacturing imprecisions, the stirrups were placed further from the column than the design distance. Also, the stirrups in the C-50 STR4 were longer than specified, reaching closer to the bottom of the slab. The influence of these manufacturing imprecisions will be addressed further.

Comparing the C-50 STR1 and C-50 STR2 hysteretic charts in Figures 4.43 and 4.44 no significant differences were observed besides the fact that the C-50 STR2 specimen was able to fulfil a complete cycle at 3.0% drift whereas C-50 STR1 was not. This happened because both specimens failed by punching outside the shear reinforcement area, so the increase in the cross section of the reinforcement was not completely mobilized. In Figure 4.45 an increase in the maximum horizontal load for C-50 STR3, when compared to the previous specimens, is depicted. In this case, the shear reinforcement effect was noticeable and more cycles were achieved. Nevertheless, the narrowness of the hysteretic charts suggests a low

energy dissipation capacity by all specimens that failed due to punching. The final tested specimen, C-50 STR4, had a behaviour like that of the C-50 STR3 specimen until the 3.0% drift step was reached. From that moment on, punching failure was avoided due to the higher shear reinforcement ratio, and a progressive loss of stiffness was depicted (Figure 4.46) instead of the brittle failure observed in the other tested specimens. This behaviour also led to a higher energy dissipation. These results are summarised in Table 4.1.

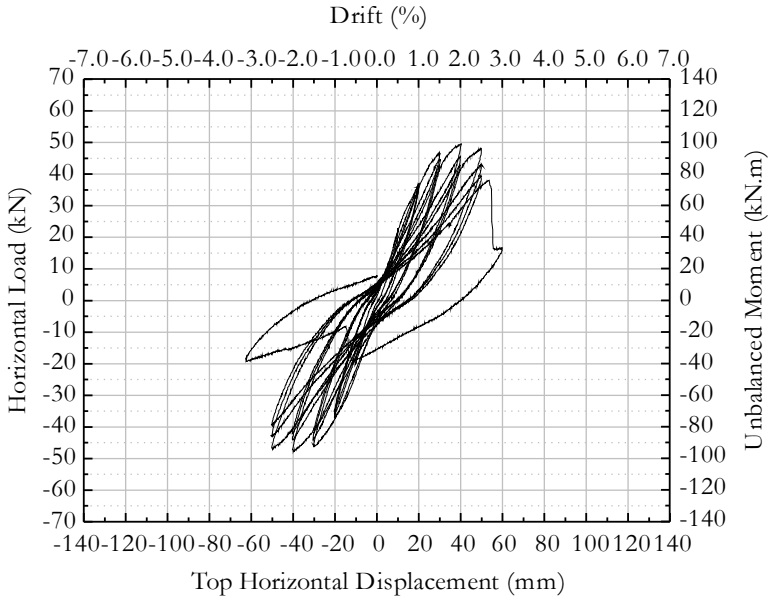

Figure 4.43: Hysteretic chart of the C-50 STR1 specimen.

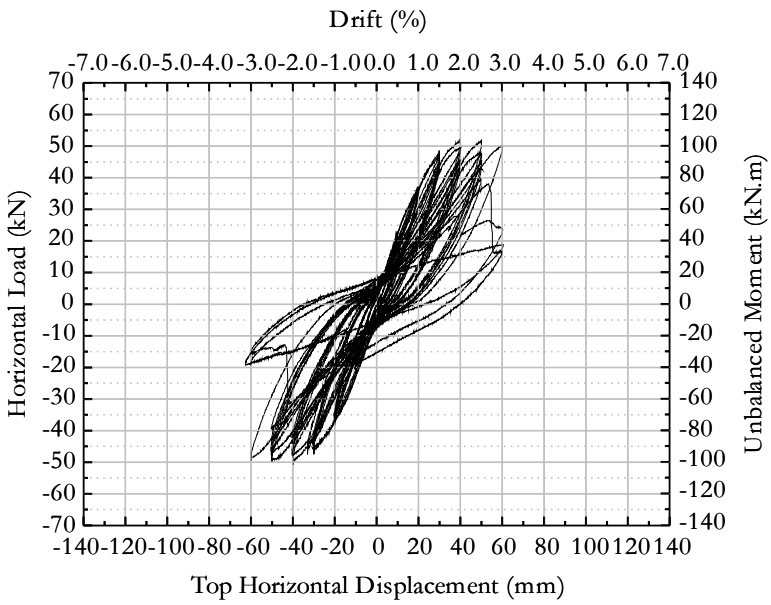

Figure 4.44: Hysteretic chart of the C-50 STR2 specimen.

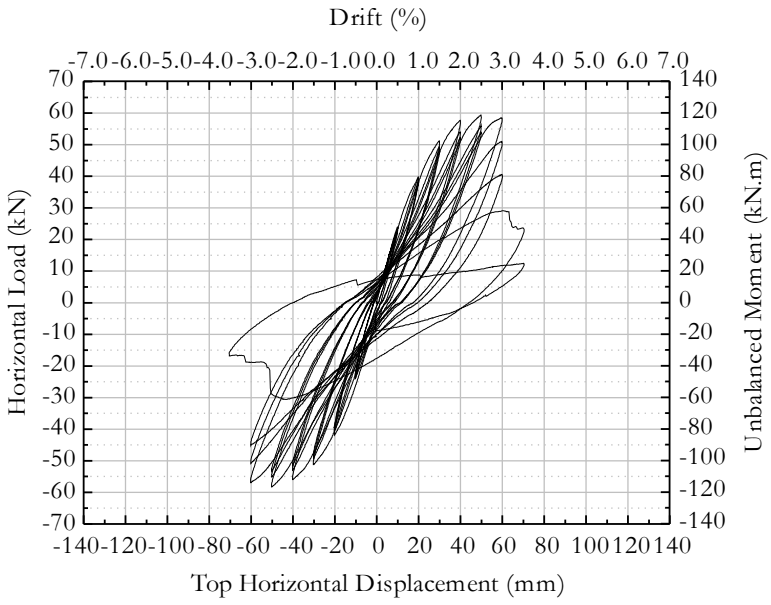

Figure 4.45: Hysteretic chart of the C-50 STR3 specimen.

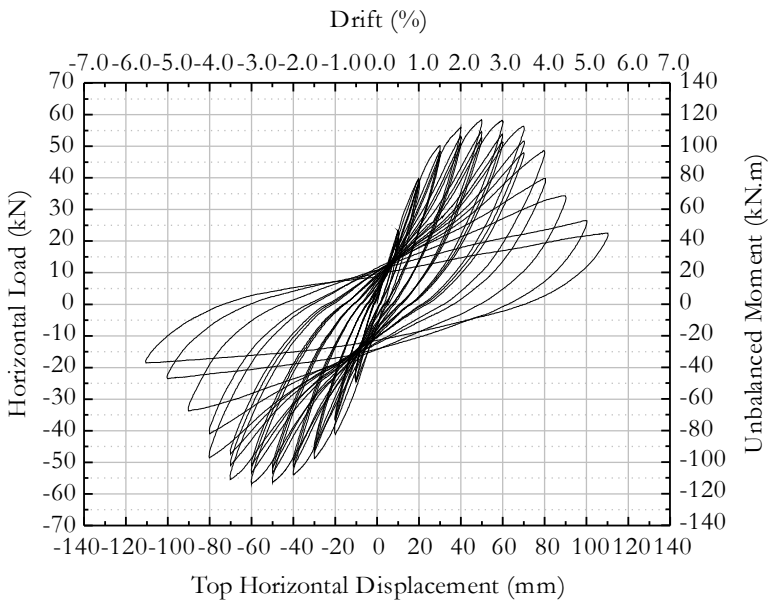

Figure 4.46: Hysteretic chart of the C-50 STR4 specimen.

Vertical deformation

The deformations of the slabs along the N-S axis for the vertical load and for different horizontal drifts are shown in Figures 4.47, 4.48, 4.49, and 4.50. The first stage (0.0%) refers to the completion of the application of the vertical load, before the horizontal displacements were applied. The following stages refer to the first time the specimen reached the respective horizontal drift (S side) due to the application of horizontal displacements at the top of the column. From Figures 4.47 to 4.50, a similar behaviour can be observed for the vertical load imposition phase, however, the specimens C-50 STR3 and C-50 STR4 present smaller vertical displacements at the edges, due to the use of real time control of the rotation compatibilization system as referred in Subchapter 3.3.3. Higher horizontal drifts result in higher vertical deformations under a constant vertical load, due to the decrease in stiffness caused by the cyclic action.

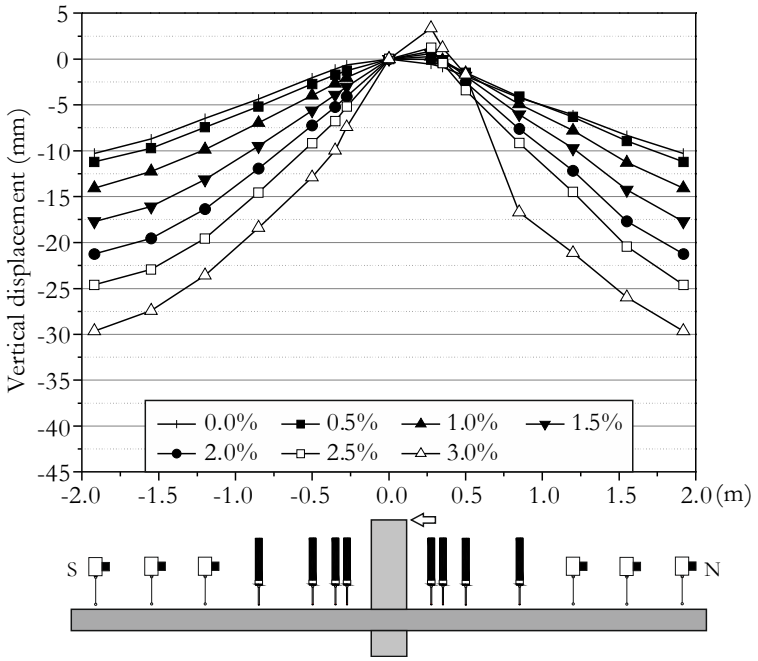

Figure 4.47: Vertical displacement of the N-S axis of the C-50 STR1 specimen.

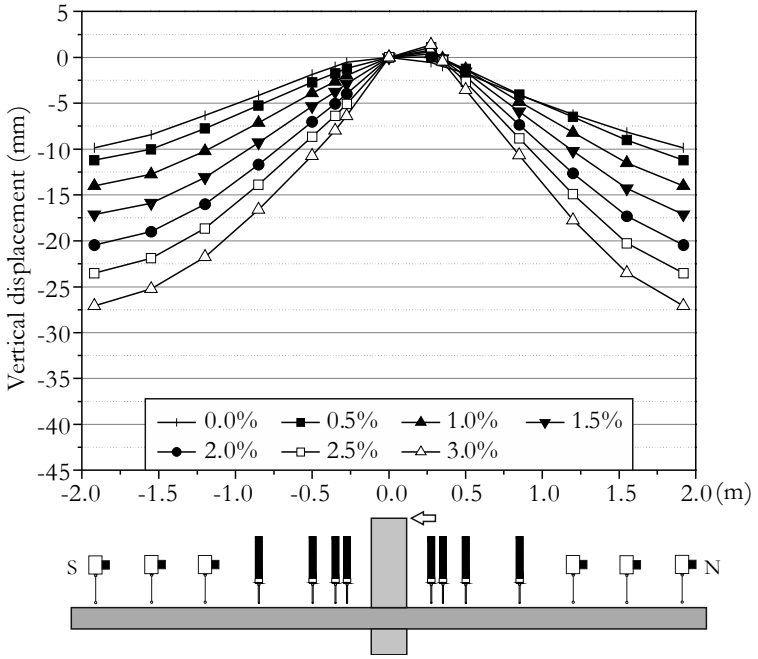

Figure 4.48: Vertical displacement of the N-S axis of the C-50 STR2 specimen.

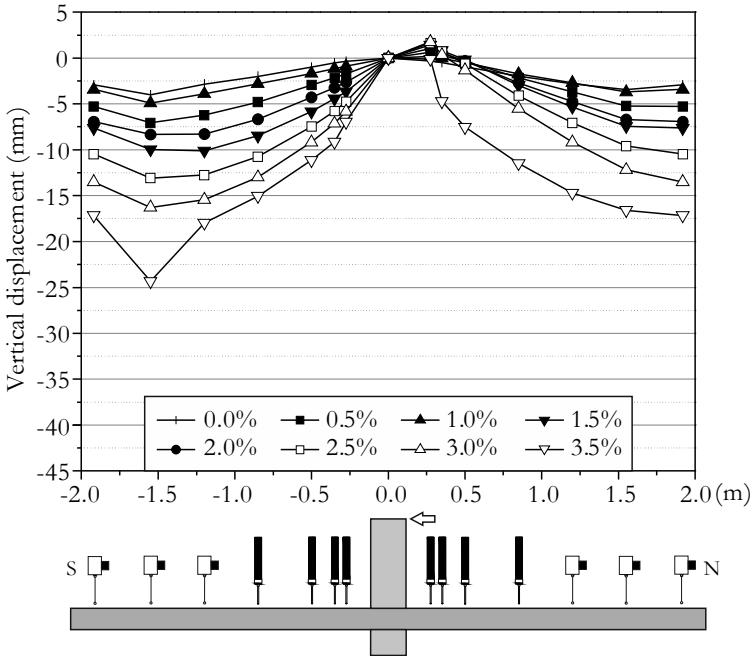

Figure 4.49: Vertical displacement of the N-S axis of the C-50 STR3 specimen.

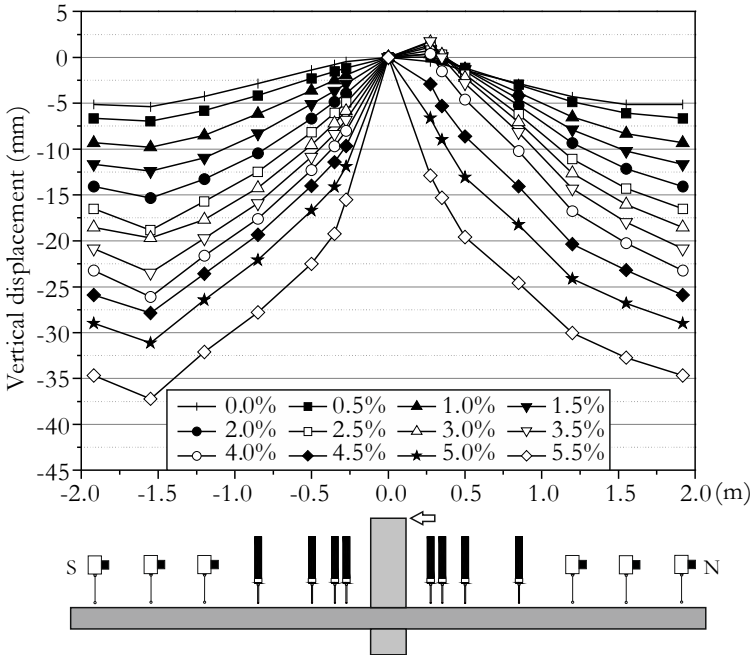

Figure 4.50: Vertical displacement of the N-S axis of the C-50 STR4 specimen.

Information about the inflection points was obtained from the vertical displacement transducers in the N-S axis and showed in Figures 4.51, 4.52, 4.53 and 4.54. The inflexion point position at each moment was computed through the approximate equation of the deformed shape of the specimen along the N-S axis for each side of the column. For the vertical load only, inflection lines were near 0.25 of the span for C-50 STR1 and C-50 STR2, and near 0.20 for C-50 STR3 and C-50 STR4, which are close to the expected theoretical

value of 0.22. These results show that the test setup is effective in representing the middle span simplification. When horizontal displacement takes place, the inflection line moves along the span. This information corroborates the observed and described cracking pattern in the inferior side of the specimen, which for higher drifts, cracks appear closer to the column region.

As the drift increases, the amplitude of the movement of the inflexion point increases because the moment due to vertical load loses magnitude when compared to the eccentrically induced moment. For higher horizontal drift ratios, a change in the bending moment signal can be observed in the vicinity of the column. This means that the moment due to the horizontal action is higher than the bending moment due to the vertical loading. This leads to opposite signal bending moments in opposite sides of the column.

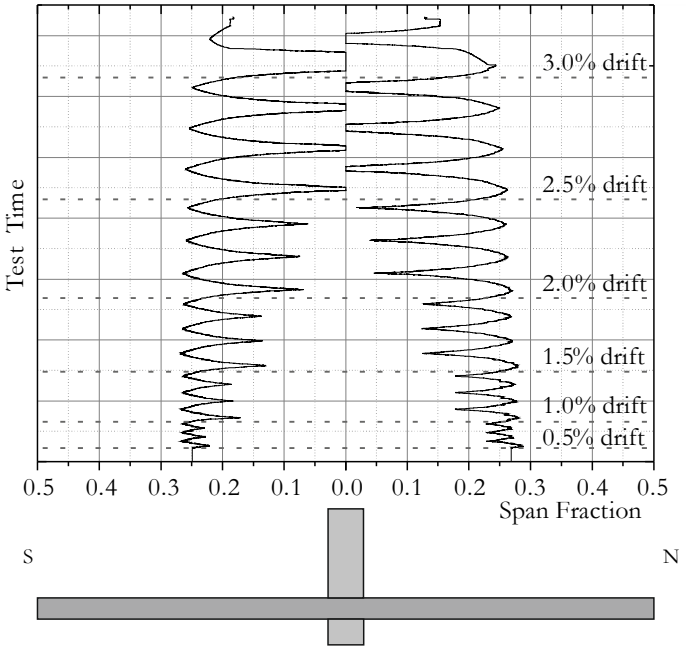

Figure 4.51: Position of the zero moment point in the N-S axis of the C-50 STR1 specimen.

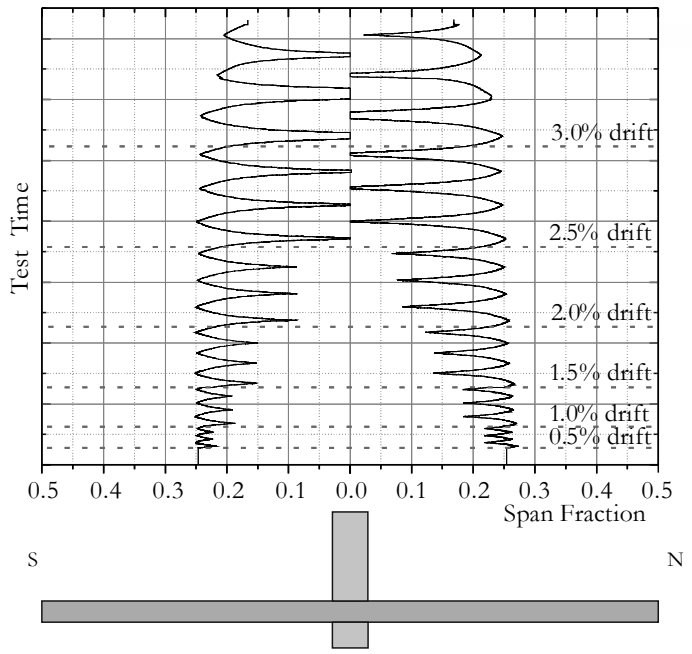

Figure 4.52: Position of the zero moment point in the N-S axis of the C-50 STR2 specimen.

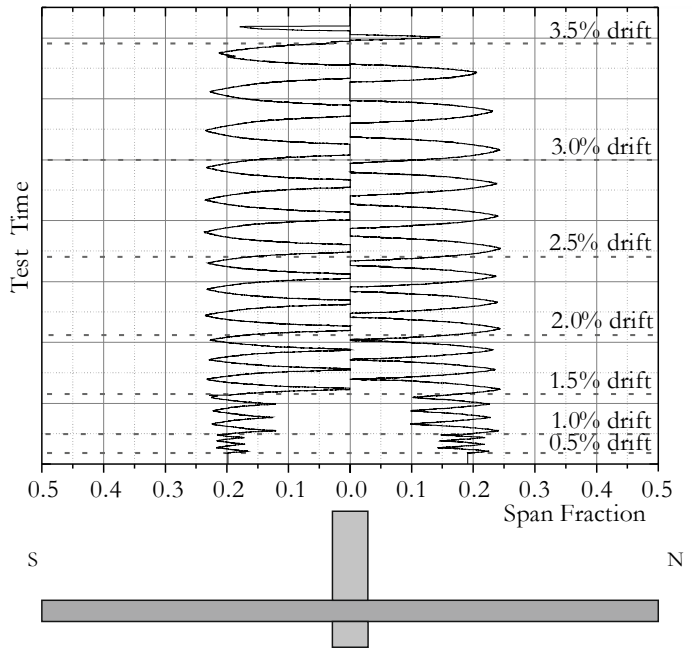

Figure 4.53: Position of the zero moment point in the N-S axis of the C-50 STR3 specimen.

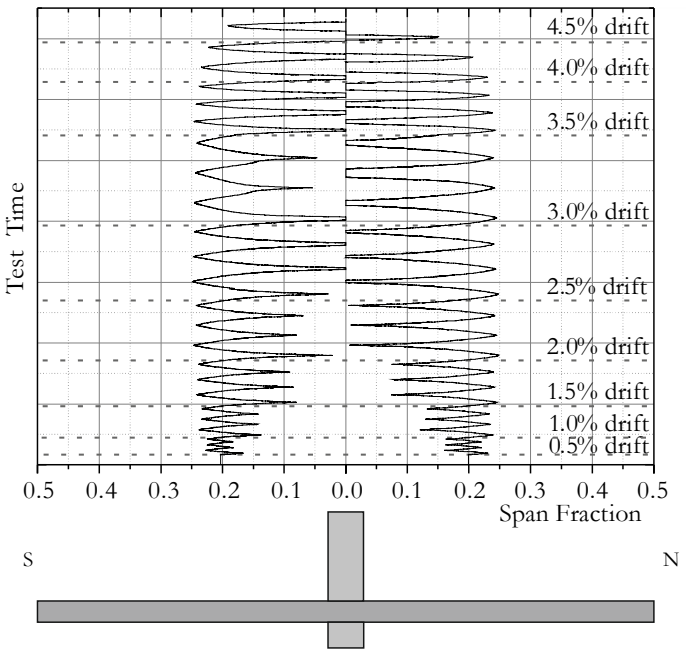

Figure 4.54: Position of the zero moment point in the N-S axis of the C-50 STR4 specimen.

Flexural reinforcement strains

At the end of the first phase (imposition of the vertical load) no reinforcement bars yielded, as can be seen by observing the points corresponding to 0.0% drift in Figures 4.55, 4.56, 4.57 and 4.58. It can also be seen that the closer to the column, the most stressed the reinforcement bars were.

The reinforcement bars closest to the column contribute the most for moment transfer from the column to the slab as they show a higher strain variation between opposite drift peaks. Reinforcement bars further from the column showed a smaller strain variation throughout the test. For imposed horizontal displacements, when strained, the reinforcement bars closer to the vicinity of the column yielded for the first 0.5% drift step. During the horizontal drift steps of 1.5% for C-50 STR1 and C-50 STR2 and 1.0% for C-50 STR3 and C-50 STR4, the upper reinforcement bars went into a compression state. This occurred because the magnitude of the negative bending moment from the vertical loads was smaller than that from the positive moment caused by the horizontal action. These results suggest a local bending moment inversion at the vicinity of the column, corroborated also by the stresses measured in the lower reinforcement bars, depicted in Figures 4.59 and 4.60.

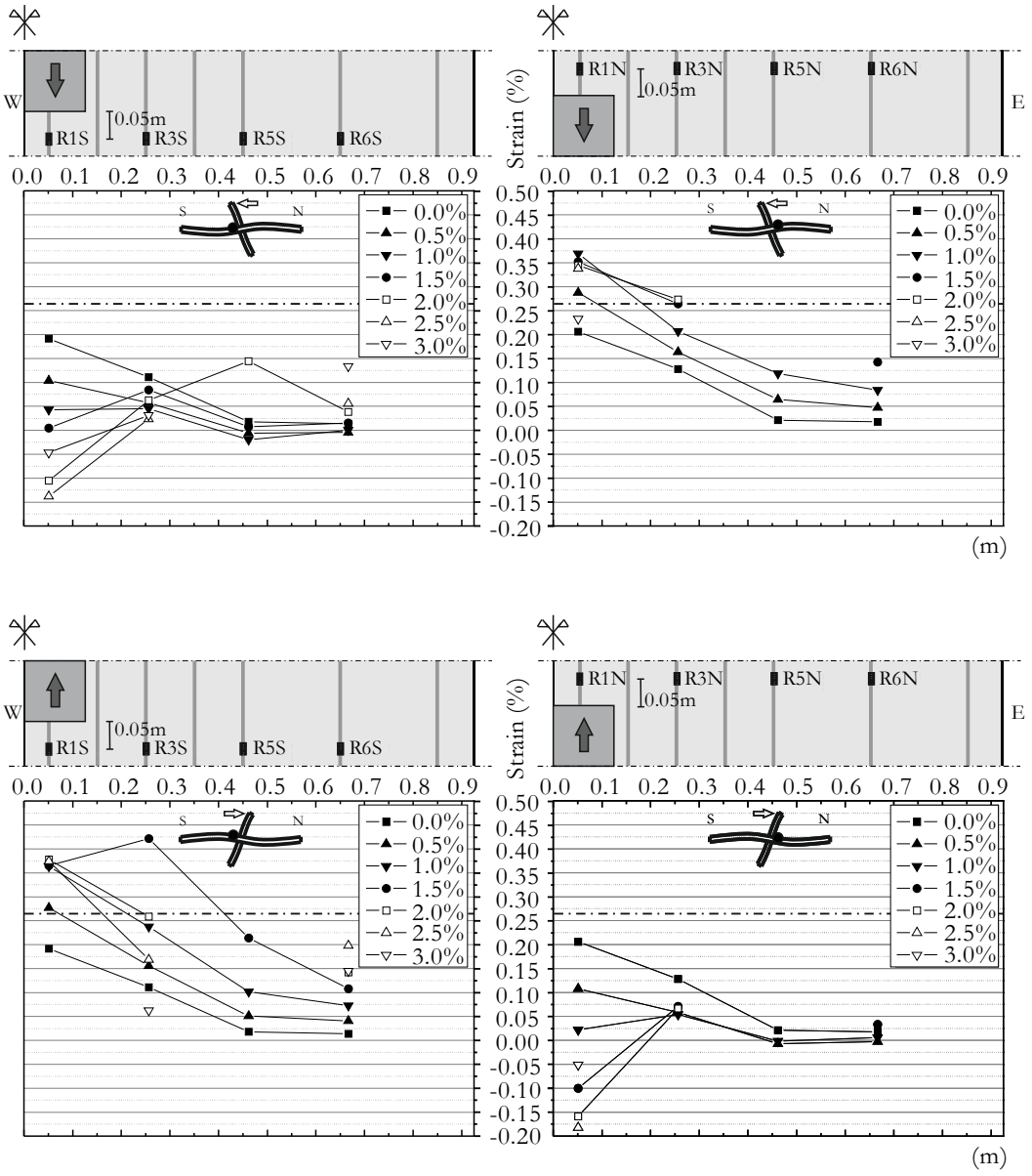

Figure 4.55: Strains in the top flexural reinforcement of the C-50 STR1 specimen.

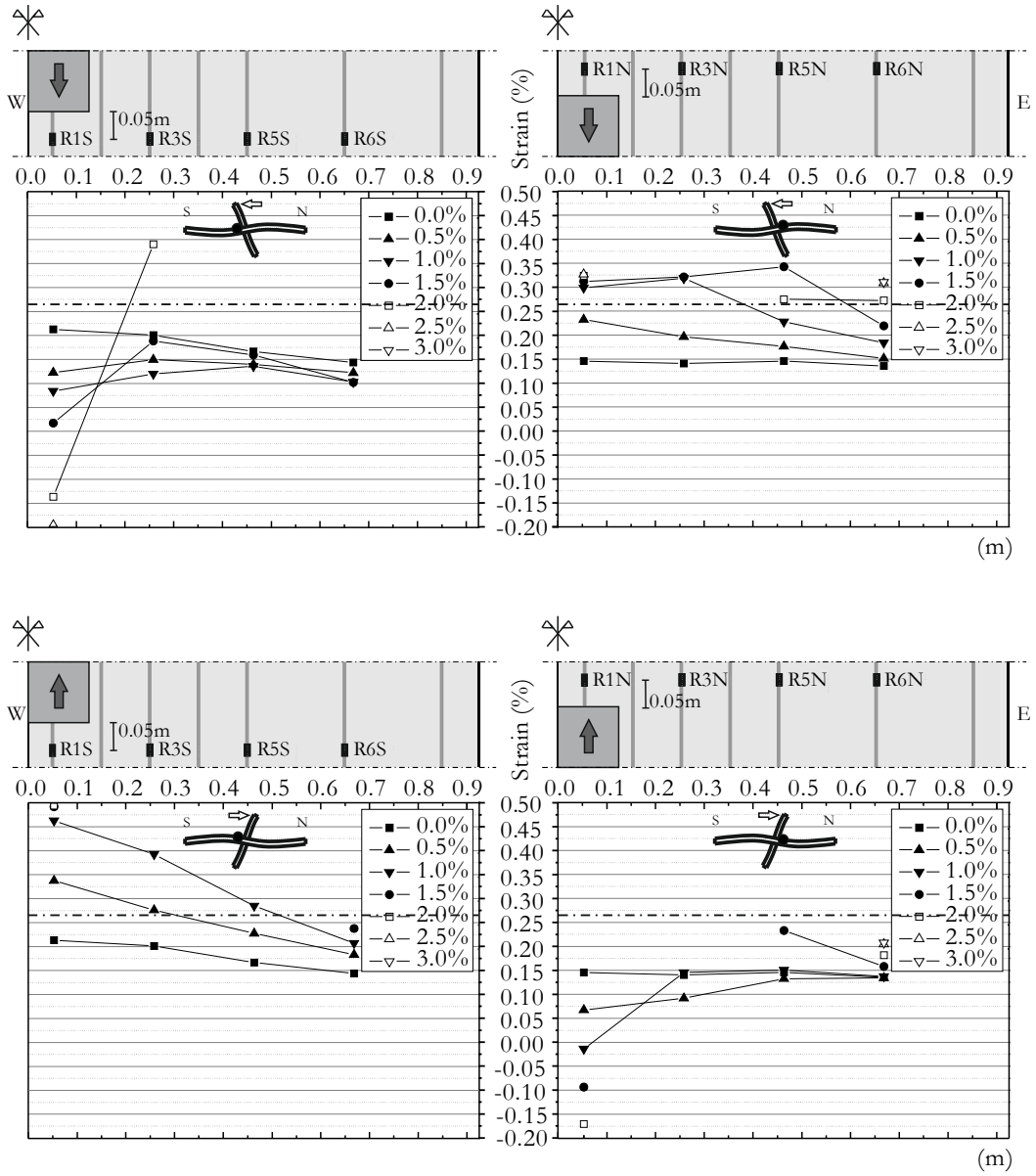

Figure 4.56: Strains in the top flexural reinforcement of the C-50 STR2 specimen.

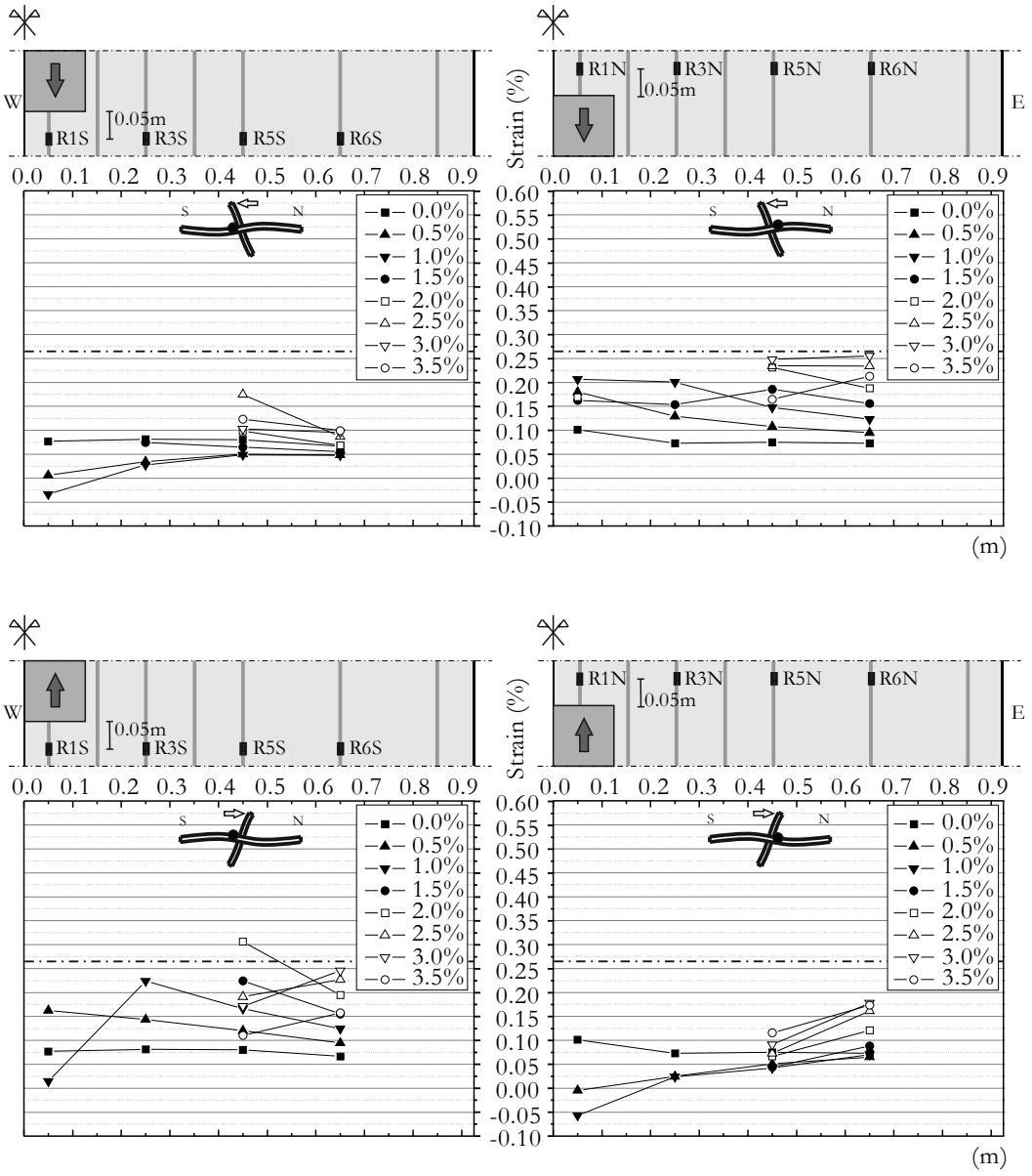

Figure 4.57: Strains in the top flexural reinforcement of the C-50 STR3 specimen.

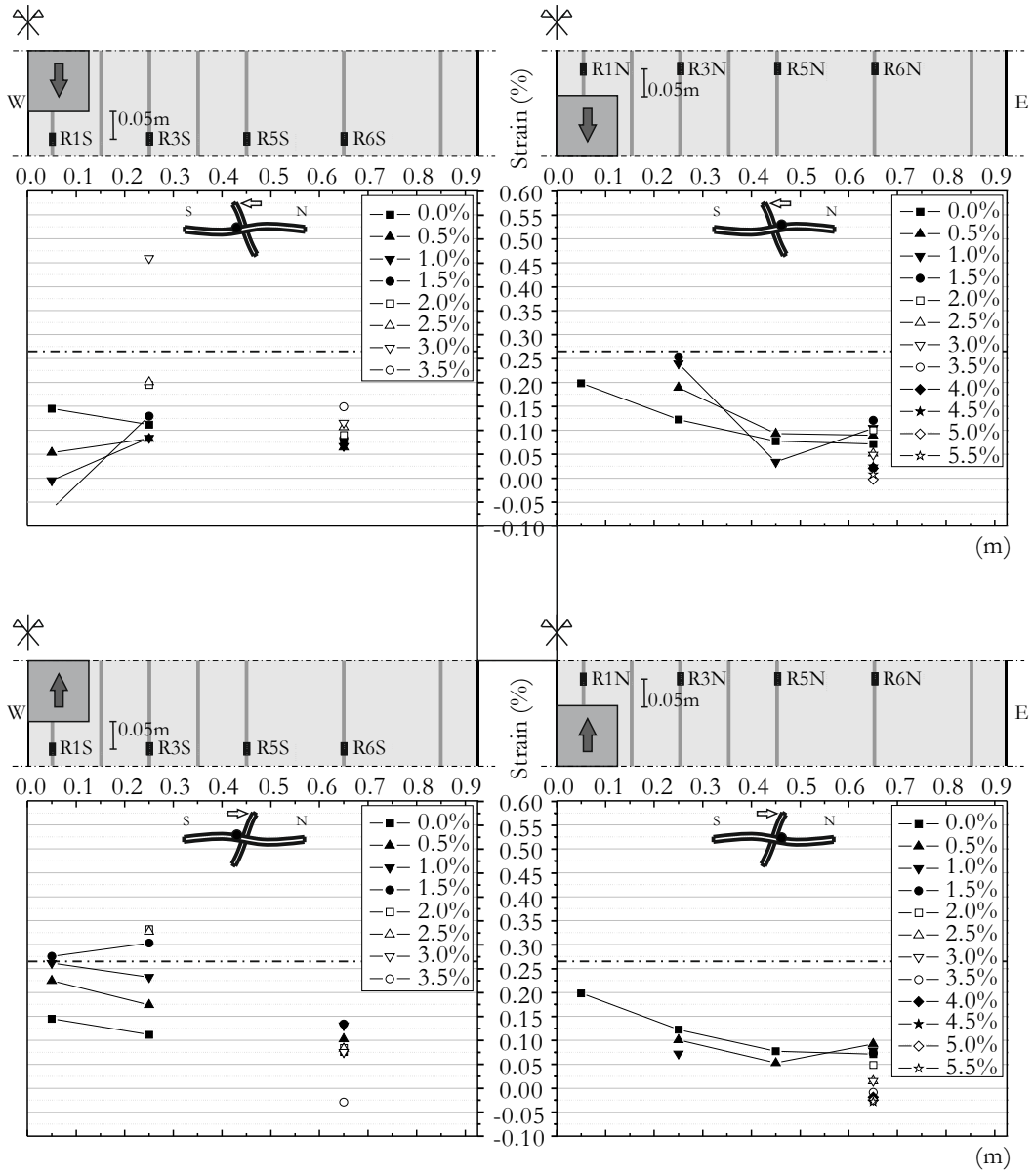

Figure 4.58: Strains in the top flexural reinforcement of the C-50 STR4 specimen.

The bottom reinforcement bars in the vicinity of the column yielded at the 2.5% drift step as shown in Figures 4.59 and 4.60. These results show that at least for specimens C-50 STR3 and C-50 STR4 both upper and lower reinforcement bars positioned closer to the column yielded. The strains in the bottom reinforcement bars (IR1S and IR3S) show a similar but symmetrical behaviour to the top reinforcement bars from the analogous location (R1S and R3S). When the horizontal load was applied in the S direction, the strains in the inferior instrumented bars increase. When the horizontal load was reversed, the strains decreased.

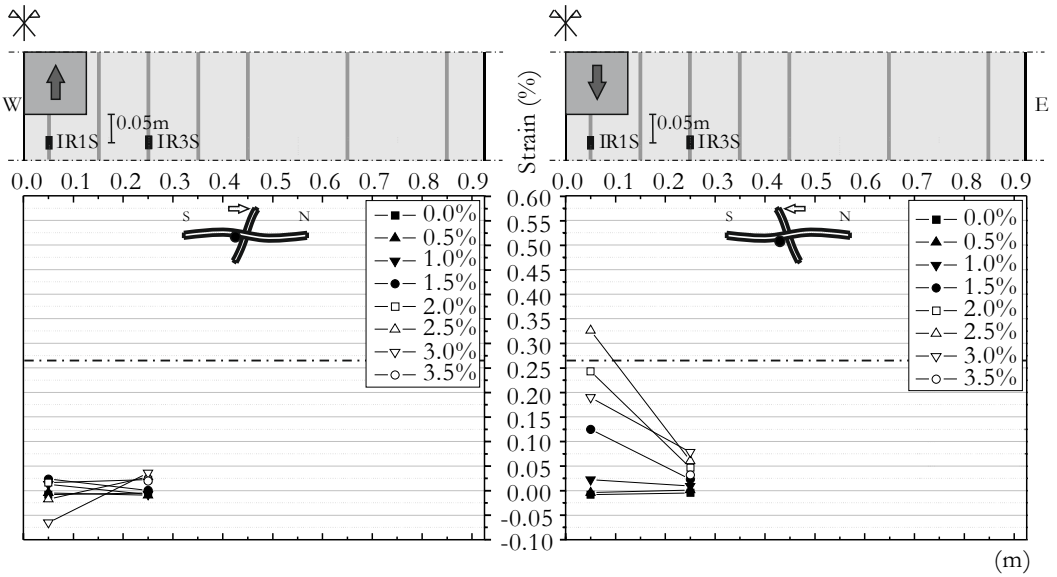

Figure 4.59: Strains in the bottom reinforcement of the C-50STR3 specimen.

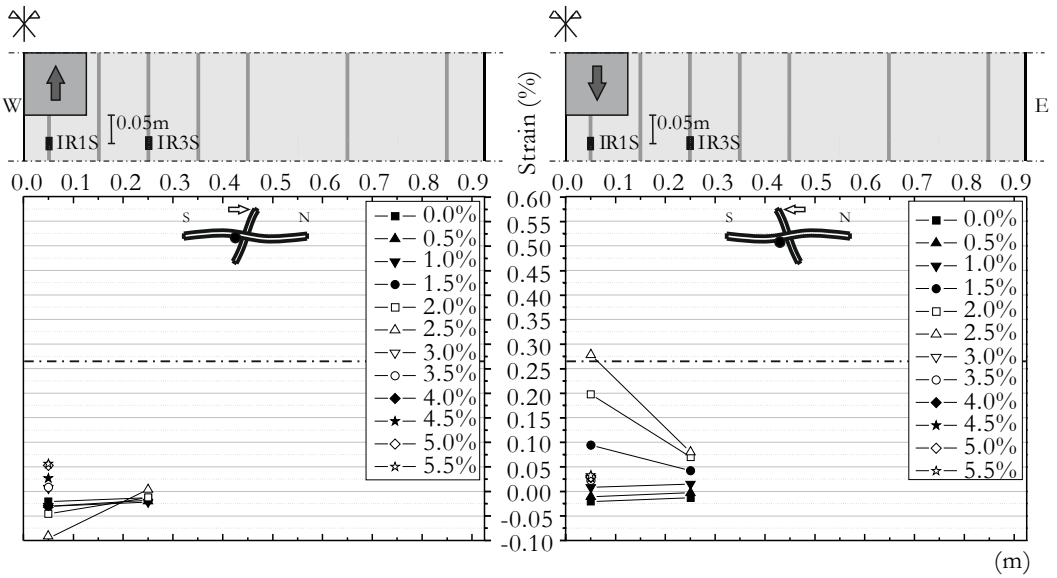

Figure 4.60: Strains in the bottom reinforcement of the C-50STR4 specimen.

At the southern edge, an increase in the bending moment was observed throughout the test, as shown in Figure 4.61. The positive bending moment was computed from the values obtained in the load cells in the struts of the Rotation Compatibilization System. The graph in Figure 4.61 shows fluctuations throughout the test. Those are the result the real time correction in the rotation of the edges (measured with the inclinometers) by using the dedicated hydraulic jacks in the struts and also the influence of the horizontal loading. The horizontal loading affects the positive bending moment in the mid-span because, for a

cracked state, the stiffness of the connection is not the same at both sides of the column. This increase in the positive bending moment shows that the specimen had moment redistribution capacity as a result of the test setup.

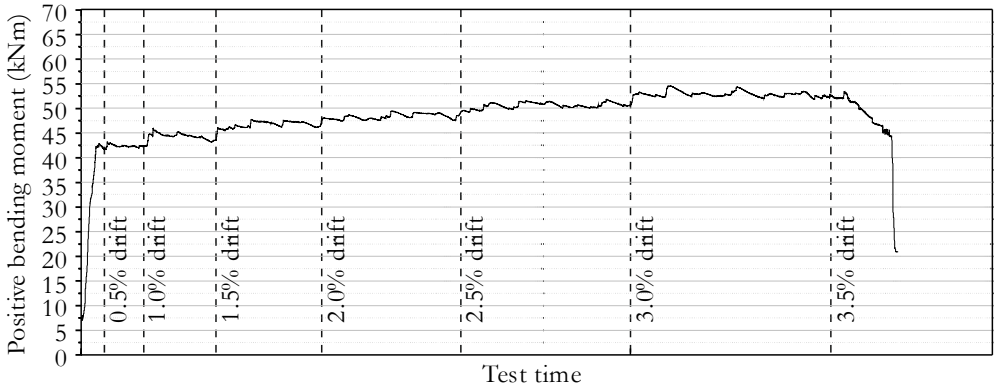

Figure 4.61: Positive bending moment at the South edge of the C-50STR3 specimen.

Cracks due to positive bending moment were present in the N and S edges (theoretical mid-span of the slab) on the bottom surface of the specimen. As the test developed, bending cracks in the bottom side of the specimen became more pronounced and new cracks appeared towards the column. For drift steps of about 2.0%, top and bottom cracks were formed in the same section, at the quarter-span region for negative and positive bending moments respectively.

Shear reinforcement strains

Figures 4.62 to 4.65 show the evolution of the strains in the shear stirrups during the test. The strain gauges were positioned in the middle of the instrumented vertical leg of the stirrup. Unlike the shear bolts from the C-50 BR and C-50 BC specimens, the stirrups are embedded in the concrete, therefore, the measured strains are localized strains. The strains are likely to be greater when a crack forms in the vicinity of the position of the strain gauge. This must be taken into account when analysing the presented data.

Figure 4.62 shows that the middle reinforcement layer (strain gauges S2 and S5) from specimen C-50 STR1 reached higher strains and all instrumented stirrups in this layer had yielded by the 2.5% drift step. This observation agrees with the formation of a diagonal shear crack crossing the stirrups that can be observed in Figure 4.39. In specimen C-50 STR2, and due to the higher cross section area of the stirrups, the strains, presented in Figure 4.63, were smaller than the ones from specimen C-50 STR1 and no stirrup yielding was spotted. The middle layer, again, showed higher strains, suggesting that a crack was formed in the middle

of the stirrups but it was not able to open, pushing the critical crack beyond the last layer of reinforcement.

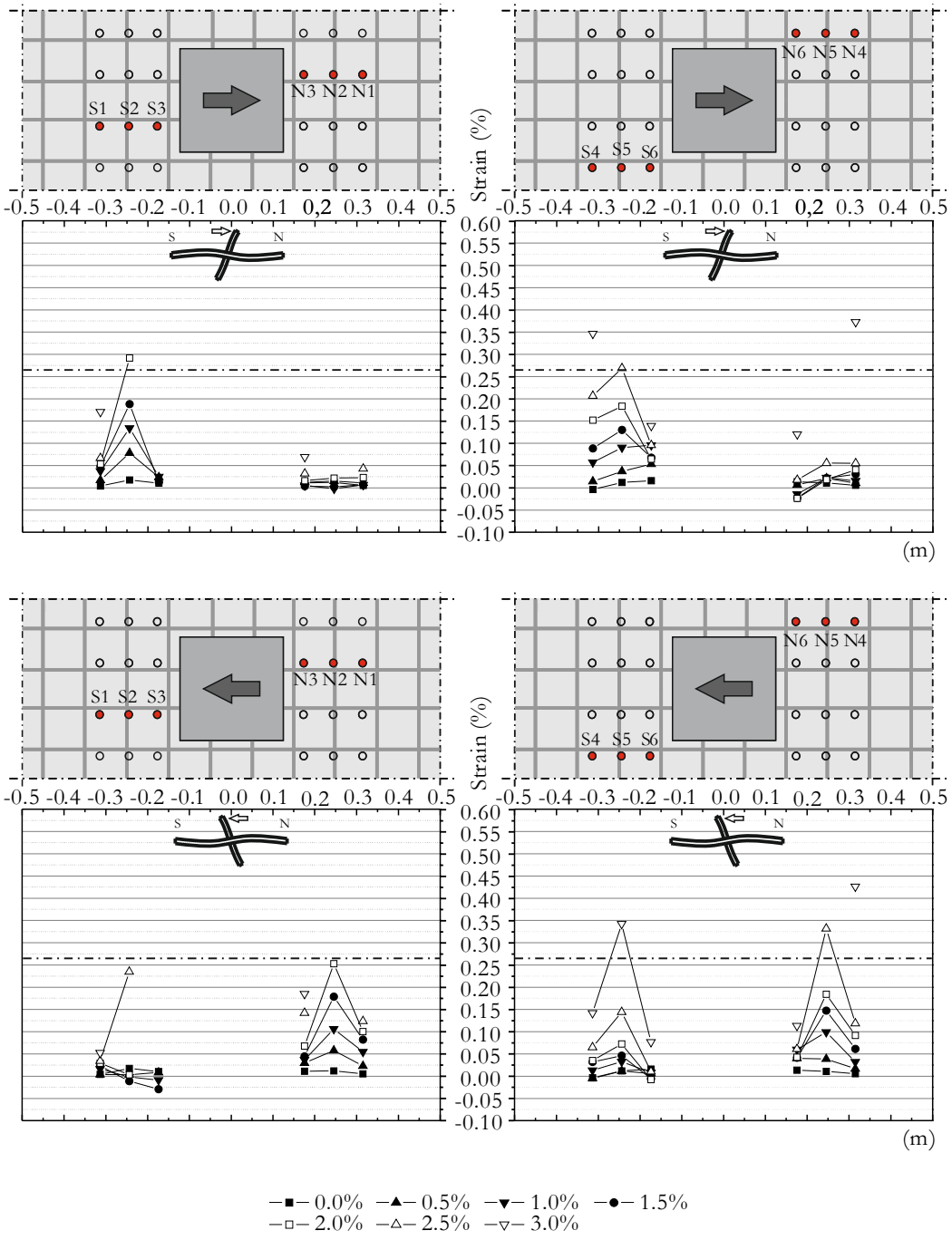

Figure 4.62: Strains in the shear reinforcement stirrups of the C-50 STR1 specimen.

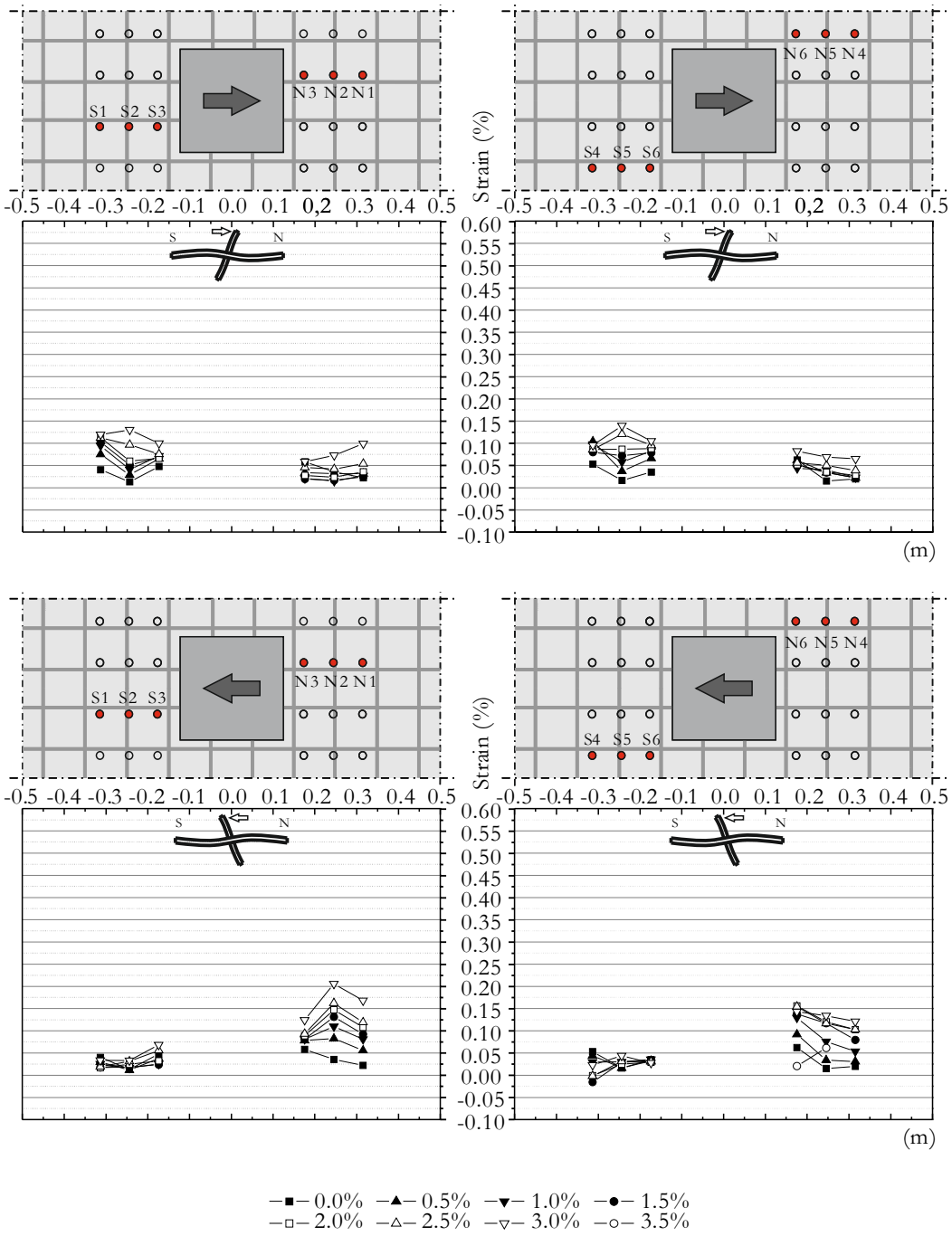

Figure 4.63: Strains in the shear reinforcement stirrups of the C-50 STR2 specimen.

The C-50 STR3 specimen failed by punching inside the stirrups zone (Figure 4.41), since the cross section area of the shear reinforcement was low, and it was not enough to prevent the punching failure near the column. From Figure 4.64 the high strains in the first and third shear reinforcement layers, counting from the column, shoe that two shear cracks occurred. This suggests the two last shear reinforcement layers were effective in preventing the outer shear crack, preventing a failure mode similar to the previous two specimens (punching outside the shear reinforced area). The strain gauges from the stirrups closer to the column

detached from the stirrup for drift steps over 2.5%. However, the post cutting inspection revealed that several stirrups had failed.

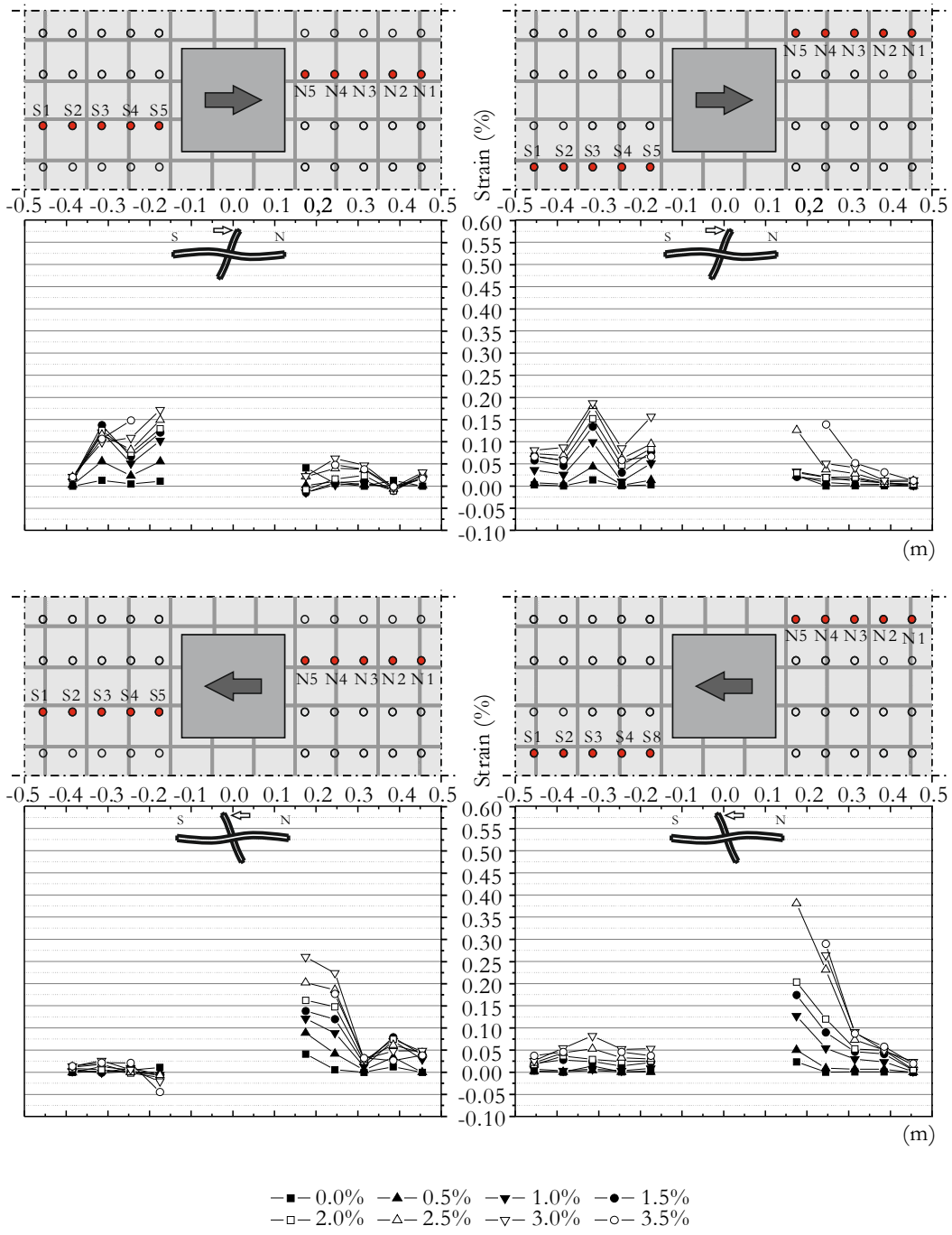

Figure 4.64: Strains in the shear reinforcement stirrups of the C-50 STR3 specimen.

The last specimen to be tested, C-50 STR4, withstood the punching failure, due to its higher shear reinforcement cross section area (Figure 4.42). The shear reinforcement strains from Figure 4.65 and post failure inspection of the specimen suggest not a punching failure but a failure with a formation of a flexural plastic hinge restricted to the vicinity of the column. In Figure 4.65 can be seen that the strain gauge S10 reached the yield strain in the last measured

cycle, which corresponds to the diagonal crack that can be observed on the left side of the column in Figure 4.42.

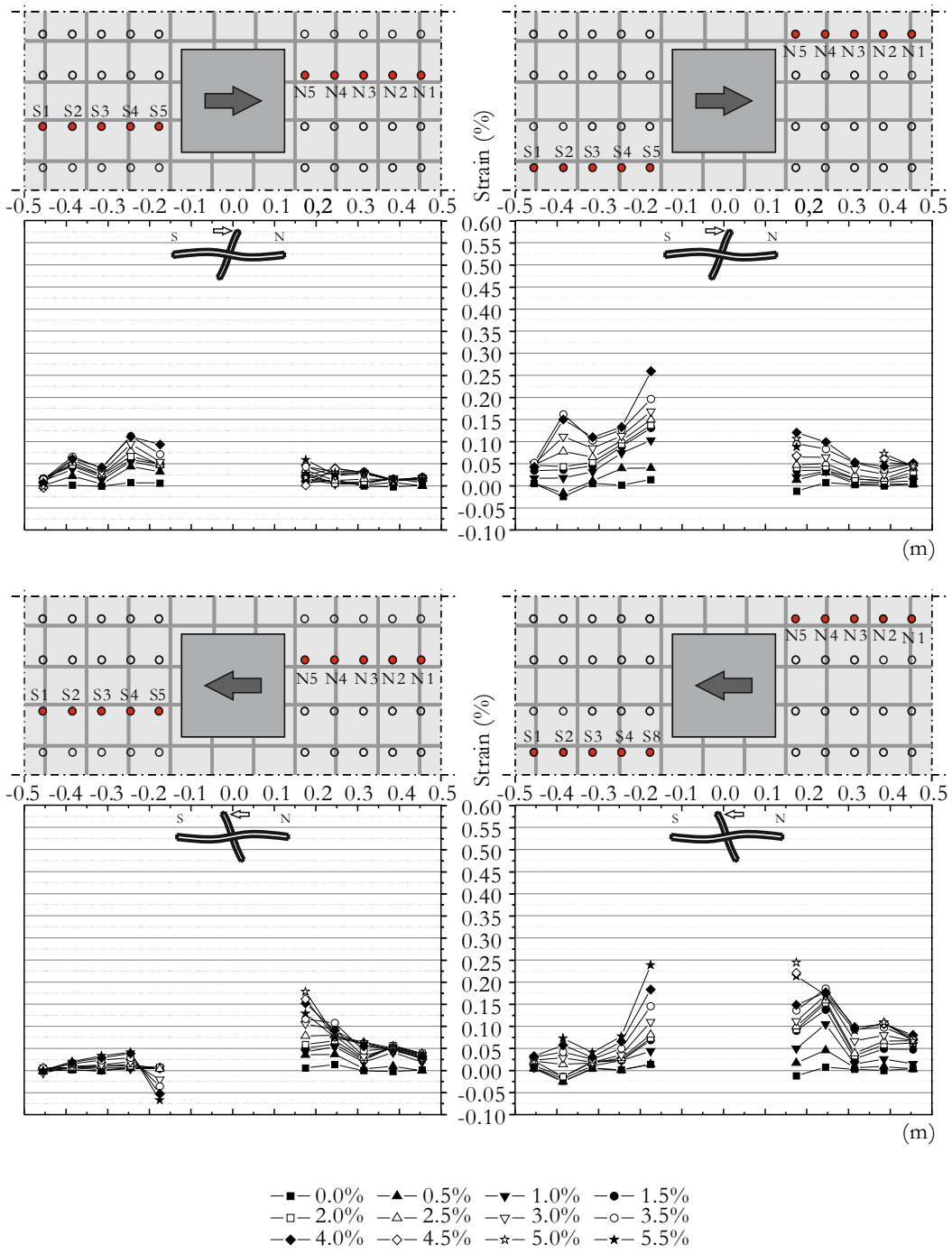

Figure 4.65: Strains in the shear reinforcement stirrups of the C-50 STR4 specimen.

Almost all the strain gauges in the stirrups stopped reading in the final cycles, due to heavy damage within the slab. It can also be concluded that the existing shear cracks did not evolve to a complete punching failure, as occurred in the case of specimen C-50 STR3. The shear

reinforcement was enough to withstand the vertical load and the imposed displacements, however, due to the large number of cycles, the concrete around the column was damaged, resulting in a plastic hinge mechanism. This led to a reduction in stiffness once the specimen could no longer endure the horizontal loading. At this time, the vertical load was supported by the bottom longitudinal reinforcement by dowel action. This conclusion is supported by Figure 4.42, where a physical separation is depicted between the concrete in the column and the remaining concrete of the specimens.

4.3 Comparison between specimens from different groups

The E-50 specimen was the only one tested with one way (S direction) eccentricity. The saw cut from E-50 (Figure 4.4) shows flexural cracks near the column in the N side only, because at the S side, the bending moment induced by the horizontal load decreases the moment due to the vertical load, while increasing the moment at the N side. The C-50 specimen shows cracks in both the N and S sides of the column, result of the two way cyclic eccentricity. The E-50 and C-50 specimens were both, at first, vertically loaded with 50% of their punching capacity, so, as expected, the behaviour of both slabs, during the vertical load imposition phase was very similar, as longitudinal vertical deformation in Figure 4.6 and Figure 4.16 and the strains from Figure 4.8 and Figure 4.21 show. The first time the 0.5% drift step was reached, both E-50 and C-50 specimens were in similar conditions. This is shown by the almost coincident longitudinal deformed profiles, although, rebar strains show some differences.

The loss of stiffness due to the cyclic loading is visible in the C-50 specimen, since, for the same applied vertical load, comparing the near failure vertical deformations at the edges of the slabs (Figure 4.6 and Figure 4.16), the E-50 and C-50 specimens, are identical, despite the fact that for the E-50 specimen, horizontal drift is almost twice the one in C-50. Cyclic related slab degradation contributed to narrowing the area around the column where the unbalanced moment is transferred, as seen when strains from E-50 and C-50 are compared (Figure 4.8 and Figure 4.21).

The saw cuts from the specimens strengthened with shear bolts (C-50 BR and C-50 BC) and the specimen with five layers of higher cross section stirrups (C-50 STR4), depicted in Figures 4.24, 4.25 and 4.42, show a different failure mode from the other tested specimens. Those three slabs did not fail by punching, instead, a hinge was formed by the degradation

of the concrete around the column, due to the horizontal cyclic loading. The specimens strengthened with shear bolts were able to achieve this failure mode with only three layers of reinforcement, while the slab with stirrups with similar reinforcement ratio and layer configuration (C-50 STR2), failed by punching outside the reinforced area. This result shows that the bolts are more efficient than stirrups because of the effective length, as the bolts confine the concrete in the whole thickness of the slab. The prestress given to the bolts when performing the strengthening of the slab is another factor that gives this solution an advantage. Contrary to the stirrups, that only start functioning when a deformation due to shear and, eventually, cracking of the slab occurs, the prestressed bolts are actively preventing concrete cracking due to shear.

The C-50 STR4 had, as stated previously, longer stirrups than the intended design, which resulted in the confinement of the inferior clear cover. This may have prevented the formation of the horizontal crack that is usually associated with punching failure outside the reinforced area, preventing this type of failure and leading to the formation of the hinge in the slab-column connection due to the resulting degradation by the cyclic action.

Comparing the hysteretic graph of the reference specimen without shear reinforcement, C-50, show in Figure 4.13, with the graphs from the specimens strengthened with shear bolts (Figures 4.26 and 4.27) and with stirrups (Figures 4.43 to 4.46), an increase in drift capacity and maximum horizontal force is observed.

The C-50 BR slab had an increase in the drift capacity of 250% and an increase of 63% in the maximum horizontal load, when compared to the C-50 specimen. The C-50 BC specimen achieved increases of 300% and 66% in the maximum drift and horizontal load, respectively.

The C-50 STR1 specimen reached a maximum drift increase of 150 % (2.5 %) over the reference specimen and an increase of 32 % (49.5 kN) in the maximum horizontal load. The C-50 STR2 and C-50 STR3 specimens reached a maximum drift of 3.0%, representing an 200 % increase and maximum horizontal loads of 52.0 kN and 59.3 kN (39 % and 59 % increases), respectively. The C-50 STR4 slab presented an increase of 300 % in the drift capacity, reaching the 4.0 % drift step and a maximum horizontal load of 58.4 kN, which corresponds to an increase of 56 %. Those conclusions are summarized in the envelope curves from Figures 4.66, 4.67, 4.68 and 4.69.

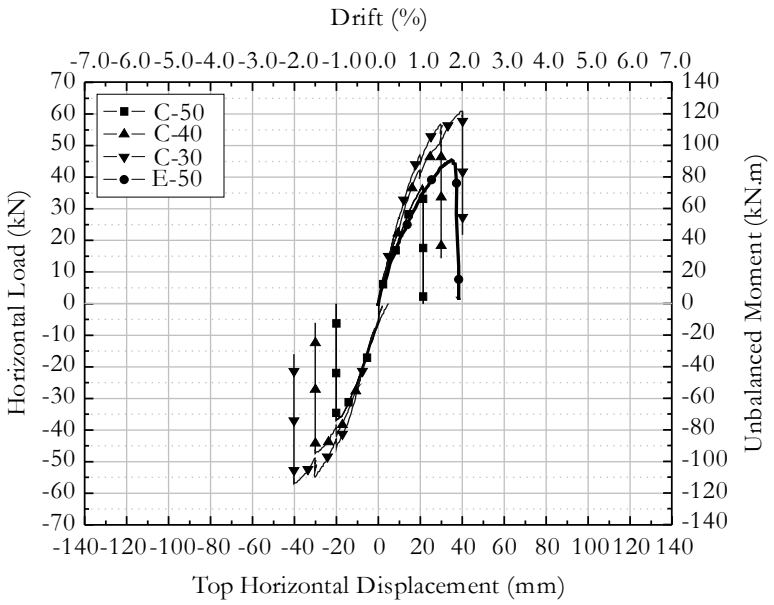

Figure 4.66: Envelope curves of the specimens without shear reinforcement.

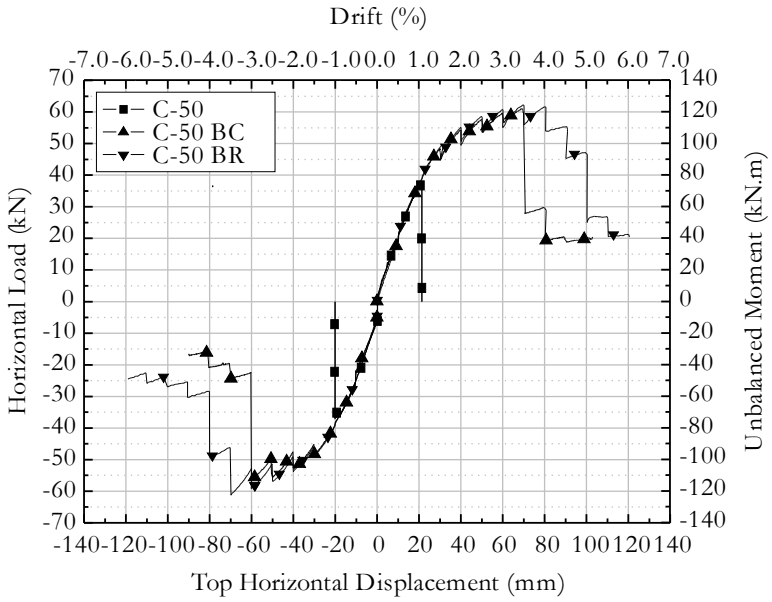

Figure 4.67: Envelope curves of the specimens with shear bolts and the reference specimen C-50.

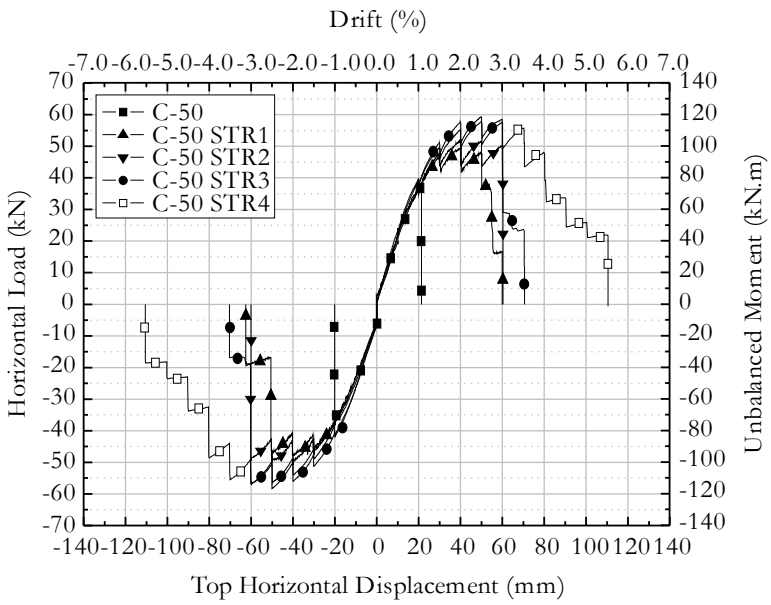

Figure 4.68: Envelope curves of the specimens with stirrups and the reference specimen C-50.

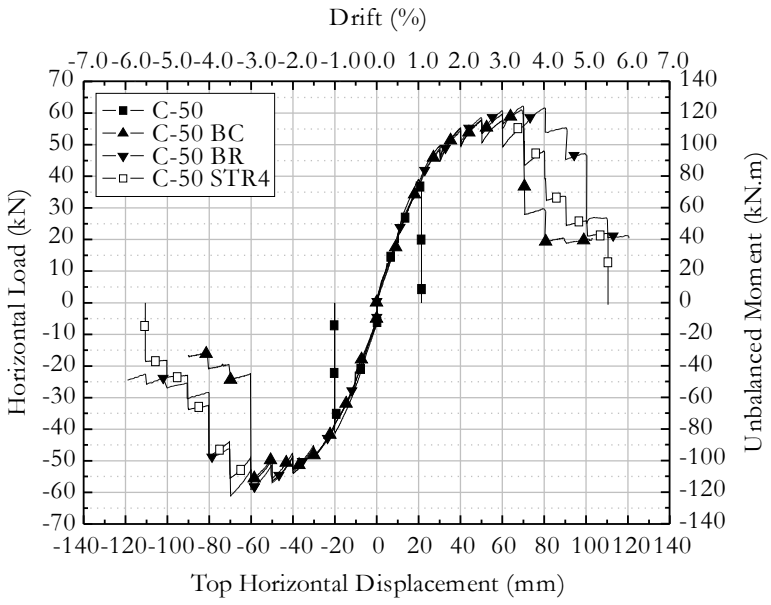

Figure 4.69: Envelope curves of the specimens that avoided punching failure and the reference specimen C-50.

The values of the increase over the reference specimen show, that the post installed shear bolts were more efficient in strengthening the slab and enhancing its behaviour under cyclic horizontal loads. With only three layers, the specimen was able to reach similar drifts and higher horizontal loads, despite having a slightly higher vertical load (13 %). This higher vertical load was due to the difference in the concrete compressive strength. The average

concrete compressive strength for the slabs with shear bolts was 58.2 MPa while for the slabs with stirrups was 49.8 MPa. Because the shear ratio was computed without taking into account the contribution of the shear reinforcement, the difference in the concrete compressive strength led to the C-50 STR4 specimen being subjected to about 10 % to 12 % less vertical load than C-50 BR, C-50 BC and C-50 STR2.

Table 4.1: Failure details of all tested specimens

Specimen	V_{exp} (kN)	Maximum horizontal load and corresponding drift		Maximum drift	Failure
C-50	203.4	37.4 kN	1.1 %	1.1 %	Punching during the 2nd 1.0% drift cycle
C-40	167.4	51.4 kN	1.5 %	1.5 %	Punching during the 1st 2.0% drift cycle (+1.2% drift)
C-30	131.3	60.8 kN	2.0 %	2.0 %	Punching during the 2nd 2.0% drift cycle
C-50 BR	220.2	61.0 kN	3.5 %	3.5 %	Plastic hinge during the 1st 3.5% drift cycle
C-50 BC	222.3	62.2 kN	3.5 %	4.0 %	Plastic hinge during the 2nd 4.0% drift cycle
C-50 STR1	209.9	49.5 kN	2.0 %	2.5 %	Punching during the 1st 3.0% drift cycle (+2.7% drift)
C-50 STR2	215.7	52.0 kN	2.0 %	3.0 %	Punching during the 2nd 3.0% drift cycle
C-50 STR3	202.3	59.3 kN	2.5 %	3.0 %	Punching during the 3rd 3.0% drift cycle
C-50 STR4	195.9	58.4 kN	2.5 %	4.0 %	Plastic hinge during the 2nd 4.0% drift cycle

The vertical deformation charts from the C-50 STR3 and C-50 STR4 slabs show the effect of the real time monitoring and adjusting of the rotations at the North and South edges for the horizontal loading. However the Rotation Compatibilization System worked as intended in the other tests, (unrecorded data from the load cells show a positive bending moment of the same order of magnitude), it benefits from the real time adjustments to reach its full performance. Those conclusions are also showed by Isufi [27]. All the comparable shear reinforced specimens presented a similar vertical deformation at the edges, between 25 mm and 30 mm. The slabs without shear reinforcement present vertical deformations between 10 mm and 15 mm. This capacity to withstand damage and deformation is essential to dissipate energy which is desirable in an earthquake situation.

To quantify the energy dissipation capacity, a viscous damping coefficient was calculated according to Hose and Seible [61]. This parameter relates the dissipated cycle energy with the energy needed to linearly reach the peak of each cycle. According to the same authors different types of behaviour are associated with different viscous damping values.

The viscous damping coefficient (ξ_{eq}) was calculated using equation (4.1).

$$\xi_{eq} = \frac{1}{2\pi}\left(\frac{E_{d1}}{E_{S1}} + \frac{E_{d2}}{E_{S2}}\right) \tag{4.1}$$

where:

E_{d1} is the energy dissipation for positive displacement cycles

E_{d2} is the energy dissipation for negative displacement cycles

E_{S1} is the elastic strain energy for positive displacement cycles

E_{S2} is the elastic strain energy for negative displacement cycles

as depicted in Figure 4.70.

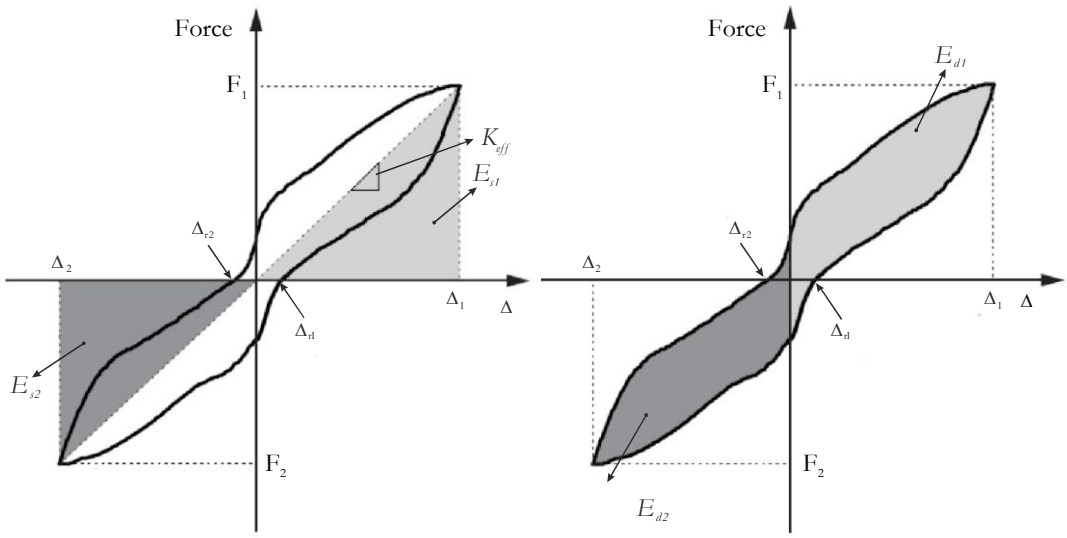

Figure 4.70: Equivalent viscous damping for asymmetric hysteretic loops (adapted from Marreiros [62]).

The narrowness of the hysteretic charts, where the load and unload branches are very close, presented in the first drift steps for all the tested specimens, indicates low energy dissipation capacity, which is verified by the Viscous Damping Coefficients, shown in Figures 4.71 to 4.73. All specimens presented Viscous Damping Coefficients that were generally smaller than 10 % for drifts up to 3.0 %. According to Hose and Seible [61], viscous damping coefficient

values under 10 % are indicative of a structural system with a non-linear elastic behaviour and therefore with low energy dissipation capacity.

The calculated viscous damping coefficients show a tendency to increase with the drift ratio. Between different cycles for the same drift ratio, the values for the viscous damping coefficients decrease, meaning less energy dissipation capacity.

The energy dissipation capacity of specimens C-50, C-40 and C-30 present similar viscous damping coefficients, showing that this parameter is almost unaffected by vertical load, although the total dissipated energy is higher, because for smaller shear ratios, higher horizontal drift ratios and more cycles are achieved.

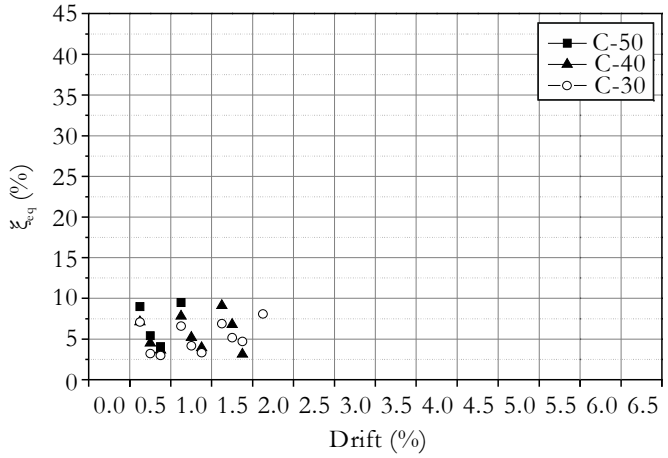

Figure 4.71: Equivalent viscous damping for slabs without shear reinforcement.

The slabs with shear reinforcement, by achieving higher drifts, were able to dissipate more energy in each of the cycles of the higher drifts, as shown in Figures 4.72, 4.73 and 4.74.

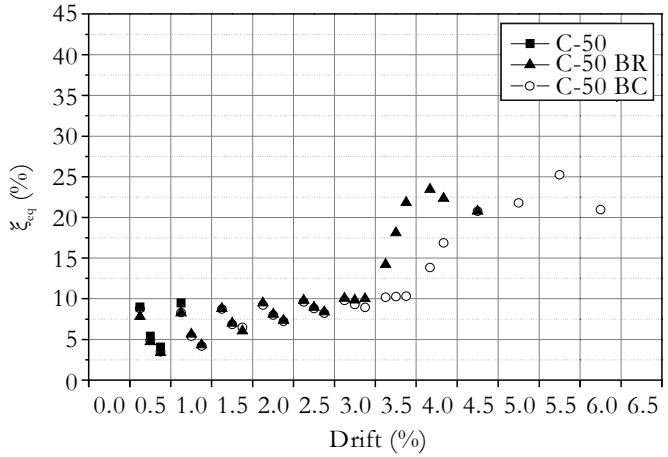

Figure 4.72: Equivalent viscous damping for slabs with bolts as shear reinforcement, compared with the reference specimen C-50.

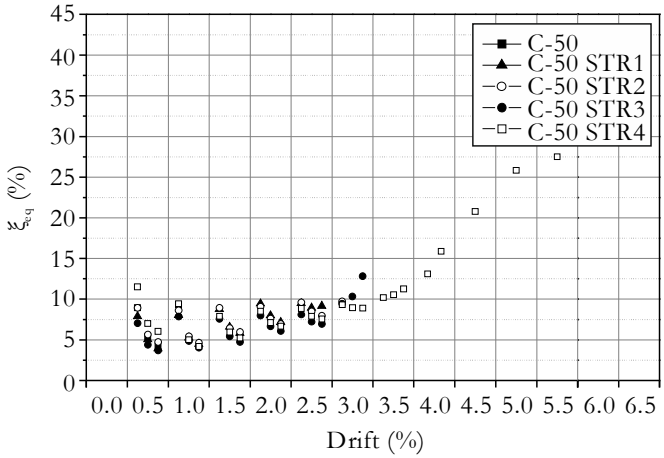

Figure 4.73: Equivalent viscous damping for slabs with stirrups as shear reinforcement, compared with the reference specimen C-50.

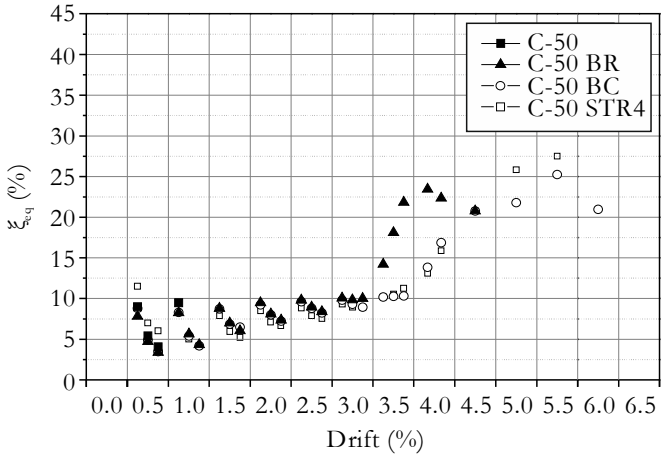

Figure 4.74: Equivalent viscous damping for slabs that avoided punching failure, compared with the reference specimen C-50.

The specimens that failed by punching, due to the fragile nature of the failure do not present an increase in the energy dissipation capability. In the slabs were punching failure was avoided, (C-50 BR, C-50 BC and C-50 STR4), the last drift step before the failure criteria was achieved presented an increase in the capability to dissipate energy. This increase was also observed for drifts after the horizontal load had dropped under 80 % of the maximum load. However, this is not relevant if, as expected in a real world scenario, drifts of that magnitude are not reached in the real structure.

Chapter 5

Design considerations

In this chapter, the results of the experimental campaign are studied regarding building design. Some inherent problems to the subject are noted and design recommendations, based in the experimental results, are provided.

5.1 Gravity shear ratio values predicted by the codes

Although the Eurocodes do not provide a definitive way to design slab-column connection for seismic actions, the American codes provide some guidance, as presented previously in this document. The first step is to assess if the connection requires shear reinforcement, which is accomplished by applying the diagram showed in Figure 2.17. Ramos et all [59] presented the diagrams showed in Figures 5.1 and 5.2 that relates the gravity shear ratio with the achieved inter story drifts using data from the bibliography. Those diagrams were created by plotting the gravity shear ratio, computed using the EC2 and the MC2010 (Level of Approximation (LoA) III) without using limitations or reduction coefficients and the reported drifts for slabs without shear reinforcement. Next, an iterative process was used to change the constants *a*, *b* and *c* in equation (5.1) with the objective of achieving the optimal fit for different percentiles (50%, 95% and 99%)

$$d = a \cdot 10^{-b \cdot SR} + c \tag{5.1}$$

where:

d is the *drift*

SR is the shear ratio

The algorithm forced the drift to be zero when the shear ratio is 1.0, that way, it is assumed that a slab subjected to a gravity load equal to the shear capacity, fails without the contribution of an eccentric load.

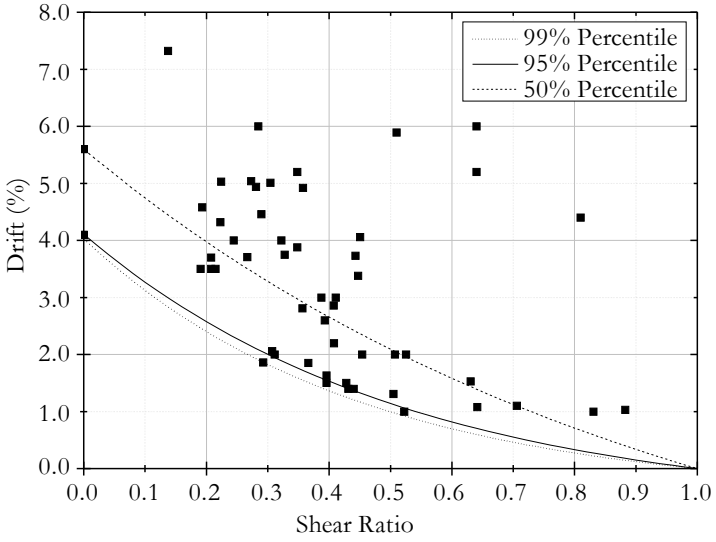

Figure 5.1: Drift as a function of the vertical shear ratio (EC2). Ramos et all [59].

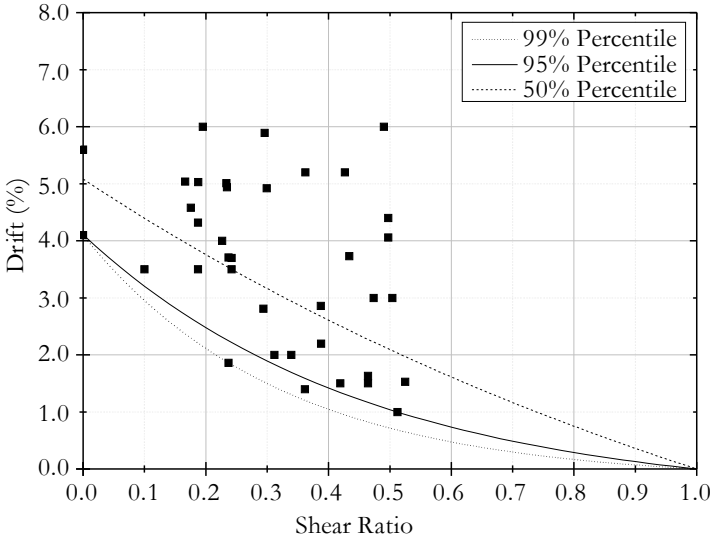

Figure 5.2: Drift as a function of the vertical shear ratio (MC2010 LoA III). Ramos et all [59].

The objective of those diagrams are to help in the design of the slab-column connection, by showing for a given shear ratio, which value of the design allowed drift can be achieved without the need to add shear reinforcement. The plots from Figures 5.1 and 5.2 show that the same test specimens are represented differently, according to the code used to calculate

the shear ratio. This leads to different curves and, therefore, different achieved drifts for a given gravity shear ratio, for the same specimen.

5.2 Factors that influence the experimental results

The plots from Figure 4.1 and Figure 4.2 show that the experimental results from the bibliography present a scattered arrangement which can be explained by the differences in the test setups and the design of the specimens. Ramos et all [59] shows that using different codes lead to different shear ratios.

The behaviour of flat slab connections under gravity and horizontal loads is complex, which makes it difficult to replicate in the laboratory, especially when trying to use smaller simplified setups. The test setups have been evolving throughout the decades, as referred in the literature review. This constant evolution tried to make use of newer technologies, new ideas and better knowhow with the goal of faithfully replicate the behaviour of a real flat slab panel in the laboratory. The test setup is a factor to take into account when considering experimental results because it can influence the value of the vertical load, the percentage of the gravity load that acts as punching load at the column, the deformation, the flexibility of the specimen and the measurement of the results.

The use of a steel column allowed to easily assembly the test setup and, because its behaviour is linear elastic, it was possible to calculate the influence of its stiffness in the total displacement. The total horizontal displacement which is converted to the inter-story drift is the sum of several effects, in which a very important one, is the column stiffness. The stiffness of the steel column used in this experimental work is 44% of an uncracked concrete column with 0.25 mm by 0.25 mm cross section. The displacement due to the flexure of the used steel column (δ_{col}) in millimetres is given by equation (5.2) as a function of the horizontal load (H) in kN.

$$\delta_{col} = 0{,}157 \cdot \mathrm{H} \tag{5.2}$$

The influence of the steel column is less important as the stiffness of the slab-column connection decreases. The specimen C-50 reached a maximum horizontal load over 35 kN which coincides with the highest horizontal displacement of 20 mm. This means that over 5.5 mm was due to the deformation of the column that, once converted to drift, results in a reduction of 0.27 % to a total drift of 0.73 %. Those results suggest that measuring the

achieved drift, however intuitive and applicable in the design of a structure, is not accurate in experimental environment where the goal is to extrapolate the results. The use of a stiffer column results in the reduction of the maximum achieved drift without changing the characteristics of the slab. A better solution is to measure the rotation of the slab-column connection as a function of the unbalanced moment. The accurate measurement of the rotation of the connection requires specific equipment that was not widely available decades ago, and, the calculation of the rotation by considering the deformation of a column made of concrete is not accurate because of its non-linear behaviour.

The thickness of the slab plays an important role in the achieved drift. The effect of the reduced scale is difficult to take into account especially when a non-linear behaviour is concerned. The literature review shows that thinner specimens reach higher drifts than thicker ones under similar conditions.

The test protocol may also present a source of scattering of the experimental results. The way the vertical load is applied, the number of horizontal cycles in each drift step, as well as the increase in each drift step may influence the overall achieved drift.

5.3 The case of the tested slabs

The dimensions of the tested specimens were the result of a 2/3 scale reduction of a standard office building. The slab was designed according to the Eurocodes EN1990 [63], EN1991 [64] and EN1992 [54]. In the design a slab with 4.0 m spans and a thickness of 0.15 m were considered, supported by columns with a 0.25 m by 0.25 m cross section.

The design loads were 8.0 kN/m^2 of permanent action and 3.0 kN/m^2 of variable action, resulting in a values of punching shear in the connection, considering the influence areas, of 244.8 kN and 142.4 kN, for the fundamental and seismic combinations, respectively.

The predicted centered punching capacity for the slab, with a concrete strength f_{ck} = 37 MPa without shear reinforcement and detailed as showed in Chapter 3, provided by the EC2 [54] is 265.0 kN, considering the safety coefficients (for the materials and a value of c = 0.12) but not limiting the thickness (k) to 0.2 m. When using the obtained values to calculate the gravity shear ratio for an earthquake situation, the result is a 53 % shear ratio.

In the experimental campaign, the punching capacities of the tested specimens were extrapolated from the result of the MSL slab, as referred in Chapter 3. Those results are very

similar to the ones obtained by using EC2 without the safety coefficients. For this case, when no safety coefficients are used (c = 0.18), the EC2 predicts a punching capacity of 425.3 kN, that results in a gravity shear ratio of 33 %. Those results show that, when compared to the experimental results, the safety coefficients of the EC2 gives a 20% safety factor in the calculation of the shear ratio and consequently, a safety factor in the achieved drift. To quantify, for the particular case of the tested slabs, the increase in the drift capacity achieved by considering the safety coefficients, the results presented for the C-50 and C-30 slabs, can be compared. It is expected for a tested slab, subjected to the design conditions, to perform similarly to the C-30 slab.

5.4 Use of shear reinforcement

It was previously showed that, for the specific case of the tested slabs, according to design, a standard slab should present a behaviour similar to the C-30 slab. The test results presented in Chapter 4 show that for the used horizontal displacement protocol, a slab with a 30 % gravity shear ratio reached a drift of 2.0 %. Assuming that the behaviour of the C-30 slab is a good approximation for the behaviour of the average slab, the value of 2.0 %, presented in the Chapter 4 can be taken as the reference of the maximum achieved drift, taking into account that this value is a function of the test conditions (number of cycles, column flexibility, for example), and, as so, can change both conservatively or non-conservatively. Also, the test conditions are not as severe as the real seismic action. The value of the demand design drift is debatable, however, values up to 2.5% are commonly used.

As a result of these uncertainties, and based in the experimental results in Chapter 4, it is advised the use of shear reinforcement in all the flat slab-column connections, in seismic regions, with the sole function of enhancing the seismic performance.

5.5 Minimum shear reinforcement

The slab-column connections should be designed to withstand the horizontal displacements of the building of which they are part of. The obtained results, as well as the results from the bibliography, suggest that flat slabs without shear reinforcement may not present sufficient ductility to achieve drifts in the magnitude of the design drifts. For that reason, even if no shear reinforcement is required to ensure the punching resistance, it is recommended to strengthen all the flat slab-column connections with a minimum shear reinforcement, in

seismic regions. The minimum shear reinforcement, should be designed to prevent punching inside the shear reinforced area and have enough layers to prevent punching outside the reinforced area, so that if a failure occurs as the result of the seismic action, it happens by the yielding of the flexural reinforcement. Experimental results show that the higher drifts were achieved by slabs in which a punching failure was avoided.

The approach taken in the design of the minimum shear reinforcement is the notion that the efficiency of the stirrups depends on the axial strain of the reinforcement. This strain must be limited, by setting a maximum allowed value, to ensure that the shear reinforcement is mobilized for smaller drifts. As presented in Subchapter 2.3.2, a limitation to the strain is steel stirrups is provided by EC2 [54] to ensure proper anchorage of the shear reinforcement. The proposed formulation allows that for thicker slabs the shear reinforcement may be fully mobilized. In order to control the opening of the shear crack, a smaller maximum strain is suggested. The Experimental results show that the strains in the stirrups in the C-50 STR4 present a maximum strain of 0.15 % before starts losing horizontal force. The value to be used for the maximum allowed strain ($\varepsilon_{w,\,max}$) is suggested in equation (5.3) and must be smaller than the design yield strain ($\varepsilon_{yk,\,w}$).

$$\varepsilon_{w,max} = 0.15\ \% \leq \varepsilon_{yk,\,w} \tag{5.3}$$

The experimental tests in shear reinforced slabs where punching failure inside the shear reinforced was avoided (Table 5.1), where considered.

Table 5.1: Details of the considered tested specimens

Author	Specimen	f_{cm} (MPa)	ρ (%)	d (mm)	Column size (mm)	A_{sw}/layer (cm²)	V_c (kN)	V_{exp} (kN)
Hawkins [24], [40]	SS1	27,6	1,3	123	305x305	5,67	457,8	133
	SS2	25,7	0,9	123	305x305	2,57	396,5	126
	SS3	25,9	1,1	123	305x305	5,67	425,0	139
	SS4	27,6	1,1	123	305x305	5,67	434,1	150
	SS6	24,2	0,9	123	305x305	5,67	388,7	271
Robertson [45]	2CS	31,4	0,8	100	254x254	2,26	288,9	34
	3SL	43,4	0,8	100	254x254	2,26	321,8	25
Gayed [14]	IPS-0	26	1,11	114	250x250	5,67	355,5	240
Song [32]	SR1	38,7	1,11	113,5	300x300	4,52	436,8	125
	SR2	38,7	1,11	113,5	300x300	6,28	436,8	125
Almeida	C-50 STR4	43,7	0,96	118	250x250	6,28	421,3	196

The plot from Figure 5.3 shown the dispersion of the shear reinforcement ratio, (calculated by the ratio of the total cross section area of the first layer of shear reinforcement by its area of influence) versus the experimental shear ratio from the slabs from literature (Table 5.1), without considering the shear reinforcement. The formulation from EC2 was used to calculate the punching capacity of the slabs. The safety coefficients were used but the 200 mm limitation for the slab thickness was neglected. The trend line represents the weighted distribution of the plotted dots and its slope represents the linear relationship of the ratio between the area of the shear reinforcement in the first perimeter by the area of influence of that layer (Figure 5.4) A_{sw}/A_{cw} as a function of V_{exp}/V_c.

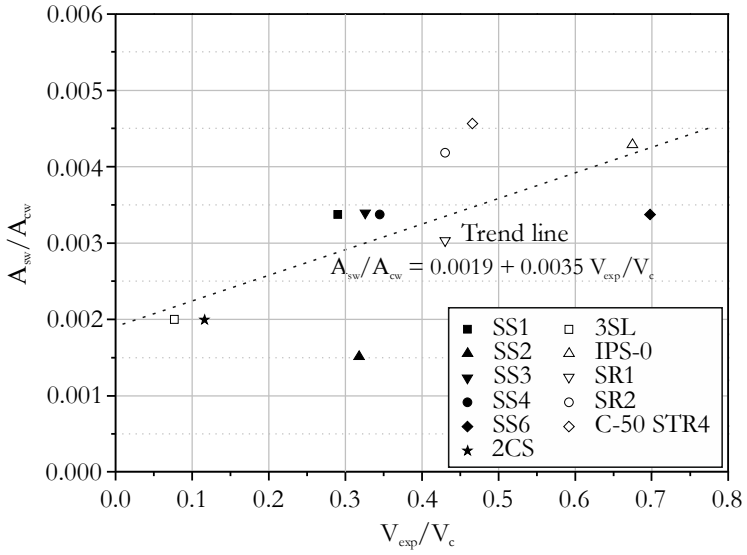

Figure 5.3: Shear reinforcement ratio (A_{sw}/A_{cw}) versus experimental shear ratio (V_{exp}/V_c) from slabs from the literature.

Because all the considered specimens had steel shear reinforcement, considering the limit from (5.3) and a modulus of elasticity of 200 GPa, the slope of the trend line can be normalized, resulting in equation (5.4)

$$\frac{A_{sw}}{A_{cw}} = \frac{0{,}06}{\varepsilon_{w,\,max} E_w}\left(1+1.75\,\frac{V_{exp}}{V_c}\right) \qquad (5.4)$$

which can be written, considering the design vertical load for the seismic combination, as equation (5.5), that allows to calculate a proposed value for the shear reinforcement cross section by layer ($A_{w,\,s}$), to be used in all slab-column connections subjected to lateral loads due to the seismic action.

$$A_{w,\,s} \geq \frac{0{,}06\,A_{cw}}{\varepsilon_{w,max} E_w}\left(1+1.75\,\frac{V_{Ed,\,s}}{V_{Rd}}\right) \qquad (5.5)$$

where:

$A_{w,\,s}$ is the area of the cross section of the shear reinforcement in a single perimeter around the column, in cm^2

A_{cw} is the the influence area of the first layer of shear reinforcement in cm^2 acording to Figure 5.4

V_{exp} is the experimental vertical load

$V_{Ed,\,s}$ is the design vertical load for the for the seismic combination

V_{Rd} is the design punching capacity of the slab, without shear reinforcement

V_c is the punching capacity without shear reinforcement

$\varepsilon_{w,max}$ is the maximum allowed strain for the shear reinforcement in percentage given by equation (5.3)

E_w is the modulus of elasticity of the shear reinforcement in GPa

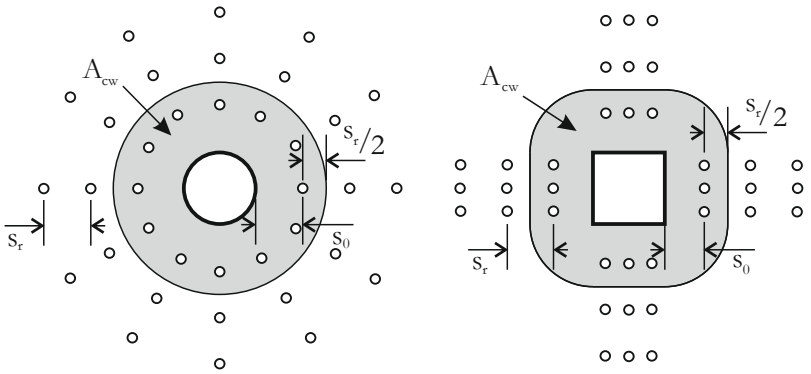

Figure 5.4: Influence area of the first layer of shear reinforcement (A_{cw})

The arrangement of the stirrups must follow the EC2 recommendations for the spacing between stirrups (s_r and s_t) and the minimum distance from the face of the column to the first layer of stirrups.

The results from the slab STR2 and also, several tests from the literature show that an insufficient distance from the face of the column to the last reinforcement layer may result in brittle punching failure outside the shear reinforced area. The ACI [52] suggests a higher

distance from the face of the column to the outer layer than the EC2, of four times the effective depth. It is then suggested that the shear reinforcement arrangement follows the rules from EC2 (section 9.4.3) with the distance from the face of the column to the last layer of shear reinforcement as suggested in ACI, as shown in Figure 5.5.

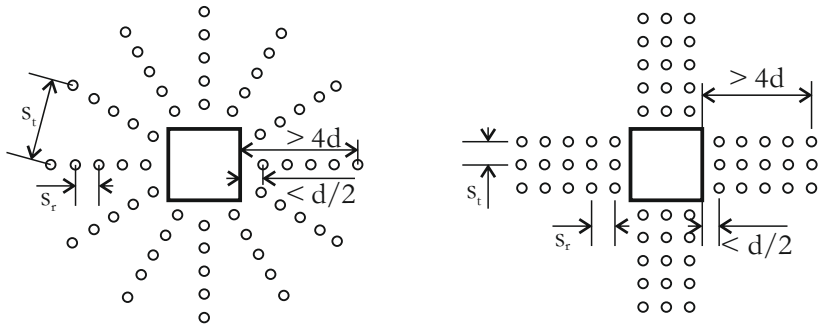

Figure 5.5: Proposed stirrup arrangement.

Further experimental tests are needed to better validate the proposed shear reinforcement and the distance from the face of the column to the last layer of shear reinforcement.

Applying the proposed methodology to the slabs tested in this experimental campaign, C-50 STR3 and C-50 STR4, with an experimental total shear reinforcement cross section by layer of 2.54 cm² and 6.28 cm², respectively, and comparing it to the obtained value from equation (5.5) of 5.16 cm², the result corroborates the experimental results. The stirrup arrangement used in the C-50 STR3 slab, although had the same number of layers as the C-50 STR4 slab, had a smaller shear reinforcement cross section by layer, being unable to prevent punching inside the shear reinforced zone.

Chapter 6

Summary, conclusions and future works

In this work, the subject of the behaviour of column to flat slab connections was studied. The first step of the experimental works involved the design and assembly of a new test setup, attempting a more realistic approximation to the real phenomenon. A prototype flat slab building was pre-designed and eleven test specimens were designed and cast, representing a 2/3 reduced scale of the prototype building. The slabs ware used to perform different kinds of tests, including a centred punching test, an eccentric punching test and nine tests that combined vertical load and cyclic horizontal load. In the cyclic tests, the variables of vertical shear ratio, the use of post installed bolts as shear reinforcement and several stirrup arrangements were tested. Finally, design considerations and a methodology to calculate a minimum shear reinforcement to be used in seismic regions were suggested.

6.1 Conclusions

The test setup performed as intended. The results show that the system designed to apply equal moments and rotations and the system designed to apply equal vertical displacements and symmetric shear forces successfully fulfilled the function for which they were designed. Therefore, a constant vertical load was applied to the slab-column connection, and a more realistic deformation was applied to the tested specimen. The ability to read the real time data from the instrumentation of the test setup (load cells of the struts and inclinometers at the borders), allowed to a more precise control of the rotations of the borders, however, the results obtained without these resources were proven to be valid.

For the same vertical shear ratio, the slab tested with an increasing horizontal load, reached a higher drift and horizontal load. Cyclic loading leads to an increase in the vertical deformation of the slab. When subjected to the same vertical shear ratio, the slab in which was imposed the horizontal cyclic loading, presented a higher vertical deformation at the moment of failure. This is due to the fact that cyclic loading damages the slab-column connection in both sides of the column (N and S sides, in this case). The ability of the test

setup to allow vertical deformations, also contributes to the increase damage under cyclic loading, leading to an increase in the flexural reinforcement strains for each cycle.

The achieved horizontal drift increases (1%, 1.5% and 2%) as the vertical load ratio decreases (0.5, 0.4 and 0.3). The unbalanced moments, due to the horizontal action, were transferred to the column by the surrounding slab region. Lower vertical loads allows the unbalanced moment to be transferred by a wider area surrounding the column. The higher shear ratio increases the difference in magnitude of the strains of the flexural reinforcement. The higher strains were measured in the reinforcement bars in the column region, however, the strains in the flexural reinforcement of slab subjected to the smaller vertical shear ratio were more even.

All the cyclically tested slabs without shear reinforcement showed a narrow hysteretic chart with low energy dissipation and drift capacity. Those results suggest that flat slabs without shear reinforcement may not have an adequate behaviour to resist horizontal loads, even for moderate horizontal drifts. The calculated viscous damping coefficients show a tendency to increase with the drift ratio. Between different cycles for the same drift ratio, the values for the viscous damping coefficients decrease, meaning less energy dissipation capacity. This phenomenon is due to the fact that damping is associated with yielding, which happens mainly when a new drift step is achieved.

Post installed steel bolts were proven to be an effective way to enhance seismic performance of flat slab structures. When compared to the specimen tested with the same vertical shear ratio, C-50, the use of steel bolts as shear reinforcement provided higher drift capacity (from 250% up to 300% increase), higher maximum horizontal load, higher ductility and higher energy dissipation capacity. The Energy dissipation by cycle was similar to the ones presented by the slab without shear reinforcement, however, because more cycles were achieved, the total energy dissipation was higher. In the tested specimens, three layers of bolts was enough to efficiently prevent punching failure. The achieved failure, which consisted in the formation of a plastic hinge in the vicinity of the column, showed that the ratio and number of layers were adequate in this case.

Although the C-50 BC specimen performed slightly better, this may be due to the fact that in that case, the bolts were closer to each other and also closer to the longitudinal reinforcement providing a better confinement of the concrete. As such, it was concluded that both solutions (radial and cross distribution) can be recommended for shear

reinforcement purpose, but special attention must be taken in the arrangement of the shear bolts. Strains in the shear bolts show that the first layer is the most effective.

All the specimens that were reinforced with stirrups presented a better overall behaviour when compared to the specimen tested with the same vertical shear ratio, C-50. Stirrups provided higher drift capacity (from 150% up to 300% increase), higher maximum horizontal loads, higher ductility and by consequence higher energy dissipation capacity, due to the higher number of cycles achieved. For both specimens with only three shear reinforcement layers (C-50 STR1 and C-50 STR2), the punching failure surface was outside the shear reinforcement perimeter. Although the C-50 STR1 specimen punched outside the shear reinforcement perimeter, a failure inside the shear reinforced perimeter was eminent. This is corroborated by the fact that the behaviours of C-50 STR1, C-50 STR2 and C-50 STR3 were very similar. This suggests that the smaller shear reinforcement ratio used in this work is, for a three layer configuration, near the minimum to have a failure outside the shear reinforcement. None of the specimens with five layers of stirrups had a failure outside the reinforcement perimeter, meaning that the five layer configuration was sufficient to prevent punching outside the reinforcement perimeter, in this studied case. C-50 STR4's failure was due to the formation of a plastic hinge in the vicinity of the column. In this case, the shear reinforcement prevented punching failure. This specimen, having five layers and a higher shear reinforcement ratio, performed better, reaching higher drifts and dissipating more energy, by achieving a higher number of cycles. The strains in the shear reinforcement, as well as the rupture of some stirrups in the C50-STR3 specimen, show that closed stirrups were efficient, when correctly detailed and executed, despite the relatively low thickness of the slab.

Comparing the slabs C-50 BR and C-50 BC (shear reinforced with 3 layers of post installed bolt) with the slab C-50 STR3 (shear reinforced with 3 layers of stirrups) shows that the shear bolts are more efficient than stirrups. The slab C-50 STR3 presented a punching failure outside the reinforced area, (which did not happened with the bolts) and its saw cut shows a horizontal crack at the level of the bottom flexural reinforcement. This crack is not present in the slabs reinforced with bolts, which indicates that the efficiency of the shear reinforcement increases if the shear reinforcement is placed at the bottom of the slab. The higher efficiency of the post installed bolts is also due to their initial prestress.

The obtained results suggest that flat slabs without shear reinforcement may not be adequate to be safely used in seismic regions. An approach to calculate a minimum shear reinforcement

to be used in every flat slab-column connection is given. A simple methodology was suggested to calculate the minimum shear reinforcement area to be used in each layer. The arrangement must follow the Eurocode 2 specifications except for the minimum distance from the face of the column to the farther layer, which is advised to be at least four times the effective depth of the slab.

6.2 Future works

In the end of this work, several questions were raised and should be addressed in future works.

Slabs with more extreme vertical shear ratios must be tested in order to collect information missing in the drift-Shear ratio response.

Different details of shear reinforcement must be tested, focussing in solutions that reach the bottom of the slab. Corrosion resistant stirrups or studs must be tested, for example, steel studs with a polymer, lacquer or epoxy coating, at least in their lower section.

Lower shear reinforcement ratios must be tested to achieve a more efficient use of materials. The methodology presented in Chapter 5 to calculate the minimum shear reinforcement area by layer must be verified with more experimental tests.

The speed in which the horizontal loading was applied, showed to be relevant. Higher horizontal loading application speeds must be tested.

The test protocol for the application of the horizontal load is similar to the ones presented in the literature. Different test protocols must be tested, for instance, cycles in a constant higher drift step until failure or the use of pseudo-dynamic protocols.

A bigger test setup to test thicker slabs should be used to study the scale effect. This will also allow for the test of slabs with different slenderness.

Bibliography

[1] N. W. Hanson and J. M. Hanson, "Shear and Moment Transfer Between Concrete Slabs and Columns," *J. Portl. Cem. Assoc.*, vol. 10, no. 1, pp. 2–16, 1968.

[2] I. N. Robertson and A. Durrani, "Gravity Load Effect on Seismic Behavior of Interior Slab-Column Connections," *ACI Struct. J.*, vol. 89, pp. 37–45, 1992.

[3] I. N. Robertson and A. Durrani, "Gravity Load Effect on Seismic Behavior of Exterior Slab-Column Connections," *ACI Struct. J.*, vol. 88, pp. 255–267, 1991.

[4] A. Durrani and Y.Du, "Seismic Resistance of Slab-Column Connections in Existing Non-Ductile Flat-Plate Buildings," *ACI Struct. J.*, vol. 92, no. 4, pp. 479–487, 1995.

[5] A. Durrani, Y. Du, and Y. Luo, "Seismic Resistance of Nonductile Slab-Column Connections in Existing Flat-Slab Buildings," *ACI Struct. J.*, vol. 92, pp. 479–487, 1995.

[6] D. Dechka, "Response of Shear-Stud-Reinforced Continuous Slab-Column Frames to Seismic Loads," University of Calgary, 2001.

[7] S. J. Hwang and J. P. Moehle, "Vertical and lateral load tests of nine-panel flat-plate frame," *ACI Struct. J.*, vol. 97, no. 1, pp. 193–203, 2000.

[8] C. Rha, T. H. K. Kang, M. Shin, and J. B. Yoon, "Gravity and lateral load-carrying capacities of reinforced concrete flat plate systems," *ACI Struct. J.*, vol. 111, no. 4, pp. 753–764, 2014.

[9] N. M. Hawkins, A. Bao, and J. Yamazaki, "Moment Transfer from Concrete Slabs to Columns," *ACI Struct. J.*, vol. 86, no. 6, pp. 705–716, 1989.

[10] A. D. Pan and J. P. Moehle, "An Experimental Study of Slab-Column Connections," *ACI Struct. J.*, no. 89, pp. 626–638, 1993.

[11] I. A. Tegos and A. Tsonos, "Punching Strength Decay of Slab-Column Connections Under Seismic Loading," in *Eleventh World Conference on Earthquake Engineering*, 1996.

[12] P. Warnitchai, S. Pongpornsup, U. Prawatwong, and A. Pimanmas, "Seismic Performance of Post-Tensioned Iinterior Flat Slab-Column Connections," in *New Technologies for Urban Safety of Mega Cities in Asia*, 2004.

[13] I. N. Robertson and G. P. Johnson, "Cyclic lateral loading of nonductile slab-column connections," *ACI Struct. J.*, vol. 103, no. 3, pp. 356–364, 2006.

[14] R. B. Gayed and A. Ghali, "Seismic-resistant joints of interior columns with prestressed slabs," *ACI Struct. J.*, vol. 103, no. 5, pp. 710–719, 2006.

[15] M. Ritchie and A. Ghali, "Seismic-resistant connections of Edge Columns with Prestressed Slabs," *ACI Struct. J.*, vol. 102, pp. 314–323, 2006.

[16] S.-W. Han, S. H. Kee, Y.-M. Park, L. H. Lee, and T. H. K. Kang, "Hysteretic behavior of exterior post-tensioned flat plate connections," *Eng. Struct.*, vol. 28, no. 14, pp. 1983–1996, 2006.

[17] Y.-M. Park, S.-W. Han, and J. H. Ryu, "Comparison of seismic behaviors of interior joints in PT and RC flat plate systems," *Key Eng. Mater.*, vol. 348–349, pp. 741–745, 2007.

[18] A. Benavent-Climent, X. Cahís, and A. Catalán, "Seismic behavior of interior connections in existing waffle-flat-plate structures," *Eng. Struct.*, vol. 30, no. 9, pp. 2510–2516, 2008.

[19] A. Benavent-Climent, X. Cahís, and A. Catalán, "Reinforced Concrete Exterior Waffle Flat Plate-Column Connections Subjected to Lateral Earthquake Loading," *J. Earthq. Eng.*, vol. 13, no. 3, pp. 275–292, 2009.

[20] A. Benavent-Climent and J. Donaire-Ávila, "Moment transfer and influence of transverse beams in interior waffle flat plate-column connections under lateral loading," *Eng. Struct.*, vol. 49, pp. 146–155, 2013.

[21] E. Anggadjaja and S. Teng, "Edge-column slab connections under gravity and lateral loading," *ACI Struct. J.*, vol. 105, no. 5, pp. 541–551, 2008.

[22] M. A. Eder, R. L. Vollum, and A. Y. Elghazouli, "Performance of ductile RC flat slab to steel column connections under cyclic loading," *Eng. Struct.*, vol. 36, pp. 239–257, 2012.

[23] A. Himawan and S. Teng, "Cyclic behavior of post-tensioned slab-rectangular column connections," *ACI Struct. J.*, vol. 111, no. 1, pp. 177–187, 2014.

[24] N. M. Hawkins, D. Mitchell, and S. N. Hanna, "The Effects of Shear Reinforcement on Reversed Cyclic Loading Behavior of Flat Plate Structures," *Can. J. Civ. Eng.*, vol.

2, pp. 572–582, 1975.

[25] I. N. Robertson, T. Kawai, J. Lee, and B. Enomoto, "Seismic performance of flat-slab shear reinforcement," in *12WCEE2000*, 1998, pp. 1–11.

[26] S. Megally and A. Ghali, "Seismic behavior of edge column-slab connections with stud shear reinforcement," *ACI Struct. J.*, vol. 97, no. 1, pp. 53–60, 2000.

[27] B. Isufi, A. P. Ramos, and V. Lúcio, "Reversed horizontal cyclic loading tests of flat slab specimens with studs as shear reinforcement," *Struct. Concr.*, Sep. 2018.

[28] H. G. Park, K. S. Ahn, K. K. Choi, and L. Chung, "Lattice Shear Reinforcement for Enhancement of Slab-Column Connections," *ACI Struct. J.*, vol. 104, no. 3, pp. 294–303, 2007.

[29] M. R. Esfahani, "Effect of cyclic loading on punching shear strength of slabs strengthened with CFRP sheets," *Int. J. Civ. Eng.*, vol. 6, no. 3, pp. 208–215, 2008.

[30] T. H. K. Kang and J. W. Wallace, "Seismic performance of reinforced concrete slab-column connections with thin plate stirrups," *ACI Struct. J.*, vol. 105, no. 5, pp. 617–625, 2008.

[31] M. Cheng and G. J. Parra-Montesinos, "Evaluation of Steel Fiber Reinforcement for Punching Shear Resistance in Slab-Column Connections — Part II : Lateral Displacement Reversals," *ACI Struct. J.*, vol. 107, pp. 110–118, 2010.

[32] J. K. Song, J. Kim, H. B. Song, and J. W. Song, "Effective punching shear and moment capacity of flat plate-column connection with shear reinforcements for lateral loading," *Int. J. Concr. Struct. Mater.*, vol. 6, no. 1, pp. 19–29, 2012.

[33] M. M. Al-nasra, I. A. Duweib, and A. S. Najmi, "The Use of Pyramid Swimmer Bars as Punching Shear Reinforcement in Reinforced Concrete Flat Slabs," *J. Civ. Eng. Res.*, vol. 3, no. 2, pp. 75–80, 2013.

[34] A. Stark, B. Binici, and O. Bayrak, "Seismic upgrade of reinforced concrete slab-column connections using carbon fiber-reinforced polymers," *ACI Struct. J.*, vol. 102, no. 2, pp. 324–333, 2005.

[35] Widianto, O. Bayrak, J. O. Jirsa, and Y. Tian, "Seismic Rehabilitation of Slab-Column Connections," *ACI Struct. J.*, vol. 107, pp. 237–247, 2011.

[36] E. F. El-Salakawy, K. Soudki, and M. A. Polak, "Punching Shear Behavior of Flat

Slabs Strengthened with Fiber Reinforced Polymer Laminates," *J. Compos. Constr.*, vol. 8, no. 5, pp. 384–392, 2004.

[37] M. A. Polak, "Ductility of reinforced concrete flat slab-column connections," *Comput. Civ. Infrastruct. Eng.*, vol. 20, no. 3, pp. 184–193, 2005.

[38] N. Lawler and M. A. Polak, "Development of FRP Shear Bolts for Punching Shear Retrofit of Reinforced Concrete Slabs," *J. Compos. Constr.*, vol. 15, no. 4, pp. 591–601, 2011.

[39] D. Topuzi, M. A. Polak, and S. Narasimhan, "A new technique for the seismic retrofit of Slab-Column connections," *ACI Struct. J.*, vol. 114, no. 6, pp. 1471–1481, 2017.

[40] N. M. Hawkins, D. Mitchell, and M. S. Sheu, "Seismic Resistance of Concrete Slab to Column and Wall Connections," University of Washington, Washington, 1974.

[41] D. W. Symonds, D. Mitchell, and N. M. Hawkins, "Slab-Column Connections Subjected to High Intensity Shear and Transferring Reversed Moments," University of Washington, Washington, 1976.

[42] A. Ghali, M. Z. Elmasri, and W. Dilger, "Punching of Flat Plates Under Static and Dynamic Horizontal Forces," *ACI J. Proc.*, vol. 73, no. 10, pp. 566–572, 1976.

[43] D. G. Morrison, I. Hirasawa, and M. A. Sozen, "Lateral- Load Tests of R/C Slab-Column Connections," *J. Struct. Eng.*, vol. 109, no. 11, pp. 2698–2714, Nov. 1983.

[44] J. Soares, "Eccentric punching in reinforced concrete flat slabs [In Portuguese]," MsC. thesis, Universidade Técnica de Lisboa;, 1993.

[45] I. N. Robertson, T. Kawai, J. Lee, and B. Enomoto, "Cyclic testing of slab-column connections with shear reinforcement," *ACI Struct. J.*, vol. 99, no. 5, pp. 605–613, 2002.

[46] S. Megally, "Punching Shear Resistance of Concrete Slabs to Gravity and Earthquake Forces," 1998.

[47] U. Prawatwong, P. Warnitchai, and C. H. Tandian, "Bonded PT Slab-Column Connections with and without Drop Panel Subjected to Earthquake Loading," in *15th World Conference on Earthquake Engineering (15WCEE)*, 2012.

[48] M. Inácio, A. P. Ramos, and D. Faria, "Strengthening of flat slabs with transverse reinforcement by introduction of steel bolts using different anchorage approaches,"

Eng. Struct., vol. 44, pp. 63–77, 2012.

[49] W. Bu, "Punching Shear Retrofit Method Using Shear Bolts for Reinforced Concrete Slabs under Seismic Loading," University of Waterloo, 2008.

[50] I. N. Robertson, "Seismic Response of Connections in Indeterminate Flat-Slab Subassemblies," 1990.

[51] ACI Committee 318, *Building Code Requirements for Structural Concrete (ACI 318M-19)*. 2019.

[52] ACI-ASCE Committee 421, *Guide to Seismic Design of Punching Shear Reinforcement in Flat Plates (ACI 421.2R-10)*. 2010.

[53] ASCE/SEI, *Minimum Design Loads for Buildings and Other Structures*. 2010.

[54] CEN, *Eurocode 2: Design of concrete structures - EN 1992-1-1*. 2010.

[55] CEN, *Eurocode 8: Design of structures for earthquake resistance - EN 1998-1*. 2004.

[56] Fib, *Model Code 2010*, September. 2011.

[57] A. Muttoni, "Punching shear strength of reinforced concrete slabs without transverse reinforcement," *ACI Struct. J.*, vol. 105, no. 4, pp. 440–450, 2008.

[58] M. F. Ruiz and A. Muttoni, "Applications of critical shear crack theory to punching of reinforced concrete slabs with transverse reinforcement," *ACI Struct. J.*, vol. 106, no. 4, pp. 485–494, 2009.

[59] A. P. Ramos, A. Almeida, B. Isufi, M. Inácio, and R. Marreiros, "Punching of flat slabs under reversed horizontal cyclic loading," *ACI Spec. Publ.*, vol. 315, pp. 253–272, 2017.

[60] N. S. Mamede, A. P. Ramos, and D. Faria, "Experimental and parametric 3D nonlinear finite element analysis on punching of flat slabs with orthogonal reinforcement," *Eng. Struct.*, vol. 48, pp. 442–457, 2013.

[61] Y. D. Hose and F. Seible, "Performance Evaluation Database for Concrete Bridge Components Concrete Bridge Components and Systems under Simulated Seismic Loads," San Diego, 1999.

[62] R. Marreiros, "Precast Concrete Wall-Foundation Connection - Development of a seismic dissipative connection," PhD. thesis, Universidade Nova de Lisboa, 2014.

[63] CEN, *Eurocode: Basis of structural design - EN 1990*. 2002.

[64] CEN, *Eurocode 1: Actions on structures - EN 1991-1-1*. 2002.